

Fakultät für Maschinenwesen

Name der promotionsführenden Einrichtung

Improvement and validation of a computer model for the thermo-mechanical fuel rod behavior during reactivity transients in nuclear reactors

Titel der wissenschaftlichen Abhandlung

Lars Holt

Vorname und Name

Vollständiger Abdruck der von der promotionsführenden Einrichtung

Fakultät für Maschinenwesen

der Technischen Universität München zur Erlangung des akademischen Grades eines Doktor-Ingenieurs genehmigten Dissertation.

Vorsitzende/-r: Prof. Dr.-Ing. Thomas F. Sattelmayer

Prüfende/-r der Dissertation:

1. Prof. Rafael Macián-Juan, Ph.D.

2. Prof. Dr. rer. nat. Hans-Josef Allelein (RWTH Aachen)

Die Dissertation wurde am 06.10.2016 bei der Technischen Universität München eingereicht und durch die promotionsführende Einrichtung Fakultät für Maschinenwesen am 11.04.2017 angenommen.

„Aus der Kraft zu träumen, zu zweifeln und querzudenken erwachsen die Kreativität, die wissenschaftliche Potenz und der Erfindungsreichtum [...]. Aber diese eher subjektive und nicht direkt messbare Gabe oder Leidenschaft für Innovationen wird [ab und zu] zugunsten der objektiv messbaren Umsetzung von Effizienz, Kontrolle und Verwaltung vernachlässigt.“

Stephan Grinewald

„Innovation hat so viele Barrieren zu durchbrechen, so viele Hürden zu überspringen und ein komplexes Gewusel von ‚unerwarteten‘ Problemen zu lösen, dass ein Innovator sehr viel Herzblut für ‚sein Baby‘ aufbringen muss, um die Last allein [...] tragen zu können.“

Gunter Dueck

For my family

Abstract

This work deals with specific improvements and validation of the TRANSURANUS fuel performance code for the analysis of reactivity initiated accidents (RIA) as well as the development of a general coupling interface between TRANSURANUS and thermal hydraulics and/or reactor dynamics core analysis codes. TRANSURANUS is a best estimate fuel performance code which can be used for operational as well as accidental analysis.

Nuclear safety analysis has to demonstrate that the RIA safety criteria which limit the maximum fuel enthalpy increase, the maximum fuel temperature, and the departure from nucleate boiling (DNB) / the maximum clad surface temperature are ensured. Today's safety analysis is based on reactor dynamics codes and thermal hydraulics codes containing simplified fuel behaviour models applying a set of conservative initial and boundary conditions. Subsequent calculations with a fuel performance code complete the safety analysis. The coupling with DYN3D enhances the level of confidence of accident analysis by simultaneous interaction of great degree in detail in fuel performance, thermal hydraulics and neutron kinetics modelling. It allows a more realistic modelling of transients in comparison with usual practise.

Because the RIA version of the fuel performance code TRANSURANUS is still under development it has to undergo additional evaluation. Thence its performance was evaluated thanks to participation in the OECD/NEA RIA Fuel Codes Benchmark for highly irradiated fuel rods (2011-2012). The TRANSURANUS results showed a (very) good agreement in comparison with other codes in terms of injected energy, variation of enthalpy, central fuel temperature, maximum fuel temperature and radial location of the maximum fuel temperature. Nevertheless, the results also indicated that the code doesn't comprise a fission gas behaviour model and cladding material properties capable for RIA conditions. Furthermore, the TRANSURANUS thermal hydraulics covers heat regimes observed before DNB only.

A part of the work was devoted to the improvement of the modelling of the Xe depletion in the high burnup structure (HBS) in TRANSURANUS to allow a more accurate RIA safety analysis. This work was performed during a research stay at JRC-ITU in Karlsruhe. It resulted in a properly described Xe depletion, which in turn will lead to a more precise modelling of the transient fission gas release during RIA. The influence of local burn-up and irradiation temperature on the Xe concentration were investigated using a multi-physics approach. The

temperature influence was modelled by means of the temperature dependent effective burn-up. Good agreement was found between the modelled temperature threshold for the effective burn-up (1049 ± 17 °C) and the experimental temperature threshold for distinguishing between un- and restructured fuel in the High Burnup Rim Project (HBRP), irradiated in the Halden reactor. The new model was integrated in the TRANSURANUS code.

Moreover, in this work the benefit and potential of replacing a simplified fuel behaviour model in reactor dynamics codes for the RIA analysis were analysed and demonstrated. The overall interaction between neutron kinetics, thermal hydraulics and detailed fuel behaviour modelling has been rarely analysed in the open literature so far. Thence a general TRANSURANUS coupling interface was developed to enable the coupling of the fuel performance code with thermal hydraulics system, sub-channel thermal hydraulics, CFD and reactor dynamics codes. A variety of features ensure the generality, e.g. the application at either fuel assembly or fuel rod level. As first application of this interface, the reactor dynamics code DYN3D was coupled at assembly level in order to describe the fuel behaviour in more detail. For the two-way coupling approach, TRANSURANUS replaces the call of the simplified DYN3D fuel behaviour model, and is part of the iteration process in each time-step in DYN3D. Results of the coupled code system are shown for two RIA scenarios in a PWR.

For a control rod ejection, it appeared that for all burn-up levels the two-way coupling approach systematically leads to higher maximum values of both the node fuel enthalpy (max. difference of 46 J/g) and the node centreline fuel temperature (max. difference of 180.7 K), compared to DYN3D standalone best estimate calculations. The differences could be explained by the more detailed TRANSURANUS modelling of fuel thermal conductivity, radial power density profile and heat transfer in the gap. Since in this scenario no DNB occurred and the fuel enthalpy increases were relatively small, the impact of a great degree in online fuel behaviour modelling on the thermal hydraulics and neutron kinetics behaviour was very limited.

To analyse this feedback more precisely, a boron dilution transient with occurrence of DNB was determined based on boron concentrations from the Rossendorf Coolant Mixing (ROCOM) model facility. The results showed that the thermal hydraulics can already be strongly affected in fresh fuel assemblies, i.e. film boiling appeared in one node with the two-way coupling approach in spite of no film boiling appearing with the one-way coupling approach. For nodes with film boiling occurring in both coupling approaches, the two-way approach determined always higher peak values for both the node average fuel enthalpy and

the node clad surface temperature. Therefore, the coupled code system can potentially improve the assessment of safety criteria, at a reasonable computational cost.

Keywords: Nuclear fuel; reactor safety analysis; RIA; OECD RIA Fuel Codes Benchmark; fuel performance modelling; high burn-up structure; Xe depletion; general TRANSURANUS coupling interface; code coupling; DYN3D-TRANSURANUS; control rod ejection; boron dilution transient.

Contents

List of Figures	i
List of Tables	vii
List of Abbreviations	ix
Nomenclature	xii
Latin variables.....	xii
Greek variables	xiv
1 Introduction	1
1.1 Background.....	1
1.2 Research objectives and stages	6
1.3 Thesis outline	9
1.4 Verification and validation.....	10
2 Literature review	12
2.1 Characteristics of the high burnup structure (HBS).....	12
2.2 Fuel rod behaviour and cladding failure during RIA.....	14
2.2.1 Early phase during RIA (Pre-DNB).....	15
2.2.2 Late phase during RIA (Post-DNB).....	16
2.3 State-of-the-art modelling in fuel performance codes for RIA.....	19
2.3.1 Range of application.....	20
2.3.2 Geometrical representation	21
2.3.3 Clad tube representation.....	24
2.3.4 Pellet-clad contact modelling.....	25
2.3.5 Ongoing model developments regarding TRANSURANUS.....	26
2.4 State-of-the-art modelling of fuel behaviour in RIA licensing calculations.....	28
2.4.1 Overview about traditional licensing approach.....	28
2.4.2 General features of the reactor dynamics code DYN3D.....	31
2.4.3 Fuel behaviour modelling in the reactor dynamics code DYN3D.....	32
2.5 Trend toward coupled code systems with detailed fuel behaviour modelling.....	35

3	OECD RIA Fuel Codes Benchmark for highly irradiated fuel rods	39
3.1	Experimental data	39
3.2	Generation of TRANSURANUS inputs	43
3.2.1	Pre-irradiation in power reactor	44
3.2.2	Refabrication in hot cells and RIA transient in research reactor.....	48
3.3	Analysis of TRANSURANUS results	51
3.3.1	Spectrum of fuel performance codes.....	51
3.3.2	Use of input data (comparison to other fuel performance codes)	52
3.3.3	Thermal behaviour (comparison to other fuel performance codes)	54
3.3.4	Mechanical behaviour (comparison to other fuel performance codes)	58
3.4	Summary and recommendations for future work	64
4	Improved modelling of high burnup structure in the TRANSURANUS code	66
4.1	Experimental data of high burn-up fuel (High Burnup Rim Project)	67
4.2	Temperature dependent modelling of the Xe depletion.....	69
4.2.1	New standalone Xe depletion model.....	69
4.2.2	Implementation of the Xe depletion model in TRANSURANUS	71
4.3	Results of the sensitivity analysis	72
4.3.1	Impact of threshold burn-up.....	72
4.3.2	Impact of threshold temperature	74
4.3.3	Impact of Xe yield.....	75
4.4	Summary and recommendations for future work	76
5	Development of the general TRANSURANUS coupling interface	78
5.1	Main features	79
5.1.1	One-way and two-way coupling	79
5.1.2	Flexibility in time-step length and numerical stability.....	80
5.1.3	Freely selectable level of detail in fuel behaviour modelling	80
5.1.4	Pre- and post-calculations with TRANSURANUS standalone.....	81
5.1.5	Automatic switch from steady-state to transient conditions	81
5.1.6	Parallelization.....	81
5.1.7	Further features	82
5.2	Applicability for various scenarios	83

5.3	General guidelines for applications	84
5.3.1	TRANSURANUS input	84
5.3.2	Modifications in the code coupled to TRANSURANUS.....	85
5.3.3	Maintenance of the code system	88
5.4	Summary and recommendations for future work	89
6	Application of the new code system DYN3D-TRANSURANUS for RIA	91
6.1	Description of the new code system DYN3D-TRANSURANUS.....	91
6.2	Variants of the code system differing in detail of fuel behaviour modelling	95
6.3	Specification of simulated RIA scenarios for German PWR.....	96
6.3.1	Control rod ejection.....	97
6.3.2	Boron dilution transient.....	98
6.4	Results and discussion	99
6.4.1	Pre-calculations for critical boron concentration	99
6.4.2	Comparison of DYN3D standalone and two-way coupling approach.....	100
6.4.2.1	Analysis of differences in global and local parameters	100
6.4.2.2	Impact of fuel thermal conductivity	105
6.4.2.3	Impact of power density profile.....	107
6.4.2.4	Impact of heat transfer in gap	108
6.4.2.5	Impact of all three factors	110
6.4.3	Comparison of one-way and two-way coupling approach.....	110
6.4.3.1	Analysis of differences in feedback on neutron kinetics	110
6.4.3.2	Analysis of differences in feedback on thermal hydraulics.....	115
6.5	Computational costs.....	123
6.6	Outlook on DYN3D-TRANSURANUS	125
6.7	Summary and recommendations for future work	126
7	Summary and conclusion	128
8	Bibliography	132
	Acknowledgements	145
	Publications	149

List of Figures

Figure 1:	Most thresholds are within the upper shaded area. The two lower shaded zones represent the envelope of conservative calculations for actual PWR cores. As seen, the core enthalpy can exceed the lower failure thresholds – i.e. for cases with large oxidation and brittle cladding. [23]	5
Figure 2:	Simplified flow structure of research objectives and stages (*due to participation in the OECD RIA Fuel Codes Benchmark in 2011/2012)	6
Figure 3:	SEM images of the high burnup structure (HBS). Left, subdivided grains due to restructuring; right, view in a HBS pore surrounded by subdivided grains [33]	12
Figure 4:	Possible mechanisms for fuel and cladding damage under RIA [45]	15
Figure 5:	PCMI failure mode observed in the NSRR test VA-1 (PWR, 71 MWd/kgU, cladding ZIRLO™) [47].....	16
Figure 6:	Boiling crisis mechanism in stationary and transient conditions (based on visual observation in NSRR tests performed under subcooled pool boiling conditions) [54]	19
Figure 7:	Clad inner and outer temperatures calculated by the Japanese fuel performance code RANNS for the NSRR RIA test FK-10 (peak power at 0 s). Left, experimental pulse width of 5.2 ms; right, larger pulse of 40 ms. [3, 70].....	24
Figure 8:	External (a) and internal (b) coupling methodology according to neutron kinetics/reactor dynamics code and thermal hydraulics system code in core wide analysis (red arrows denote data exchange) [3]	36
Figure 9:	Stages of the fuel rod in a complex irradiation experiment compared to its simulation in TRANSURANUS (individual figures taken from [125])	43
Figure 10:	First methodology to combine different axial resolutions/discretisations in power reactors and research reactors (example on linear heat rate with resolution of two locations in power reactor and three locations in research reactor)	46
Figure 11:	Second methodology to combine different axial resolutions/discretisations in power reactors and research reactors (example on linear heat rate with resolution of two locations in power reactor and three locations in research reactor)	47

Figure 12:	Node linear heat rate over time (benchmark case #1). Left, during pre-irradiation in the power reactor [25]; right, during RIA test CIP0-1 in the research reactor CABRI (extracted from TRANSURANUS (HZDR) results).	50
Figure 13:	Energy deposited over time in the whole rodlet (benchmark case #1) [25].....	53
Figure 14:	Gap width over time at peak power node (benchmark case #3) [25].....	54
Figure 15:	Variation of enthalpy over time in the whole rodlet with respect to initial conditions of the transient (benchmark case #3). Left, results provided by all participants of the benchmark; right, selected results from the left side. [25]	55
Figure 16:	Fuel maximum temperature over time at peak power node (benchmark case #3). Left, results provided by all participants of the benchmark; right, selected results from the left side. [25]	56
Figure 17:	Radial location of the maximum of the fuel temperature over time at peak power node defined as distance from the centre of the pellet (benchmark case #3). Left, results provided by all participants of the benchmark; right, selected results from the left side. [25].....	57
Figure 18:	Clad outer temperature over time at peak power node (benchmark case #2). Left, results provided by all participants of the benchmark; right, selected results from the left side. [25].....	58
Figure 19:	Outer fuel radius over time at peak power node (benchmark case #3). Left, results provided by all participants of the benchmark; right, selected results from the left side. [25].....	60
Figure 20:	Inner clad radius over time at peak power node (benchmark case #3). Left, results provided by all participants of the benchmark; right, selected results from the left side. [25].....	60
Figure 21:	Outer clad permanent hoop strain at the end of the transient as a function of height with respect to the bottom of fissile column (benchmark case #1). Left, experimental data and results provided by all participants of the benchmark; right, experimental data and selected results from the left side. [25].....	62

Figure 22:	Outer clad permanent hoop strain at the end of the transient as a function of height with respect to the bottom of fissile column (benchmark case #2). Left, results provided by all participants of the benchmark; right, selected results from the left side. [25].....	63
Figure 23:	Total axial clad elongation containing thermal, elastic and plastic components with respect to cold state conditions over time (benchmark case #1). Left, experimental data and results provided by all participants of the benchmark; right, experimental data and selected results from the left side. [25].....	64
Figure 24:	Burn-up and average irradiation temperature of the 16 stacks of HBRP. The extremes represent the temperature difference between the surface and the centre of the discs, obtained by a finite element calculation [142].....	68
Figure 25:	Comparison between predicted and measured local xenon concentrations as a function of the local burn-up for data from HBRP. The prediction is based on the depletion model in Ref. [27] with the threshold burn-up varied between 40 and 70 GWd/tU in steps of 10 GWd/tU. Rod numbering corresponds to the numbering in Figure 24.	73
Figure 26:	Main principle of the general TRANSURANUS coupling interface, whereas one fuel rod is calculated per call of the interface.....	78
Figure 27:	Local restructuring of DYN3D to allow determination of the whole fuel rod behaviour at once (i: count variable; n: total number of axial nodes in the coolant channel). Left, previous local DYN3D code structure; right, new local DYN3D code structure after restructuring.....	87
Figure 28:	Coupling approaches with the reactor dynamics code DYN3D.....	92
Figure 29:	Data transfer between DYN3D and TRANSURANUS via the general TRANSURANUS coupling interface for one-way coupling (prospective in combination with the thermal hydraulics system code ATHLET) [10]. As shown, a later planned extension to DYN3D-ATHLET-TRANSURANUS was already taken into account, e.g. applicable to ATWS in the future (G_{in} : coolant mass flow density at the core inlet; G_{out} : coolant mass flow density at the core outlet; h_{in} : coolant specific enthalpy at the core inlet; h_{out} : coolant specific enthalpy at the core outlet; p_{in} : coolant pressure at the core inlet; p_{out} : coolant pressure at the core outlet).....	94

Figure 30: Data transfer between DYN3D and TRANSURANUS via the general TRANSURANUS coupling interface for two-way coupling (prospective in combination with the thermal hydraulics system code ATHLET) [10]. As shown, a later planned extension to DYN3D-ATHLET-TRANSURANUS was already taken into account, e.g. applicable to ATWS in the future (G_{in} : coolant mass flow density at the core inlet; G_{out} : coolant mass flow density at the core outlet; h_{in} : coolant specific enthalpy at the core inlet; h_{out} : coolant specific enthalpy at the core outlet; p_{in} : coolant pressure at the core inlet; p_{out} : coolant pressure at the core outlet)..... 94

Figure 31: Total nuclear power over time (left) and global average fuel temperature over time (right) for CR ejection at 30% of nominal reactor power. 101

Figure 32: Maximum assembly-average fuel enthalpy increase Δh calculated by DYN3D-TRANSURANUS for CR ejection at 30% of nominal reactor power (bordered fuel assembly represents the location of the ejected CR)..... 102

Figure 33: For CR ejection with no onset of DNB, relative difference $\Delta(\Delta h)_{rel}$ in maximum assembly-average fuel enthalpy increase Δh between DYN3D and DYN3D-TRANSURANUS at 30% of nominal reactor power ($> 0\%$: value of DYN3D is larger; $< 0\%$: value of DYN3D is lower; bordered fuel assembly represents the location of the ejected CR) 102

Figure 34: Node-wise differences in maximum centreline fuel temperature over node burn-up for CR ejection without DNB. Differences are defined as two-way coupling approach DYN3D-TRANSURANUS (realistic) minus DYN3D. Left, at 30 % of nominal reactor power; right, at HZP conditions. 104

Figure 35: Node-wise differences in maximum centreline fuel temperature over node burn-up for CR ejection at 30% of nominal reactor power for (a) variant I with identical fuel thermal conductivity, (b) variant II with identical power density profile, (c) variant III with identical heat transfer coefficient in gap, and (d) variant IV as combination of (a), (b) and (c). Left, difference defined as two-way coupling approach DYN3D-TRANSURANUS (variant I, II, III or IV) minus DYN3D (standalone); right, differences defined as two-way coupling approach DYN3D-TRANSURANUS (variant I, II, III or IV) minus DYN3D-TRANSURANUS (realistic). 106

Figure 36: Heat transfer coefficient (HTC) in gap as function of (a) node linear heat rate and (b) node average fuel enthalpy. Left, two-way coupling approach of DYN3D-TRANSURANUS (realistic) for CR ejection with no onset of DNB initiated at 30 % of nominal reactor power (slice with maximum linear heat rate of the fuel assembly containing the ejected CR, cf. Figure 32); right, TRANSURANUS standalone for CR ejection case #3 of OECD RIA Fuel Codes Benchmark with onset of DNB [24] (slice in the middle of the test rodlet). 109

Figure 37: Total reactivity vs. time (a), total nuclear power zoomed in for showing differences vs. time (b) and global average fuel temperature vs. time (c) [values of the 1-way approach taken from the DYN3D part in the coupled code system] 111

Figure 38: Node average injected energy vs. time. (a) For the node at the bottom of the fresh fuel assembly B6 (left) and for the 2nd lowest node of the same assembly (right). (b) For the node at the bottom of fuel assembly D5 with average assembly burn-up of 31.7 MWd/kgHM (left) and for the node at the bottom of fuel assembly E6 with average assembly burn-up of 50.0 MWd/kgHM (right)..... 113

Figure 39: Maximum assembly-average fuel enthalpy increase Δh calculated by DYN3D-TRANSURANUS (two-way approach) [bordered fuel assembly contains the stuck CR] 114

Figure 40: (a) Node-wise differences in maximum average fuel enthalpy as a function of the node burn-up. Differences are defined as the result of the two-way coupling approach minus the corresponding result of the one-way coupling approach of DYN3D-TRANSURANUS. (b) Maximum node average fuel enthalpy calculated by the two-way coupling approach versus the corresponding value of the one-way coupling approach. The ratio between the CHF and the actual heat flux, at which DNB is assumed, amounted to 1.0 (best estimate value) on the left and to 2.0 (conservative value) on the right. 116

Figure 41: Node average fuel enthalpy vs. time. (a) For the node at the bottom of the fresh fuel assembly B6 (left) and for the 2nd lowest node of the same assembly (right). (b) For the node at the bottom of fuel assembly D5 with average assembly burn-up of 31.7 MWd/kgHM (left) and for the node at the bottom of fuel assembly E6 with average assembly burn-up of 50.0 MWd/kgHM (right)..... 117

- Figure 42: (a) Node-wise differences in maximum clad surface temperature as a function of the node burn-up. Differences are defined as the result of the two-way coupling approach minus the corresponding result of the one-way coupling approach of DYN3D-TRANSURANUS. (b) Maximum node clad surface temperature calculated by the two-way coupling approach versus the corresponding value of the one-way coupling approach. The ratio between the CHF and the actual heat flux, at which DNB is assumed, amounted to 1.0 (best estimate value) on the left and to 2.0 (conservative value) on the right. 120
- Figure 43: Node clad surface temperature vs. time. (a) For the node at the bottom of the fresh fuel assembly B6 (left) and for the 2nd lowest node of the same assembly (right). (b) For the node at the bottom of fuel assembly D5 with average assembly burn-up of 31.7 MWd/kgHM (left) and for the node at the bottom of fuel assembly E6 with average assembly burn-up of 50.0 MWd/kgHM (right). 121
- Figure 44: Node heat transfer coefficient (HTC) in the gap vs. time. (a) For the node at the bottom of the fresh fuel assembly B6 (left) and for the 2nd lowest node of the same assembly (right). (b) For the node at the bottom of fuel assembly D5 with average assembly burn-up of 31.7 MWd/kgHM (left) and for the node at the bottom of fuel assembly E6 with average assembly burn-up of 50.0 MWd/kgHM (right). 123

List of Tables

Table 1 –	Potential reactivity initiated scenarios in BWR and PWR (taken from [4] and extended by information in [3]).....	3
Table 2 –	Values of critical heat flux, critical surface temperature and film-boiling heat flux measured in PATRICIA tests under steady-state conditions and RIA-like transients [3, 51, 55]	18
Table 3 –	(Transient) fuel performance codes applicable to RIA taken from Ref. [3]	20
Table 4 –	Features of the simplified fuel behaviour model in DYN3D [94] compared to the fuel performance codes TESPARD [95-97] and TRANSURANUS [60] (according to RIA).....	34
Table 5 –	Cases of the OECD RIA Fuel Codes Benchmark [24].....	41
Table 6 –	Main characteristics of the CABRI tests determined in the OECD RIA Fuel Codes Benchmark [24]	42
Table 7 –	Thermal hydraulics conditions in power reactor vs. research reactor (CIP0-1) [25]	44
Table 8 –	Codes applied by participants in OECD RIA Fuel Codes Benchmark [24].....	52
Table 9 –	States of stress relevant to the mechanical testing for RIA (assuming isotropic plasticity) [13]	61
Table 10 –	Burn-up and calculated temperature at end of life (EOL) reached for the 16 stacks [142].....	68
Table 11 –	Values of the merit function χ^2 for temperature values given in Ref. [140]	74
Table 12 –	Values of the fitted parameters bu_{eff0} and T_{thres} with 68% confidence intervals.	75
Table 13 –	Values of the fitted parameters bu_{eff0} and T_{thres} with their standard errors (dependence on Xe creation rate).	76
Table 14 –	Critical boron concentration of the initial reactor state for CR ejection transient	100
Table 15 –	Relative difference $\Delta(\Delta h)_{rel}$ in maximum assembly-average fuel enthalpy increase Δh in relation to the fuel assembly burn-up for CR ejection transient	103

List of Tables

Table 16 – Differences in maximum values of the node centreline fuel temperature for CR ejection transient (defined as DYN3D-TRANSURANUS minus DYN3D standalone).....	104
Table 17 – Maximum node average fuel enthalpy for nodes with film boiling (simulation with increased ratio between CHF and actual heat flux).....	119
Table 18 – Maximum node clad surface temperature for nodes with film boiling (simulation with increased ratio between CHF and actual heat flux).....	122
Table 19 – Overview of computation times without parallelization [159].....	124

List of Abbreviations

AOO	Anticipated Operational Occurrence
ASTRID	Advanced Sodium Technological Reactor for Industrial Demonstration
ATWS	Anticipated Transient Without Scram
BIGR	Bystry Impulsny Graphitovy Reaktor, Russia
BOC	Begin Of Cycle
BOCHVAR	Joint Stock Company “A.A. Bochvar High-technology Research Institute of Inorganic Materials” (JSC “VNIINM”), Russia
BWR	Boiling Water Reactor
CABRI reactor	Research reactor in Cadarache, France
CEA	Commissariat à l’énergie atomique et aux énergies alternatives, France
CFD	Computational Fluid Dynamics
CHF	Critical Heat Flux
CIEMAT	Centro de Investigaciones Energéticas, Medioambientales y Tecnológicas, Spain
CPU	Central Processing Unit
CR	Control Rod
CRIEPI	Central Research Institute of Electric Power Industry, Japan
CS	Control System
CZP	Cold Zero Power
DBA	Design Basis Accident
DiD	Defence In Depth concept
DNB	Departure from Nucleate Boiling
EAC-2	European Accident Code (improved version 2)
EDF	Electricité de France
EOC	End Of Cycle
EOL	End Of Life
EPMA	Electron Probe Microanalysis
EPRI	Electric Power Research Institute, United States
FR	Fast Reactor
FUMAC	FUel Modelling in Accident Conditions (ongoing IAEA benchmark)
FUMEX	FUel Modelling at EXtended burnup (IAEA benchmark with three phases)
FWHM	Full Width at Half Maximum

List of Abbreviations

Gen-IV	GENeration IV reactors (next generation nuclear energy systems)
GRS	Gesellschaft für Anlagen- und Reaktorsicherheit, Germany
HBRP	High Burnup Rim Project
HBS	High Burnup Structure
HFP	Hot Full Power
HRP	OECD Halden Reactor Project, Norway
HTC	Heat Transfer Coefficient
HWR	Heavy Water Reactor
HZDR	Helmholtz-Zentrum Dresden-Rossendorf e.V., Germany
HZP	Hot Zero Power
IAEA	International Atomic Energy Agency, Austria
IFE	Institute for Energy Technology, Norway
IFPE	International Fuel Performance Experiments database (OECD/NEA)
IGR	Impulsny Graphitovy Reaktor, Russia
INL	Idaho National Laboratory, United States
IRSN	Institut de Radioprotection et de Sûreté Nucléaire, France
JAEA	Japan Atomic Energy Agency
JNES	Japan Nuclear Energy Safety organization
JRC-ITU	European Commission, Joint Research Centre, Institute for Transuranium Elements, Germany
KINS	Korea Institute of Nuclear Safety
KIT	Karlsruhe Institute of Technology, Germany
Konvoi	Design of the last three constructed PWRs in Germany (Siemens)
LMFBR	Liquid Metal Fast Breeder Reactor
LOCA	Loss Of Coolant Accident
LWR	Light Water Reactor
MOC	Mid Of Cycle
MOOSE	INL Multiphysics Object Oriented Simulation Environment
MOX	Mixed OXide fuel
MTA EK	Nuclear Security Department of the Hungarian Academy of Sciences, Centre for Energy Research
MYRRHA	Multi-purpose hYbrid Research Reactor for High-tech Applications
NEA	Nuclear Energy Agency of OECD
NFIR	Nuclear Fuel Industry Research program
NRC	Nuclear Regulatory Commission, United States
NRI	Nuclear Research Institute Řež plc, Czech Republic

List of Abbreviations

NSRR	Nuclear Safety Research Reactor, Japan
NURESIM	European platform for Nuclear Reactor Simulator
NURISP	NUclear Reactor Integrated Simulation Project
OECD	Organisation for Economic Co-operation and Development
PCI	Pellet Clad Interaction
PCMI	Pellet Cladding Mechanical Interaction
PIE	Post Irradiation Examination
PNNL	Pacific Northwest National Laboratory, United States
PSI	Paul Scherrer Institut, Switzerland
PWR	Pressurized Water Reactor
RDA	Reactivity control rod/blade Drop Accident (BWR)
REA	Reactivity control rod Ejection Accident (PWR)
RIA	Reactivity Initiated Accident
ROCOM	ROssendorf COolant Mixing model (test facility)
SAPR	Semi-Analytical Perturbation Reconstruction model
SEM	Scanning Electron Microscopy
SGTR	Steam Generator Tube Rupture
SIMS	Secondary Ion Mass Spectrometry
SSM	Strål säkerhets myndigheten (Swedish Radiation Safety Authority)
TEM	Transmission Electron Microscopy
TEPCO	Tokyo Electric Power Company Holdings, Inc., Japan
TRACTEBEL	Tractebel Engineering S.A. (ENGIE Group), Belgium
TÜV NORD	Technischer Überwachungsverein NORD EnSys Hannover GmbH & Co. KG, Germany
UNIPI	Università di Pisa, Italy
VTT	Technical Research Centre of Finland
VVER	Vodo-Vodyanoy Energetichesky Reaktor (Russian PWR)
WGFS	OECD/NEA Working Group on Fuel Safety

Nomenclature

Latin variables

a	Fitting constant for thermal conductivity $\left(\frac{mK}{W}\right)$
a	Fitting constant in the Xe rate equation $\left(\frac{kgU}{MWd}\right)$
a	Summarizing all fitted parameters of the correlation $y(x_k, a)$
a_1	Fitting constant for thermal conductivity $\left(\frac{m\ kgU\ K}{MWd\ W}\right)$
a_2	Fitting constant for thermal conductivity $\left(\frac{mK}{W\ wt\%}\right)$
b	Fitting constant for thermal conductivity $\left(\frac{m}{W}\right)$
b_1	Fitting constant for thermal conductivity $\left(\frac{m\ kgU}{MWd\ W}\right)$
b_2	Fitting constant for thermal conductivity $\left(\frac{m}{W\ wt\%}\right)$
bu	Local burn-up $\left(\frac{MWd}{kgU}\right)$
Δbu	Increment of local burn-up $\left(\frac{MWd}{kgU}\right)$
bu_0	Local threshold burn-up for onset of Xenon depletion $\left(\frac{MWd}{kgU}\right)$
bu_{eff}	Local effective burn-up $\left(\frac{MWd}{kgU}\right)$
Δbu_{eff}	Increment of local effective burn-up $\left(\frac{MWd}{kgU}\right)$
bu_{eff0}	Reference value of local effective burn-up $\left(\frac{MWd}{kgU}\right)$
c	Specific heat capacity $\left(\frac{J}{kgK}\right)$
c	Fitting constant for thermal conductivity $\left(\frac{WK}{m}\right)$
\dot{c}_{Xe}	Xenon creation rate $\left(\frac{wt\%*kgU}{MWd}\right)$
d	Fitting constant for thermal conductivity (K)
$[D]$	Tensor of the elastic constants $\left(\frac{m^2s}{N}\right)$
$f(T)$	Factor specifying the temperature influence in the range of defect healing (–)
F_l	Friction forces (N)
G_{in}	Coolant mass flow density at the core inlet $\left(\frac{kg}{m^2s}\right)$
G_{out}	Coolant mass flow density at the core outlet $\left(\frac{kg}{m^2s}\right)$
Gd	Local gadolinium concentration ($wt\%$)
h	Assembly-average specific fuel enthalpy $\left(\frac{J}{g}\right)$

Δh	Maximum assembly-average specific fuel enthalpy increase ($\frac{J}{g}$)
h_{in}	Specific enthalpy of the coolant at the core inlet ($\frac{kJ}{kg}$)
h_{out}	Specific enthalpy of the coolant at the core outlet ($\frac{kJ}{kg}$)
k	Counter variable referring to x_k and y_k (—)
k_d	Factor taking into account the effects of the initial fuel structure (—)
LHR	Linear rod power or rather linear heat rate ($\frac{W}{mm}$)
N	Number of data points referring to x_k and y_k (—)
p_{cool}	Coolant pressure (MPa)
p_{in}	Coolant pressure at the core inlet (MPa)
p_{out}	Coolant pressure at the core outlet (MPa)
P	Local porosity (—)
q'''	Power density ($\frac{W}{m^3}$)
r	Radius (m)
r_{ref}	Radius of reference radius (m)
R	Radius of deformed geometry (m)
δR_{clad}	Total change in clad radius (m)
δR_{fuel}	Total change in fuel radius (m)
$\delta R_{clad,el}$	Total change in clad radius due to elastic deformation (m)
$\delta R_{fuel,el}$	Total change in fuel radius due to elastic deformation (m)
$\delta R_{clad,pl}$	Total change in clad radius due to plastic deformation (m)
$\delta R_{clad,th}$	Total change in clad radius due to linear thermal expansion (m)
$\delta R_{fuel,th}$	Total change in fuel radius due to linear thermal expansion (m)
t	Time (s)
Δt	Time step length (h)
T	Temperature (K)
T	Local fuel temperature for effective burn-up (°C)
T_1	Onset-temperature for partial healing in the fuel (°C)
T_2	Temperature limit for complete healing of defects in the fuel (°C)
$T_{clad,sf}$	Clad surface temperature (°C)
T_{cool}	Coolant temperature (°C)
T_{fuel}	Fuel temperature (K) ¹
T_{mod}	Moderator temperature (K)

¹ Unit °C in the section 6.1

T_p	Absolute temperature (K)
T_{thres}	Temperature threshold for effective burn-up ($^{\circ}C$)
u	Radial deformation (m)
Xe	Local xenon concentration ($wt\%$)
x_k	Data point with index k
$y(x_k, \mathbf{a})$	Correlation fitted iteratively by minimization of $\chi^2(\mathbf{a})$
y_k	Data point with index k

Greek variables

$\alpha_{clad,sf}$	Heat transfer coefficient between clad to coolant $\left(\frac{W}{mm^2K}\right)$
ε_1	Axial strain (–)
ε_2	Hoop strain (–)
ε_a	Axial strain component (–)
ε_r	Radial strain component (–)
ε_s	Volumetric ratio of the restructured fuel domain (–)
ε_t	Tangential strain component (–)
$\{\varepsilon^{cr}\}$	Vector of creep strain as component of inelastic strain (–)
$\{\varepsilon^{el}\}$	Vector of elastic strain (–)
ε_a^{el}	Axial component of elastic strain (–)
ε_r^{el}	Radial component of elastic strain (–)
ε_t^{el}	Tangential component of elastic strain (–)
$\{\varepsilon^{ex}\}$	Vector of sum of inelastic strains (–)
$\{\varepsilon^f\}$	Vector of crack strain as component of inelastic strain (–)
$\{\varepsilon^{pl}\}$	Vector of instantaneous plastic strain as component of inelastic strain (–)
$\{\varepsilon^s\}$	Vector of solid & gaseous swelling strain as component of inelastic strain (–)
$\{\varepsilon^{sin}\}$	Vector of hot-pressing strain as component of inelastic strain (–)
$\{\varepsilon^{th}\}$	Vector of thermal strain as component of inelastic strain (–)
$\{\varepsilon^{tot}\}$	Vector of total strain (–)
ε_a^{tot}	Axial component of total strain (–)
ε_r^{tot}	Radial component of total strain (–)
ε_t^{tot}	Tangential component of total strain (–)
λ	Thermal conductivity $\left(\frac{W}{mK}\right)$

Nomenclature

λ_{fuel}	Fuel thermal conductivity ($\frac{W}{mK}$)
ρ	Density ($\frac{kg}{m^3}$)
ρ	Reactivity (—)
ρ_{cs}	Reactivity component due to control system (—)
$\{\sigma\}$	Vector of stress ($\frac{N}{mm^2}$)
σ_a	Axial stress component ($\frac{N}{mm^2}$)
σ_k	Experimental uncertainty of y_k (e.g. standard deviation)
σ_r	Radial stress component ($\frac{N}{mm^2}$)
σ_{stand}	Error band of each fitted parameter related to a 68% confidence interval
σ_t	Tangential stress component ($\frac{N}{mm^2}$)
ϕ_{mod}	Void volume fraction of the moderator (—)
$\chi^2(\mathbf{a})$	Merit function with \mathbf{a} summarising all fitted parameters of the correlation $y(x_k, \mathbf{a})$ (—)

1 Introduction

1.1 Background

The public has to be protected against civilization related radiation exposure occurring additionally beside the natural one, e.g. from medical devices, from nuclear power plants and in airplanes. For nuclear power plants the defence in depth (DiD) concept should ensure this [1]. This concept “consists of a hierarchical deployment of different levels of equipment and procedures in order to maintain the effectiveness of physical barriers placed between radioactive material and workers, the public or the environment, during normal operation, anticipated operational occurrences (AOOs) and, for some barriers, accidents at the plant.” [2] For example, level 1 refers to normal operation, level 2 to abnormal operation, and level 3 to design basis accidents (DBA) like loss of coolant accident (LOCA) and reactivity initiated accident (RIA).

The operational reactor control system and the safety protection systems must ensure either no radiological impact in the level 1 and level 2 or no radiological impact outside the exclusion area in the level 3 of the DiD concept [1]. Due to the impossibility to consider in each safety analysis the full chain of causation from the release of fission products located in the fuel pellets up to the determination of the radiological doses of a person in the power plant’s environment advanced surrogate criteria were defined. Their compliance has to be guaranteed by the licensee for the operation of its nuclear power plant. These criteria also allow a direct comparison to results of neutron kinetics codes, thermal hydraulic system codes and fuel performance codes. For RIA core coolability/integrity of fuel rods and reactivity control represent the main advanced surrogate criteria. The total change of the reactivity rate $\dot{\rho}$ is defined as following [3]:

$$\dot{\rho} = \dot{\rho}_{cs} + \frac{\partial \rho}{\partial T_{fuel}} T_{fuel} \dot{} + \frac{\partial \rho}{\partial T_{mod}} T_{mod} \dot{} + \frac{\partial \rho}{\partial \phi_{mod}} \phi_{mod} \dot{} \quad (1)$$

where ρ is the reactivity, its component ρ_{cs} symbolizes the reactivity due to the control system (CS) and its actuating variables, T_{fuel} presents the fuel temperature in K, T_{mod} the moderator temperature in K, and ϕ_{mod} the void volume fraction of the moderator. The rates of change are marked by a point above the symbol in the equation. In light water reactors

(LWR), the coolant medium represents also the moderator at the same time. Regarding the first term on the right side in eq. (1), the control rods and additionally boron acid in a PWR (dissolved in the coolant/moderator) are normally used by the CS as actuating variables for management the neutron economy in LWR, hence the control of the reactivity. The control of the reactivity due to CS can be disturbed in case of RIA. For example, the reactivity can be (strongly) influenced by a control rod ejection due to a mechanical failure. In that short time period the CS can't balance the effect of the control rod ejection. In general various classes of RIA scenarios exist considering for instance control system failure, control rod ejection (PWR) or control blade/rod drop (BWR), coolant/moderator temperature and void effects, and dilution or removal of coolant/moderator poison [3, 4] (cf. Table 1). In some case, the core power can rise rapidly, although the Doppler Effect limits simultaneously the rise in power thanks to the fuel temperature increase (cf. second term on the right hand side in eq. (1)). The last two terms in eq. (1) describe the influence of the change in moderator temperature T_{mod} and moderator void volume fraction ϕ_{mod} . Nevertheless, the time constant of the clad-to-coolant heat transfer is larger than that of a sharp power pulse. This leads to an almost adiabatic heating of the fuel [5] in the case of very fast reactivity insertion (see subsection 2.2.1 and subsection 3.3.3).

A few of the events in Table 1 result in a relatively low rate of increase in reactivity (e.g. increase in heat removal by the secondary side in PWR). Thence the category of these events is named as reactivity initiated transients [3]. On the other side reactivity control rod/blade drop accident (RDA) in BWR and reactivity control rod ejection accident (REA) in PWR belong to the category of reactivity initiated accidents due to a sharp increase in reactivity into the reactor core over a short power pulse width [6]. The separation of drive mechanism and control blade leads to RDA in BWR. REA is caused by mechanical failure of the control rod drive mechanism housing (conservative ejection time of 0.1 s for a fully inserted control rod in a German PWR [7]). The induced power pulse during RIA is influenced by the reactor state, the reactivity worth of control rod, the position of control rod, the insertion of control rod in the core, the axial power distribution and the rod burn-up [8]. In general the power pulse can be characterized by width and shape as core-wide parameters and by amplitude as local parameter. Calculations for a hypothetical REA in a German PWR show pulse widths around 30 milliseconds and larger [9]. The amplitude varies over the core because of the strong dependence on the distance from the ejected control rod occurring in large reactor cores, where the reactor point kinetics approach is not valid. It's obvious that the most

affected fuel rods would be located in the neighbourhood of the ejected or dropped control rod [3, 10].

Table 1 – Potential reactivity initiated scenarios in BWR and PWR (taken from [4] and extended by information in [3])

Class of scenario	BWR	PWR
Control system failure	<ul style="list-style-type: none"> ▪ Control rod bank withdrawal 	<ul style="list-style-type: none"> ▪ Control rod bank withdrawal
Control rod (cluster) ejection/drop	<ul style="list-style-type: none"> ▪ Control rod drop due to separation of a control rod blade from its drive mechanism 	<ul style="list-style-type: none"> ▪ Control rod ejection due to mechanical failure of a control rod mechanism housing
Coolant/moderator temperature and void effects	<ul style="list-style-type: none"> ▪ Core coolant flow rate increase ▪ Core coolant temperature reduction (e.g. void collapse due to rapid cooldown) ▪ Steam line valve closure (e.g. void collapse due to overpressurization) 	<ul style="list-style-type: none"> ▪ Increase in heat removal by the secondary side ▪ Steamline break ▪ Transients during operation with positive moderator temperature coefficient
Dilution or removal of coolant/moderator poison	<ul style="list-style-type: none"> ▪ Flushing of boron during ATWS 	<ul style="list-style-type: none"> ▪ Inadvertent poison removal ▪ Injection of diluted accumulator or refuelling water at shutdown ▪ Injection of diluted water after LOCA ▪ Ingress of secondary water after SGTR ▪ Restart of primary coolant pumps with cold/dilute water in loop
Miscellaneous	<ul style="list-style-type: none"> ▪ Misloading fuel assemblies ▪ Transients while reactor is operating in unstable regions ▪ Inadvertent removal of control rods during shutdown 	<ul style="list-style-type: none"> ▪ Misloading fuel assemblies

Depending on the pulse characteristic, the thermal hydraulics conditions and the fuel rod state, the injected energy during RDA or REA can lead to fuel rod failure [11, 12]. Possible failure mechanisms are [3, 6]:

- Pellet cladding mechanical interaction (PCMI) in the low temperature range,
- Ballooning and burst in the high temperature range,
- Disruption during quenching of the cladding embrittled by high temperature oxidation,
- Melting of cladding and of fuel pellets in the high temperature range.

Typically the first failure mode is mainly representative for highly irradiated fuel rods [13]. Fuel rod failure can lead to core un-coolability and even to damages of the reactor pressure

vessel due to water hammers caused by interaction of hot fuel and coolant [3]. Thence the proof of the criteria concerning core coolability and reactivity control (defined on the DiD concept) would be difficult to achieve in this case [14]. To guarantee fuel rod integrity and hence the DiD concept, RIA tests have been performed in research reactors like the CABRI reactor in France [15], NSRR in Japan [16], as well as IGR [17] and BGR [18] in Russia. However, these experiments are only partly representative for the conditions in power reactors (at least for PWR). For example, the pulse width is sometimes very short in the experiments (e.g. BGR test RT-3 with 2.5 ms [3]). Furthermore, the coolant can differ in type of medium (e.g. sodium in the test series REP-Na in the CABRI reactor), in coolant velocity (e.g. stagnant in NSRR for PWR) and in coolant pressure (e.g. atmospheric pressure for PWR). The ongoing OECD CABRI Water Loop Project will provide more representative data for PWR conditions (see section 3.1).

Several fuel rod failure thresholds were defined worldwide, mainly referring to the peak fuel rod enthalpies as a function of burn-up in the RIA in-pile tests (cf. Figure 1). On the one side, a continuous or stepwise decrease in the thresholds is observable with increasing burn-up in Figure 1. This results from NSRR [16] and CABRI [15] tests indicating less resistance to fuel rod failure for highly irradiated fuel rods, caused by a change in the failure mechanism. For example, due to an increased discharge burn-up a so-called high burnup structure (HBS) is developed in the periphery of the pellet - characterized by recrystallized grains, micron-sized porosity and a depletion of fission gas [19] (see section 2.1). Therefore PCMI becomes more important with higher burn-up [3] as the fission gas filled pores in the HBS extend rapidly due to the sharp temperature increase and a more peaked radial temperature profile at the fuel periphery during a RIA [20]. Furthermore highly irradiated claddings feature a thicker oxide layer on the clad surface, concomitant with a higher hydrogen content [15]. On the other side, some of the failure thresholds shown in Figure 1 differ considerably in certain areas. This indicates the need for further research analysing in more detail influences on the fuel rod failure. For example, key phenomena like fuel fragmentation, transient fission gas release (see chapter 4), clad oxide layer thickness and hydrogen uptake [21]. Afterwards more refined failure thresholds should be defined, i.e. depending on oxide layer thickness as NRC proposed in Ref. [22]. In parallel, the modelling in fuel behaviour codes should be improved for increasing the reliability of safety analysis [3].

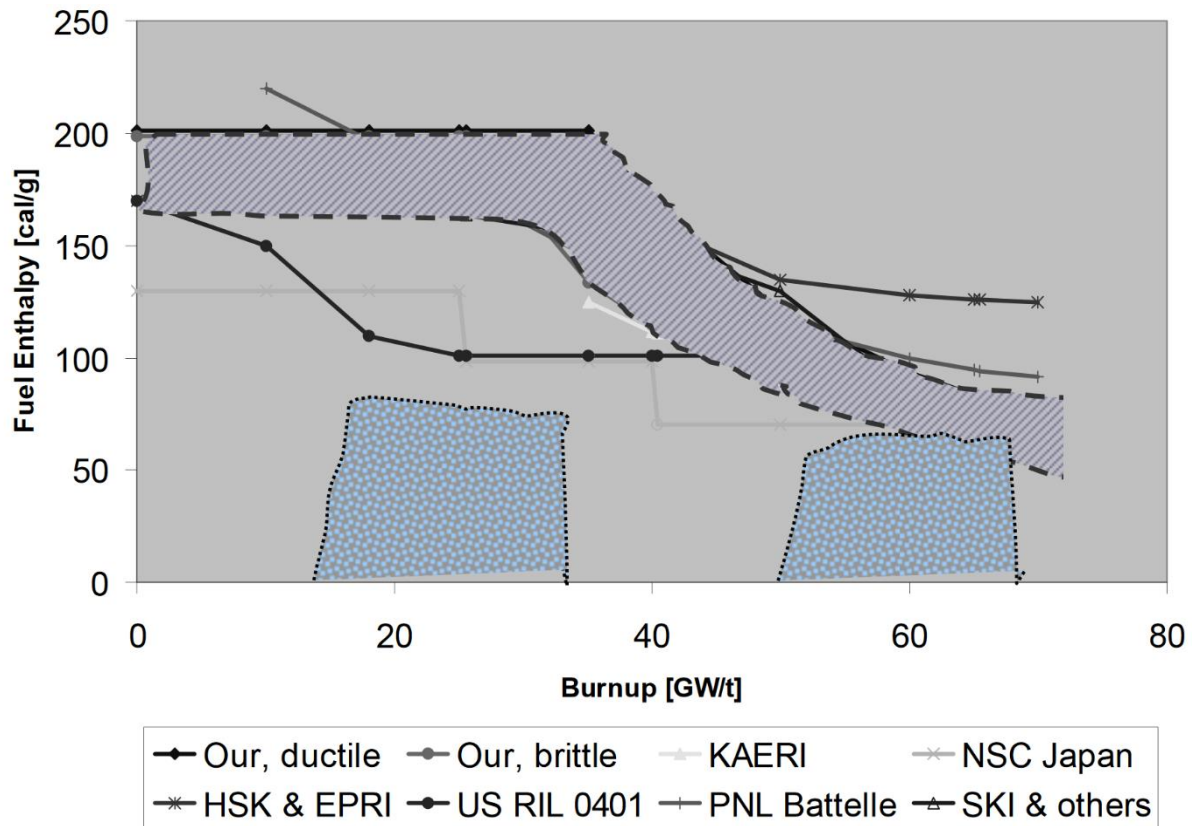


Figure 1: Most thresholds are within the upper shaded area. The two lower shaded zones represent the envelope of conservative calculations for actual PWR cores. As seen, the core enthalpy can exceed the lower failure thresholds – i.e. for cases with large oxidation and brittle cladding. [23]

Today fuel performance codes are widely used worldwide to ensure a reliable check of the safety limits for RIA. Thence an OECD RIA Fuel Codes Benchmark on highly irradiated fuel rods was initiated by the OECD/NEA Working Group on Fuel Safety (WGFS) for comparison of different modelling approaches, further validation of these models and recommendations for future work [24, 25]. A challenge for the numerical methods of fuel performance codes is the sharp increase in injected power, especially for the detailed mechanical modelling in fuel performance codes [26]. Nevertheless, fuel performance codes can handle such conditions and already showed good agreement in several parameters in the OECD benchmark, e.g. in variation of enthalpy and maximum fuel temperature (see chapter 3).

Most of the thermal hydraulics system codes, sub-channel thermal hydraulics codes, reactor dynamics codes and code systems consisting of these codes include more or less simplified fuel behaviour models (see subsection 2.4.3 and chapter 5). Thence the safety analysis of the fuel performance is often carried out in a conservative manner [10]. For example, either

1. Analysis of state-of-the-art fuel behaviour modelling in traditional licensing approaches
 - Selection of the fuel performance code TRANSURANUS after extensive literature and computer code review
 - Analysis of RIA tests in the CABRI reactor in France and NSRR in Japan
 - Participation as first TRANSURANUS user in the OECD RIA Fuel Codes Benchmark on highly irradiated fuel rods (2011/2012)
 - Evaluation of further R&D needs for the development of the RIA version of TRANSURANUS
 - Study regarding the benefits of the high-fidelity simulation tool, i.e. from replacement of the simplified fuel behaviour models in thermal hydraulics system codes, sub-channel thermal hydraulics codes and reactor dynamics codes through online coupling to a modern fuel performance code

2. Simulation of the Xe depletion in the high burnup structure (HBS)
 - Investigation of electron probe microanalysis (EPMA) performed on samples from the High Burnup Rim Project (HBRP) irradiated in the Halden reactor
 - Development of a model describing the matrix Xe depletion in the HBS based on the temperature dependent effective burn-up
 - Integration of this new model in a TRANSURANUS “point version” especially developed for this purpose in a standalone testing environment
 - Application of this new version and fitting of the effective burn-up and its temperature threshold to experimental data of the High Burnup Rim Project (HBRP)
 - Integration of the new standalone Xe depletion model for HBS in the fuel performance code TRANSURANUS

3. Developing of the general TRANSURANUS coupling interface
 - Proof that the fuel performance code TRANSURANUS can fulfil the requirements for successful couplings to thermal hydraulics system codes, sub-channel thermal hydraulics codes, CFD codes and reactor dynamics codes
 - Identification of important features for the development of a general coupling interface

- Implementation of modifications in the source code of TRANSURANUS for coupling applications (under the restriction to apply TRANSURANUS also in standalone mode)
 - Development of the general TRANSURANUS coupling interface organizing the data transfer between TRANSURANUS and the code coupled to TRANSURANUS
4. Core wide safety analysis with great degree in detail in fuel behaviour modelling for a control rod ejection scenario (no occurrence of DNB)
- Restructuring of the DYN3D source code for the “docking” of the new general TRANSURANUS coupling interface
 - Testing of the general coupling interface with the reactor dynamics code DYN3D and hence the new coupled code system DYN3D-TRANSURANUS
 - Application of the two-way coupling approach in the new coupled code system
 - Analysis of differences between DYN3D standalone and the two-way approach (identification of potential fuel behaviour processes relevant in coupled code calculations)
5. Core wide safety analysis with great degree in detail in fuel behaviour modelling for boron dilution transient (occurrence of DNB)
- Analysis of a boron dilution transient carried out in the Rossendorf Coolant Mixing model (ROCOM) facility
 - Application of both the one-way and the two-way coupling approach in the new coupled code system
 - Analysis of differences between the two approaches (“online feedback” from great degree in detail in fuel behaviour modelling)
 - Integration of this coupled code system DYN3D-TRANSURANUS in the tools applied to safety analysis at HZDR

1.3 Thesis outline

Chapter 2 gives a background about the reactivity initiated accident (RIA) as design basis accident (DBA). In this regard ongoing research on highly irradiated fuel rods shows the important role of the high burnup structure (HBS) on the fuel behaviour in such rapid transients. The reactor must be able to sustain a RIA without environmental impact, ensured by a corresponding safety analysis performed with computer codes validated on experiments. Thence an overview is given about state-of-the-art modelling of the fuel behaviour in such codes and code systems. Furthermore, general trends are outlined toward coupled code systems with great degree in detail in fuel behaviour modelling.

Chapter 3 describes shortly the RIA tests and the steps to simulate such experiments with TRANSURANUS. In addition, results and conclusions are presented for the fuel performance code TRANSURANUS based on the OECD RIA Fuel Codes Benchmark in 2011/2012. The version of TRANSURANUS for RIA simulations is still under development, hence its performance is evaluated by participation in international benchmarks. The findings in this benchmark resulted amongst others to the work in the following chapter.

Chapter 4 concerns the improved modelling of the high burnup structure (HBS) in the fuel performance code TRANSURANUS. The HBS is of special interest because it may limit the productive life of fuel and has an important potential effect on fuel behaviour during design basis accidents (DBA) such as RIA. A new model is presented for the Xe depletion from the grains in the HBS.

Chapter 5 presents the newly developed general TRANSURANUS coupling interface applicable to thermal hydraulics system codes, sub-channel thermal hydraulics codes, CFD codes and reactor dynamics codes, which enables the coupling to the fuel performance code TRANSURANUS. The main features of this interface are the application at either fuel assembly level or fuel rod level, one-way or two-way coupling and automatic switching from steady-state to transient conditions in TRANSURANUS. The interface is applicable for various scenarios. The chapter gives also a short description for maintenance and the necessary modifications in the code coupled to TRANSURANUS.

Chapter 6 focuses on the coupled code system DYN3D-TRANSURANUS as first application of the general TRANSURANUS coupling interface. After successful testing two RIA scenarios for a German PWR (Konvoi) were calculated: a control rod ejection scenario, and a boron dilution transient based on experimental data of the ROCOM facility. Firstly, the differences between DYN3D standalone and the two-way coupling approach of DYN3D-TRANSURANUS are analysed. For this purpose, several variants of the code system differing in level of detail in fuel behaviour modelling were used. In addition, the differences between the one-way and two-way coupling approach are discussed.

Chapter 7 summarizes the key results and conclusions found in this PhD thesis.

1.4 Verification and validation

Chapter 3: The RIA version of TRANSURANUS is still under development. For LWR experimental fuel behaviour data are still limited for RIA scenarios, in particular for highly irradiated fuel rods. Furthermore, it's not possible from technical point of view to measure every by a fuel performance code calculated parameter in fuel behaviour experiments, e.g. fuel stress or radial location of the maximum of the fuel temperature. Hence, TRANSURANUS are validated for the RIA test CIP0-1 and verified for the RIA tests CIP0-1 and CIP3-1 in the frame of this thesis (cf. Table 5 and Table 8). This work were performed by participation in the international OECD RIA Fuel Codes Benchmark for highly irradiated fuel rods in 2011/2012.

Chapter 4: The fission gas behaviour in HBS is modelled in the TRANSURANUS fuel performance code assuming its depletion to be dependent on the local burn-up in the HBS. Nevertheless, a scatter still exists in local burn-up values. To improve the modelling, the belonging TRANSURANUS model was extended to the influence of the local temperature by applying a temperature transition zone with related thresholds of a former work. Afterwards it was validated among new experimental data (not measured in the frame of this work). Nevertheless, the upper threshold temperature were in disagreement with the experimental data, e.g. due to partly unknown irradiation histories in the former work (see subsection 4.3.2). Hence, the temperature threshold was newly validated on the new and more detailed

experimental data (see subsection 4.3.2). Furthermore, the impact of Xe yield was verified at the end of this thesis (see subsection 4.3.3).

Chapter 6: Comprehensive verification work is presented in this chapter for the two RIA scenarios CR ejection event and boron dilution transient for the coupled code system DYN3D-TRANSURANUS. The differences between DYN3D standalone and the two-way coupling approach of DYN3D-TRANSURANUS are verified and analysed in the first RIA scenario (see subsection 6.4.2). For that purpose, several variants of the code system differing in level of detail in fuel behaviour modelling were used. In addition, the differences between one-way and two-way coupling approach are verified and discussed in the second scenario (see subsection 6.4.3). According to both scenarios, a German PWR Konvoi Design was applied for the verification.

Developers and users have been calculating and verifying these both RIA scenarios for more than one decade with DYN3D standalone. In parallel they conducted validation work for the models of DYN3D standalone. Hence this former works allows this kind of verification in the thesis. Furthermore, it allows to draw conclusions for the impact of a great degree in online fuel behaviour modelling on the thermal hydraulics and neutron kinetics behaviour.

Integral data of the design basis accident RIA would be needed to also validate the coupled code system DYN3D-TRANSURANUS. Both verified RIA scenarios didn't occur in power reactors in the past. Hence integral data didn't exist to validate both the modelling of neutron kinetics, thermal hydraulics and detailed fuel rod behavior in once and the overall interaction between them in the frame of this thesis.

2 Literature review

2.1 Characteristics of the high burnup structure (HBS)

The discharge burn-ups in power reactors increased over the last few decades. Because the highest burn-ups are achieved in the fuel pellet periphery caused by the fuel self-shielding effect [27], a so-called high burnup structure (HBS) occurs in the periphery of the fuel pellets [28, 29]. Due to the location at the pellet periphery this restructured fuel region is often named as rim. Nevertheless, this denotation can be misleading (see section 4). The restructuring of the fuel matrix at higher burn-up was already observed in studies for the uranium bearing fuel in naval reactors in the 1950's [30]. The HBS is of special interest because it may limit the productive life of nuclear fuel [31] and can have an important effect on the fuel behaviour during design basis accidents (DBA) [3]. The following main characteristics are representative for the HBS (cf. Figure 3):

- Recrystallized grains of 50-200 nm [32]
- Development of micron-sized porosity surrounded by recrystallized grains [33]
- Depletion of fission gas from the fuel matrix into the HBS pores [27]

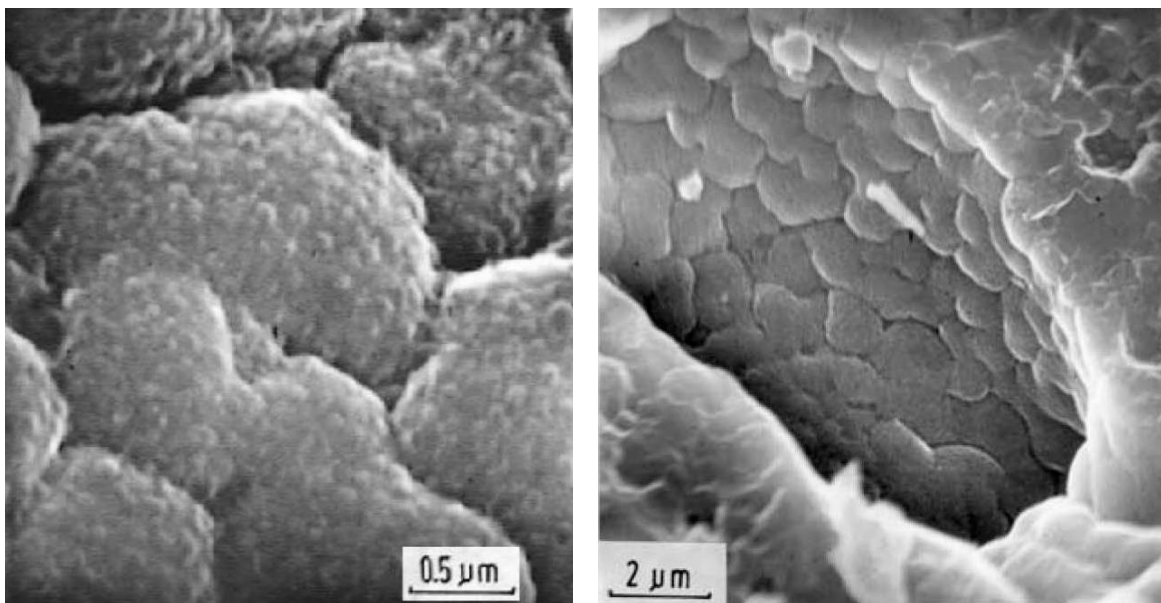


Figure 3: SEM images of the high burnup structure (HBS). Left, subdivided grains due to restructuring; right, view in a HBS pore surrounded by subdivided grains [33]

The related processes seem to occur at different points in time. Barner et al. observed first the depletion of fission gas from the fuel matrix measured by electron probe microanalysis

(EPMA) which was followed afterwards by recrystallization of the grains and finally by the development of HBS porosity as seen with optical microscopy [34]. Therefore, the HBS thickness measured by EPMA adopted larger values compared to optical microscopy. However, it may be difficult with optical devices to define an exact onset of grain recrystallization and development of pores.

The HBS formation, the onset of restructuring and the behaviour of HBS still need to be understood in better detail [35]. For example, different approaches are outlined and summarized for the formation mechanism in Ref. [36]:

- The forces due to lattice strain caused by increase in irradiation damages and/or enclosure of fission products are assumed to be an important factor driving the formation of the HBS. Alternatively Rest and Hofman explained this lattice strain by diffusion of fission products to dislocations [37]. Due to increase of lattice strain with burn-up high enough values are assumed to be achievable for formation of new grain boundaries.
- Thomas et al. postulated a formation driven by forces resulting from stored energy in fission products and nano-sized pressurized bubbles [38].

Spino et al. found reasons pro and contra for the proposed formation mechanisms [29]. Corresponding to the mechanism based on the lattice strain this would lead to a high number of subgrain boundaries in restructured regions in the first stage, which should be decorated with pores due to filling up with fission gas in a later stage. However, Spino couldn't observe recrystallized regions without pore decoration in his studies. Thence restructured regions of the first stage weren't found by Spino. Maybe the diffusion process proceeds very quickly due to the reduced diffusion length in recrystallized grains. Regarding to the stored energy mechanism, Spino et al. found high fracture toughness in restructured fuel. Thence, irradiated fuel seems to be not brittle. Based on this finding Spino et al. introduced the idea of creep induced recrystallization around locations with high pressure. In general Spino et al. pointed out the importance of further work for clarification.

The threshold for restructuring represents another open question. More precisely, a scatter in measured local Xe concentrations over local burn-ups still exists [27] (see section 4.2). Recently Baron et al. concluded that the HBS transformation mainly depends on the local

burn-up, while secondary effects arise from local temperature, instantaneous fission density, local density of fission products, initial grain size, local fuel constraint, initial additives and local oxygen potential [39]. Regarding the future, a detailed understanding is needed for accurate conclusions about safety limits for highly irradiated fuel rods. Thence highly enriched U^{235} fuel discs were irradiated under different secondary effect conditions like temperature and strain in the Halden reactor, mainly in the frame of the High Burnup Rim Project (HBRP) [40] and the Nuclear Fuel Industry Research (NFIR) program [41].

Furthermore, the HBS seems to have an important influence on the fuel behaviour during DBA [3] (see section 2.2 and chapter 3). Therefore another open issue is associated with a better understanding of the microstructure evolution, behaviour and impact of HBS on the fuel rod behaviour under transient conditions [13, 42]. In this context Wiesenack mentioned the need of detailed fuel behaviour modelling describing the fuel fragmentation and cracking in high burn-up fuel, which seems to be affected by the fission gas in HBS [43]. Today the (transient) fission gas release modelling isn't accurate enough for a reliable, high prediction of the experimental data, e.g. performed by the OECD Halden Reactor Project or by Hiernaut on high burn-up samples at JRC-ITU [44].

2.2 Fuel rod behaviour and cladding failure during RIA

The fuel behaviour under RIA depends strongly on power pulse characteristics, reactor state, coolant conditions and fuel rod state at the beginning of the transient [3, 6]. Fast RIA transients like control rod drop/ejection (cf. Table 1) can lead to sharp energy injection followed by prompt increase in fuel temperature. This can cause a rapid fuel volume expansion due to both solid thermal expansion and – becoming important with increase in burn-up – gaseous swelling. This can result in further complex and interacting fuel rod phenomena and eventually to cladding failure (cf. Figure 4). For RIA several cladding failure mechanisms are known:

- PCMI as low temperature failure in the early phase (Pre-DNB)
- Ballooning and burst as high temperature failure in the late phase (Post-DNB)
- Disruption during quenching of the cladding embrittled by high temperature oxidation in the late phase (Post-DNB)

- Melting of cladding and of fuel pellets as high temperature failure

The probability of these cladding failure mechanisms is affected by the discharged burn-up, i.e. through the occurrence of HBS. Cladding failure should be avoided because it can lead to damage of the reactor pressure vessel due to water hammers caused by thermal interaction of (molten) fuel fragments with the coolant (cf. post-failure events in Figure 4).

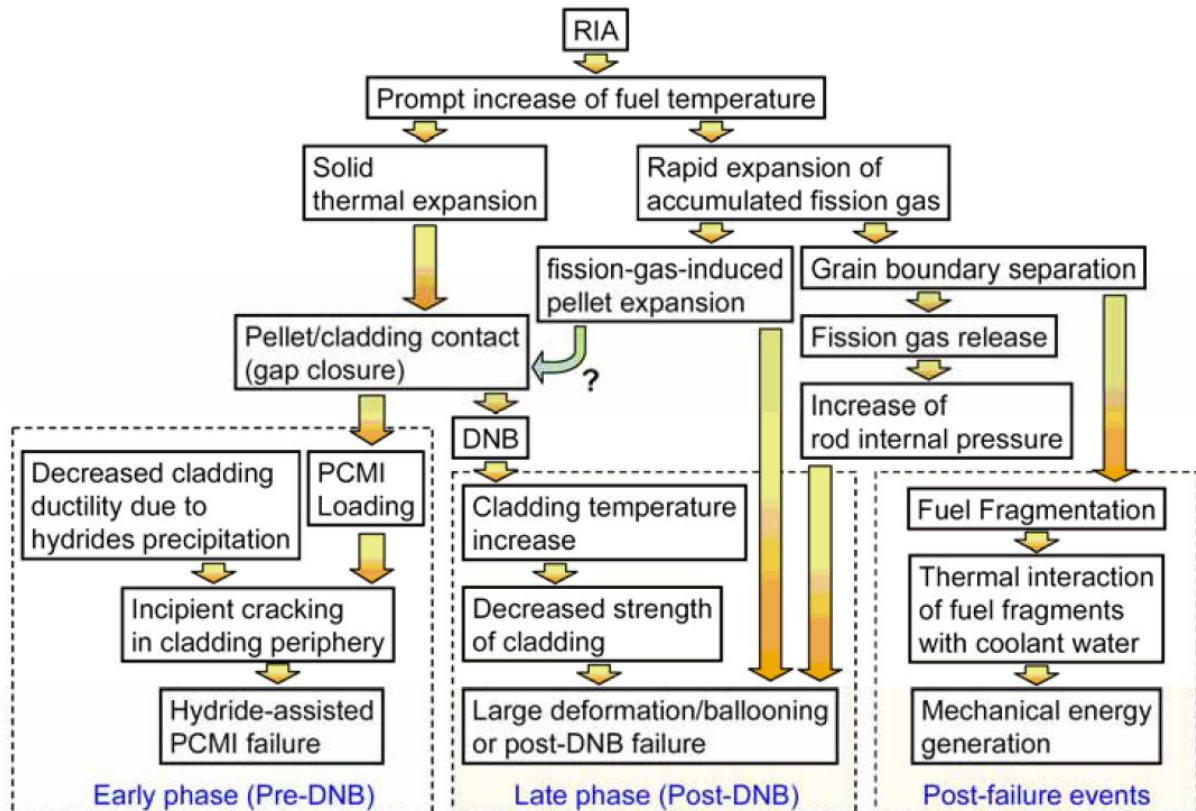


Figure 4: Possible mechanisms for fuel and cladding damage under RIA [45]

2.2.1 Early phase during RIA (Pre-DNB)

Solid thermal expansion and gaseous swelling can occur through high energy injection under RIA. Assuming isotropic plasticity, an equal biaxial tension is imposed on the cladding causing PCMI [13] and potentially followed to cladding failure (cf. Figure 5) [3]. The PCMI failure mode represents a low temperature failure because the clad temperature and hence the cladding ductility are low in the early phase [6]. Furthermore, this failure mode is only relevant for highly irradiated fuel rods. On the one hand, the expansion caused by gaseous swelling is higher due to the HBS porosity (see section 2.1) containing fission gas which

expands rapidly with the fuel temperature rise. This effect is enforced by a quasi adiabatic fuel heating. Thence the radial temperature profile can be peaked temporarily at the fuel pellet periphery decorated with HBS pores (see chapter 3) [24, 25]. In addition the pellet-cladding gap is closed in highly irradiated rods, even a bonding layer can exist between fuel and cladding [46]. Therefore, a high cladding loading can result already from less relative fuel expansion in highly irradiated fuel rods compared to fresh fuel. On the other side, the cladding material properties change in the reactor with increase in burn-up, e.g. outer oxide layer (around 80 to 90 μm for Zry-4 cladding irradiated up to 60 MWd/kgHM) and content of hydrogen (around 700 to 800 ppm for Zry-4 cladding irradiated up to 60 MWd/kgHM) [15]. Both effects can weaken the cladding, especially through the formation of zirconium hydrides.

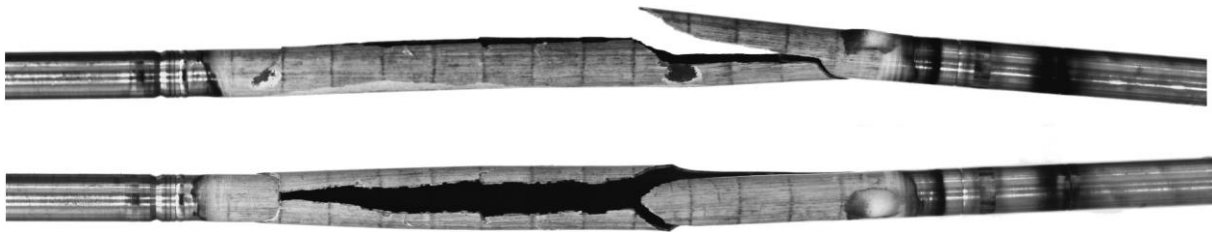


Figure 5: PCMI failure mode observed in the NSRR test VA-1 (PWR, 71 MWd/kgU, cladding ZIRLO™) [47]

2.2.2 Late phase during RIA (Post-DNB)

In the late phase cladding failure can be caused by both ballooning and disruption of the cladding during quenching. The kind of failure mode depends on fuel rod design and coolant conditions. Both failure modes are mainly limited to fresh and low burn-up fuel rods in today's standard fuel loading patterns [3]. The clad-to-coolant heat transfer is already developed in this late phase (larger time constant than for the pulse injection of energy), hence the clad temperature is higher which increases the cladding ductility (in case of high heat transfer). Thence the PCMI failure mode (cf. Figure 5) cannot be observed in the late phase during RIA. High clad and fuel temperatures lead to an increase in the inner rod pressure during this late phase. In addition, the HBS pores were shown to be mainly open after the CABRI sodium test REPNa 5 [5] and fission gas could be released from the HBS pores into the plenum. Before the transient a large amount of fission gas is expected to be held in the HBS pores. Therefore additional fuel rod pressure increase is expected from the (significant)

transient fission gas release, e.g. confirmed by 21.6 % in the mixed oxide (MOX) fuel test REPNa 6 [48].

If the inner rod pressure exceeds the coolant pressure in this high temperature phase, ballooning will take place due to creep [3, 49]. The maximal outward ballooning depends on cladding material state, pressure difference and temperature history. Measurements of the cladding hoop strain showed values of up to 123 % [50], limited to 25 % for pre-irradiated rods [3]. The ballooning leads to a thinning of the cladding. At the end the cladding can collapse both in axial and radial direction. The second potential failure mechanism appears during quenching [50]. The cladding can be brittle due to high temperature oxidation on the inner and outer clad surface (in case of clad temperatures > 1000 K in the late phase). The cladding can disrupt during quenching, if the rupture stress is exceeded.

According to the late phase the clad-to-coolant heat transfer itself is of major interest due to its strong impact on the clad temperature and hence cladding failure caused by ballooning and high temperature oxidation [51]. The boiling crisis mechanism differs between transient and steady-state conditions (cf. Figure 6). During a RIA transient a considerable number of nucleation sites can be activated due to rapid energy injection in the fuel rod and delay time of the clad-to-coolant heat transfer. This leads to a high heat flux observable in NSRR tests as temperature plateau, until coalescence of bubbles causing the boiling crises [52]. Both coolant velocity and subcooling influence the clad-to-coolant heat transfer under RIA. More precisely, NSRR tests on fresh PWR fuel showed a decrease in peak clad temperature and in duration of film boiling with increase in flow velocity and subcooling [53]. Especially the subcooling can have a strong impact on the duration of film boiling. With regard to highly irradiated fuel rods no in-pile tests were performed hitherto with representative coolant conditions for hot zero power (HZP) which is the conservative scenario in most PWRs. Therefore, the planned tests in the OECD CABRI Water Loop Project will provide important experimental data for deeper analysis in the future.

Because the NSRR tests in the 1980's were conducted under pool conditions (stagnant water, atmospheric pressure, room temperature), IRSN, EDF and CEA initiated together the out-of-pile PATRICIA experiments in France for both HZP in PWR (15 MPa, 553 K, 4 m/s) and NSRR pool conditions [51]. The temperature rates amounted 2200 K to 4900 K/s (HZP in PWR, 30 ms FWHM) and 6000 K/s to 12000 K/s (NSRR pool conditions, 5 ms FWHM).

Typical values of critical heat flux (CHF), critical surface temperature and film-boiling heat flux measured in PATRICIA are summarized in Table 2. The transient CHF values are greater than under steady-state condition in the PATRICIA tests, even up to a factor of ten/twelve for NSRR conditions [54]. This is confirmed by the different boiling crises mechanisms shown in Figure 6. The experimental uncertainty in measured CHF was estimated up to $\pm 50\%$, caused by the sharp temperature increase.

Table 2 – Values of critical heat flux, critical surface temperature and film-boiling heat flux measured in PATRICIA tests under steady-state conditions and RIA-like transients [3, 51, 55]

Measured parameter	PWR		NSRR	
	Steady-state	Transient	Steady-state	Transient
Critical heat flux [MWm^{-2}]	3	4-6	1	12
Critical temperature [K]	630	670	400	470-570
Film-boiling heat flux [MWm^{-2}]	3	1-2	0.2	1-5

Furthermore oxide spallation (break away) as observed in the REPNa 1 test in the CABRI sodium loop is assumed to reduce the clad-to-coolant heat transfer due to lower surface roughness [15, 56]. Thus the clad temperature of the bare metal surface may rise to much higher values than of cladding with an oxide layer [3]. Thence plasticity effects and high temperature oxidation might occur as local phenomena. However, the cause of the early failure in the REPNa 1 test (failure enthalpy: 117-150 J/g) and whether this test is representative are investigated by an international task force [15]. In addition, oxide spallation was only observed in tests conducted in the sodium loop of the CABRI reactor. Therefore it is unclear whether oxide spallation is likely for light water reactors, too [3].

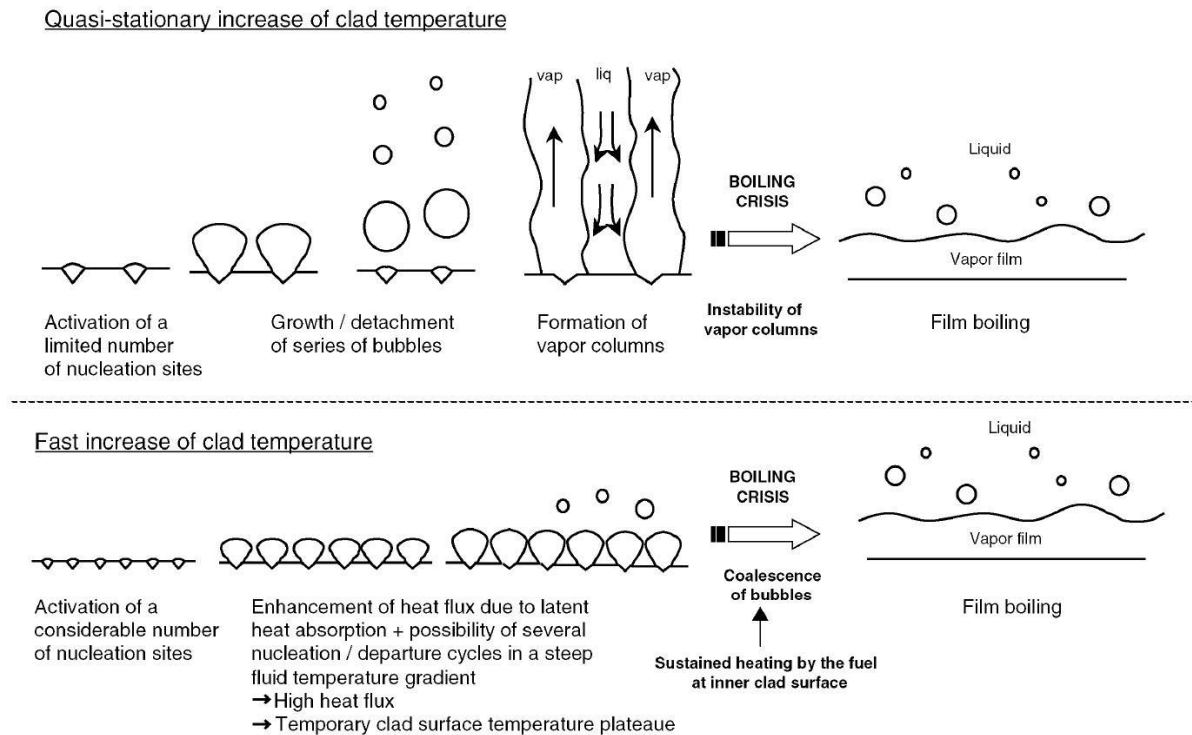


Figure 6: Boiling crisis mechanism in stationary and transient conditions (based on visual observation in NSRR tests performed under subcooled pool boiling conditions) [54]

2.3 State-of-the-art modelling in fuel performance codes for RIA

Worldwide fuel performance codes are widely in use by safety authorities, research institutions, utilities and vendors to proof the conservation of the safety limits for fuel rods [57], e.g. in case of RIA [24] (see section 1.1). Features of fuel performance codes applied by a larger number of users are listed in Table 3 [3]. Additional code features and further fuel performance codes are described in Ref. [24, 25]. This section focuses on the range of application as well as state of thermal and mechanical analysis in 1D, 1½D and 2D fuel performance codes (geometrical representation, clad tube representation, pellet-clad contact modelling). Furthermore, recent and future developments are described for the RIA version of TRANSURANUS. More precisely, gaseous fuel swelling, transient fission gas release, specific clad properties for RIA, cladding failure criterion for RIA and plenum temperature (see chapter 3).

Table 3 – (Transient) fuel performance codes applicable to RIA taken from Ref. [3]

	FALCON MOD-01	FRAPTRAN Version 1.3	SCANAIR Version 3.2	TRANSURANUS v1m1j96	RANNS Version 1
Maintaining organization	EPRI, USA	PNNL, USA	IRSN, France	JRC-ITU, Germany	JAEA, Japan
Range of application	Transients, steady-state	Transients only	Transients only	Transients, steady-state	Transients only
Geometrical representation	2D	1D	1½D ¹	1½D	1½D (2D ²)
Clad tube representation	Thick wall	Thin shell	Thick wall	Thick wall	Thick wall
Pellet-clad contact modelling	Frictional sliding	Axial sticking	Axial sticking	Frictional sliding [or axial sticking]	Frictional sliding
Fission gas release model	NRO-MT	None	RIA	NRO-MT	NRO-MT and RIA
Fuel gaseous swelling model	Steady-state only	No	Transient only	Steady-state only	Steady-state only
Cladding failure criterion for RIA	Strain energy density	Hoop strain	Nonlinear fracture mechanics	No	Linear fracture mechanics

NRO-MT: Model for normal reactor operation and mild transients.

RIA: Specific model for reactivity initiated accidents

¹Pellet-clad contact modelling assumes a perfect sticking compared to the other 1½D fuel performance codes [24] (see subsection 2.3.4).

²In RANNS, an optional 2D local model for detailed PCMI analyses can be applied to an axial segment that corresponds to the length of half a pellet [58].

2.3.1 Range of application

A few fuel performance codes in Table 3 are only applicable to transients/DBA like LOCA and RIA, other codes are validated for the whole range associated with normal operation, operational transients and transients/DBA. For codes of the first category, the initial fuel rod state at the end of the pre-irradiation/beginning of DBA has to be provided as input data. Thence these fuel rod characteristics have to be calculated by another fuel performance code capable to cope with steady-state conditions. Especially highly irradiated fuel rods can differ considerably in characteristics compared to fresh fuel, e.g. in power density profile due to radial burn-up profile in the fuel pellet or in gap width due to deformation of both fuel and cladding [3]. If the code application range contains both steady-state and transient, the fuel behaviour can be calculated by the same code in all stages/phases. This possibility represents

a consistent approach because the transfer of numerous parameters between two fuel performance codes such as the local stress state, the local fission gas amount in grains, in HBS pores and on grain boundaries might be difficult to handle. However, the “influence of the initial state of the fuel on the behaviour during RIA is difficult to assess.” [24] More experiences and computer simulations are needed to verify this influence. This might also be of interest for state-of-the-art LOCA analysis [59].

2.3.2 Geometrical representation

The fuel rod geometry can be modelled as 1D approach, quasi 2D (1½D) approach or 2D approach (cf. Table 3).

According to the 1D and quasi 2D (1½D) approaches the fuel rod is divided axially in (hollow²) cylindrical segments (cf. Figure 10 and Figure 11 in see chapter 3). TRANSURANUS discretises radially each of these axial segments in cylindrical rings (so-called coarse zones). Furthermore, each coarse zone consists of cylindrical rings (so-called fine zones). Material properties like the elasticity modulus are assumed to be constant inside a coarse zone. The mechanical formulations are based on the assumptions of plane strain and rotational symmetry in 1D and quasi 2D approaches. Regarding the thermal analysis the one dimensional energy equation is solved radially for the fuel pellet, the cladding and the surrounding structure, e.g. in TRANSURANUS [60]:

$$c\rho \frac{\partial T}{\partial t} = \frac{1}{r} \frac{\partial}{\partial r} \left(\lambda r \frac{\partial T}{\partial r} \right) + q''' \quad (2)$$

where c is the specific heat capacity expressed in $\frac{J}{kgK}$, ρ the density in $\frac{kg}{m^3}$, T the temperature in K , λ the thermal conductivity in $\frac{W}{mK}$, q''' the power density in $\frac{W}{m^3}$, t the time in s , and r the radius in m .

The mechanical analysis refers to “the principal conditions of equilibrium and compatibility together with constitutive relations” [60] which are formulated in axial, radial and tangential direction. For example, TRANSURANUS applies as constitutive relation the Hooke’s law in its differential form in three dimensions [61]:

² Hollow pellets are applied to the previous VVER fuel pellet design and to pellets owning central thermocouple.

$$\{d\sigma\} = [D]^{-1}\{d\varepsilon^{el}\} + [dD]^{-1}\{\varepsilon^{el}\} \quad (3)$$

where $\{d\sigma\}$ is the column vector of the change in stress consisting of an axial component ($d\sigma_a$), a radial component ($d\sigma_r$) and a tangential component ($d\sigma_t$) expressed in $\frac{N}{m^2s}$, the column vector of elastic strain $\{\varepsilon^{el}\}$ including also an axial component (ε_a^{el}), a radial component (ε_r^{el}) and a tangential component (ε_t^{el}) as well as its change $\{d\varepsilon^{el}\}$, the matrix $[D]$ containing the components of the elastic constants $\left[\frac{N}{m^2s}\right]$ assumed as isotropic and constant inside a coarse zone in TRANSURANUS as well as its change $[dD]$. The column vector of elastic strain $\{\varepsilon^{el}\}$ in eq. (3) can be determined by means of a semianalytical solution as follows:

$$\{\varepsilon^{el}\} = \{\varepsilon^{tot}\} - \{\varepsilon^{ex}\} \quad (4)$$

where $\{\varepsilon^{tot}\}$ is the column vector of the total strain and $\{\varepsilon^{ex}\}$ represents the column vector of the sum of inelastic strains. The change of inelastic strain $\{d\varepsilon^{ex}\}$ is assumed to be a superposition of all strains excluding the elastic strain [61]:

$$\{d\varepsilon^{ex}\} = \{d\varepsilon^{cr}\} + \{d\varepsilon^{pl}\} + \{d\varepsilon^s\} + \{d\varepsilon^{th}\} + \{d\varepsilon^f\} + \{d\varepsilon^{sin}\} \quad (5)$$

where the subscript *cr* symbolizes creep, *pl* instantaneous plastic, *s* both solid and gaseous swelling, *th* thermal, *f* crack strain, and *sin* hot-pressing. Each inelastic strain component is described by a correlation in TRANSURANUS. Eq. (5) is related to the description of the fuel and not all components are relevant for the inelastic strain $\{\varepsilon^{ex}\}$ of the cladding.

Furthermore, to solve eq. (4) Lassmann derived the components of $\{\varepsilon^{tot}\}$ based on the compatibility equations under axisymmetric and plane boundary conditions neglecting the quadratic terms:

$$\begin{aligned} \varepsilon_r^{tot} &= \frac{du}{dR} \\ \varepsilon_t^{tot} &= \frac{u}{R} \\ \varepsilon_a^{tot} &= \text{const} \end{aligned} \quad (6)$$

where ε_a^{tot} , ε_r^{tot} and ε_t^{tot} are the total strains in axial, radial and tangential direction. R represents the radius of the deformed geometry defined as $R = r_{ref} + u$, whereas r_{ref} represents the radius of the reference geometry and u the radial deformation. Assuming a

constant ε_a^{tot} along the radius is the main difference compared to 2D approaches. To close the set of equations, the equation of equilibrium in the radial equation is the last missing information for performing the mechanical analysis [61]:

$$\frac{d\sigma_r}{dR} - \frac{\sigma_r - \sigma_t}{R} = 0 \quad (7)$$

According to the 2D approach as applied by FALCON (cf. Table 3), the fuel rod geometry is solved on the basis of a finite-element numerical structure. The fuel performance code FALCON offers two modes for this approach [62]. On the one side, the 2D R-Z plane spatial model contains a fully axially and radially coupled approach assuming axisymmetric conditions. The main difference compared to 1D and quasi 2D (1½D) approaches is the solution of the equilibrium and compatibility equations in the considered element/zone taking into account also states in stress and strain of axial neighbored elements/zones. Because the axial strain isn't set constant over the radius (as e.g. in the 1.5D approach applied in TRANSURANUS), phenomena like hourglass pellet shape can be simulated. On the other side, the 2D R- Θ plane spatial model featuring a fully radial and azimuthal coupling can be applied to a cross section of a fuel rod. This second 2D mode was developed for local analysis of cracking and pellet clad interaction (PCI) in FRAPCON [62].

To take benefit from the decreasing computational costs, recently multidimensional multiphysics tools were developed. One of them is the 3D code BISON maintained by Idaho National Laboratory (INL) [63], another one is named ALCYONE developed by CEA [64]. For example, BISON includes “fully-coupled partial differential equations for energy, species and momentum conservation” [63]. To solve this system of equations on two or three-dimensional meshes (allowing higher order geometry) the INL Multiphysics Object Oriented Simulation Environment (MOOSE) [65] is applied. Due to a fine and multidimensional mesh high resolutions and 3D phenomena can be modelled, e.g. hourglass pellet shape, missing pellet surface, fuel cracking, eccentric position of the fuel stack in the fuel rod and influence of pellet chamfer on the cladding creep down during irradiation. However, one should be kept in mind that today's post irradiation examinations (PIE) provide mainly one or two dimensional data, e.g. SEM, TEM, EPMA and SIMS [66-68]. Thence the validation of 3D modelling is a challenge. Nevertheless, 3D codes give the opportunity to model, analyse and understand in more detail local effects in the fuel and the surrounded cladding. The findings

might also be useful for a more accurate modelling in 1D, quasi 2D (1½D) and 2D fuel performance codes (e.g. improvement of approximations).

2.3.3 Clad tube representation

In Table 3 FRAPTRAN represents the only fuel performance code modelling the cladding as thin shell (one zone). The clad temperature, stress, strain and material properties are assumed to be constant/uniform over the clad thickness in FRAPTRAN [69], i.e. the cladding stress of a cross section is like the mid-wall value taking into account the inner and outer pressure on the cladding. Nevertheless uniform conditions in the cladding “is hardly the case in reactivity-initiated accident” [3]. This is obvious from the sharp increase in temperatures, leading to large values in the periphery of highly irradiated pellets [58] (see chapter 3). For example, Figure 7 shows high differences between inner and outer clad temperature for the NSRR RIA test FK-10 [3, 70]. Both a high temperature gradient and a thin cladding can result in high thermal stresses over the cladding thickness. Therefore, all other fuel performance codes in Table 3 model the clad as a thick wall. A further advantage of this approach is the opportunity to take into account processes limited to one cladding surface only or that differ between the inner and outer cladding surface, e.g. oxidation, hydrogen uptake, and chemical processes due to bonding between fuel and cladding.

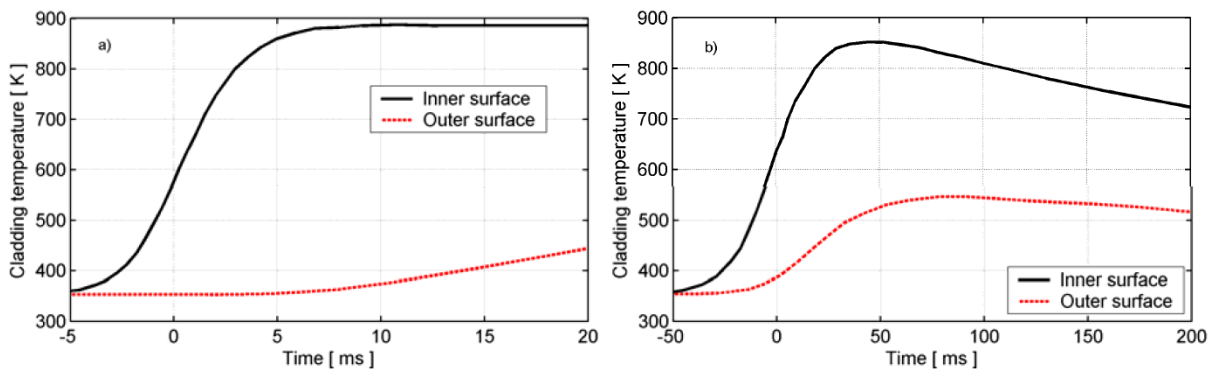


Figure 7: Clad inner and outer temperatures calculated by the Japanese fuel performance code RANNS for the NSRR RIA test FK-10 (peak power at 0 s). Left, experimental pulse width of 5.2 ms; right, larger pulse of 40 ms. [3, 70]

2.3.4 Pellet-clad contact modelling

Axial friction forces F_l between fuel and cladding are taken into account additionally in 1½D fuel performance codes, compared to 1D approaches (cf. Table 3). The 1½D fuel performance code SCANAIR is one exception because “the contact between the pellet and the clad assumes a perfect sticking” [24]³. Lassmann postulated that neglecting friction forces might lead to “major errors” [61]. Of course no friction forces are expected in fresh fuel due to an open gap (at least during normal operation). Due to fuel swelling and cladding creep down fuel rods of low and medium burn-up are expected to be modelled more reliable taking into account friction forces [3]. Finally, for highly irradiated fuel rods good simulation results were observed in the OECD RIA Fuel Codes Benchmark assuming axial perfect sticking between fuel and cladding [24, 25] (see chapter 3). This assumption refers to the bonding layer between the fuel and the cladding in case of high burn-up conditions [71].

To allow high flexibility, the fuel performance code TRANSURANUS can model the pellet-clad contact both in 1D and 1½D (quasi 2D) [60]:

- 1) Friction forces are neglected, whereas a local no-slip condition is applied.
- 2) Friction forces are neglected, whereas a slip condition is applied.
- 3) Friction forces are taken into account.

In the first approach, the local no-slip condition means an identical axial deformation ε_a^{tot} of fuel and cladding when they are in contact. Thence fuel and cladding are modelled as a unique structure for closed gap conditions (perfect axial sticking between fuel and cladding). According to the slip condition, fuel and cladding are modelled separately considering the radial contact as external force. Therefore, fuel and cladding deformations differ. The third approach takes into account the friction forces F_l in the analysis. After convergence of the thermal and mechanical solution in each axial segment, F_l is calculated for coupling the axial segments. This two-step process is iterated up to fulfilment of the convergence criteria for the friction: limited changes in F_l , identical axial deformation ε_a^{tot} of the fuel and cladding, and F_l lower than the adhesion forces. Because for each iteration loop the thermal and mechanical

³ In case of SCANAIR 1½D means strong coupling of thermal and thermal hydraulics solving (first iteration loop) as well as fission gas behavior module and mechanical solving (second iteration loop). However even if the fuel performance code TRANSURANUS model the pellet-clad contact in 1D, the thermal hydraulics (if calculated by the code), thermal behavior, mechanical behavior and fission gas behavior are still strongly coupled.

equations have to be solved again in each axial segment [61], computational costs can rise, especially under transient conditions.

2.3.5 Ongoing model developments regarding TRANSURANUS

TRANSURANUS [60] is applicable to both steady-state and transient conditions ranging from operational transients to DBA (cf. Table 3). One decade ago the TRANSURANUS code was successfully extended to LOCA as DBA [26]. As observable in Table 3 the fuel code's features provide also a basis for its successful extension to RIA conditions. Another advantageous feature is the quick and stable numerical behaviour [60]. The potential for a RIA version is confirmed by earlier work performed by Lassmann. He implemented a point kinetics model (as alternative to the specification of the linear heat rate in the input) for a RIA. Nevertheless, in order to apply TRANSURANUS to RIA conditions, several models have either to be extended or newly developed for the RIA version of TRANSURANUS:

- *Gaseous fuel swelling*: PCMI becomes more important during a RIA with higher burn-up [3] as the fission gas filled pores in the HBS extend rapidly due to a sharp temperature increase and peaked radial temperature profile at the fuel periphery (see section 2.1 and subsection 2.2.1). Thence Van Uffelen et al. pointed out the need to evaluate and extend the thermal expansion model in TRANSURANUS for highly irradiated fuel rods under such conditions [26]. This means also a more precise modelling of the fuel conditions before the transient, e.g. the fuel porosity, pore size distribution, and amount of fission gas in the grains and HBS pores affected by depletion [35, 39]. For this purpose, recently a temperature dependent effective burn-up [27] was introduced in the code taking into account the inhibition of the HBS formation due to defect annealing above a certain temperature (see section 4.2). Good agreement was found between this model and experimental results for the temperature threshold between unstructured and restructured fuel [20]. Afterwards Holt et al. applied their model to the Xe depletion performing a sensitivity study analysing the scatter in experimental data of Xe depletion. In the future this work will be extended by means of a more detailed description of the HBS porosity development and its pore size distribution in TRANSURANUS. At the end this should lead to a new model for

gaseous swelling under RIA conditions, leading to a more accurate determination of PCMI.

- *Transient fission gas release:* High fission gas release was measured in PIE carried out on fuel rods withstanding a RIA transient (see section 2.2) [3]. Lemoine mentioned the need to understand in more detail the release processes of fission gas located on grain boundaries and in HBS pores [5]. According to TRANSURANUS, on the one side, a burst release model related to grain boundary bubbles is under development based on micro-cracking [72]. On the other side, an empirical burst release model associated to the HBS porosity was introduced, which determines the temperature dependent fission gas release [73, 74]. The latter work is based on former modelling of Győri and Blair for LOCA [75, 76]. The user can actually choose to apply this model during LOCA. In the future this model will be extended to the more rapid conditions under RIA. However, the fission gas release under accident condition is more complex than described in the model. For example, it depends also on temperature rate and stress state in addition to the temperature. The stress state seems also to be relevant for fuel fragmentation, which can be correlated to fission gas release [42]. Additional experimental data has to be created in order to be able to consider these dependences.
- *Temperature in the plenum:* Today the lower and upper plenum temperatures are modelled in a simplified manner in fuel performance codes. According to the low temperature approximation in the TRANSURANUS code, the plenum temperature is set to the clad inner temperature of the considered plenum section. For the high temperature approximation, an average value of the clad inner temperature in the plenum section and the fuel temperature of the outer free surface cross section of the fuel stack represents the plenum temperature. A 2D model, assuming adiabatic conditions at the symmetry plane, is under development by Győri to describe more accurately the plenum temperatures [77]. Preliminary results for LOCA showed the influence of plenum temperature differences on the permanent tangential strain.
- *Material properties and failure criteria for cladding:* A reliable modelling of the cladding deformation is of high importance. Today no specific material properties and cladding failure criteria are included in TRANSURANUS for RIA. On the one side,

the cladding behaviour will strongly influence the stress state in the fuel, if the fuel is in contact with the cladding. Accordingly, the stress state in the fuel seems to have an important impact on the fragmentation and the burst release [78]. Thence corresponding material properties for the cladding behaviour under RIA should be built in, i.e. oriented on Ref. [79] and experiments summarized in Ref. [80]. A suitable modelling should take into account the mechanical behaviour in both the low and high temperature phase (see section 2.2). The hydrogen uptake might also play a role [22]. Nevertheless, advanced cladding materials like M5[®] (AREVA) and Optimized Zirlo[™] (Westinghouse Electric) feature low hydrogen pick up rates [81]. On the other side, the implementation and validation of a suitable cladding failure criterion represents another important milestone. The criterion modelling depends on the mechanic model in the fuel performance code, hence the material properties. Today different approaches are applied for the fuel rod failure prediction under RIA (cf. Table 3), validated on in-pile and/or out-of-pile tests.

As far as RIA is concerned, the performance of TRANSURANUS was already evaluated in international benchmarks like FUMEX-III organized by IAEA [57] and the OECD RIA Fuel Codes Benchmark [24, 25] (see chapter 3). Nevertheless, the number of validation cases are limited for RIA, compared to the code SCANAIR maintained by IRSN [82] (see subsection 3.3.1). Thence the validation work is continued by JRC-ITU and the TRANSURANUS user group through participation in further international benchmarks. Furthermore new RIA tests in France will be performed in the frame of the OECD/NEA CABRI Water Loop Project [83], hence well and representative experimental data will be available in the next years (see section 3.1).

2.4 State-of-the-art modelling of fuel behaviour in RIA licensing calculations

2.4.1 Overview about traditional licensing approach

To ensure the safety criteria for RIA like the fuel enthalpy limits (see section 1.1), core-wide simulations have to be performed for solving the equations for neutron transport, thermal hydraulics of the coolant, heat transfer between the cladding surface and the coolant, heat transfer inside the fuel rod, mechanical behaviour of the fuel rod and fission product

behaviour [3]. These phenomena are strongly coupled to each other and depend on both space and time. Today's computer codes and their coupled code systems don't yet allow simultaneously a great degree in detail in modelling of neutron kinetics, thermal hydraulics and fuel rod behaviour together. Thence state-of-the-art safety analysis still relies on offline coupled computer codes, meaning step by step analysis [10]. The following methodology is applied in the German licensing procedure for proving the RIA safety criteria:

- 1) *Lattice physics codes* like APOLLO2 [84], CASMO [85] and HELIOS [86] generate homogenized cross-sections and neutron kinetics data for each fuel assembly design of the core loading map. Every fuel rod/pin of the fuel assembly is taken into account in these calculations to allow a pin-by-pin power reconstruction in the core simulator, i.e. fuel pins differ by fuel composition (UO₂, MOX, UO₂ with Gd), fuel enrichment and in case of BWR in rod length. The dependence from feedback parameters like fuel temperature have to be considered not only for the normal operation of the reactor, as requested e.g. in fuel cycle calculations, but also in the full range of variation during the imposed transients.
- 2) *Reactor dynamics codes* like SIMULATE-3K [87] and DYN3D [88] solve the three dimensional neutron diffusion equation for two neutron energy groups as the core simulator (for LWRs). For this purpose, homogenized cross-sections and neutron kinetics data are taken from the previous step. The thermal hydraulics is modelled such that each fuel assembly is defined as vertical coolant channel, usually neglecting lateral flows that are typical for a PWR [89]. Furthermore, the fuel rod behaviour is generally determined by a simplified fuel behaviour model, integrated into the reactor dynamics code, applied to the representative fuel rod of each fuel assembly (see subsection 2.4.3). The initial fuel rod conditions like heat transfer coefficient in the gap (and radial power density profile) have to be provided as input. Nevertheless, the neutron kinetics depends (strongly) on the fuel temperature via the Doppler Effect. In addition the clad temperature influences the heat transfer between cladding and coolant [10].
- 3) *Sub-channel thermal hydraulics codes* like COBRA [90], COBRA-FLX [91] and SUBCHANFLOW [92] describe the lateral flows inside the core which allows to analyse the potential of film boiling during RIA [8]. A further goal of this step is the

definition of hot channels. The codes take into account both vertical and lateral flows in their pin-by-pin analysis. In BWR the lateral flows are smaller due to canned fuel assemblies. Furthermore, details like the pressure drop due to spacers can be modelled. As boundary conditions, previous results of the reactor dynamics code are transferred to the sub-channel code, e.g. time-dependent nodal power density. Simplified fuel behaviour models are applied as in the reactor dynamics codes, normally requiring rod initial conditions as input [91]. For the German safety criteria detailed thermal hydraulics calculations are requested to approve the avoidance of significant film boiling during RIA [8].

- 4) *Fuel performance codes* like FRAPTRAN [69] and TRANSURANUS [60] calculate fuel enthalpy and fuel temperature with respect to fuel rod failure thresholds (cf. Figure 1). The fuel rod behaviour is modelled in great detail (see section 2.3 and cf. Table 4). Some of the fuel performance codes like SCANAIR [93] (cf. Table 3 and see subsection 3.3.1) offer well validated thermal hydraulics modules and clad-to-coolant heat transfer correlations for RIA [51]. In contrast, the TRANSURANUS thermal hydraulics models cover the phases for normal operating conditions only. The thermal hydraulics conditions have to be provided as input to TRANSURANUS for accident simulations (e.g. taken from sub-channel codes). Furthermore, the node power density calculated by the reactor dynamics codes has to be supplied.

The methodology represents a generic analysis, hence core designs of different cycles should be covered [8]. Therefore, the boundary conditions depend on conservative assumptions trying to meet all potential conditions:

- Conservative values are selected for the initial reactor state, e.g. thermal power, peaked power distribution in the upper core and cycle status (begin of cycle (BOC), mid of cycle (MOC) and end of cycle (EOC) including or neglecting Xe equilibrium).
- During the transient, the Doppler coefficient, the moderator temperature coefficient, the boron reactivity worth, the void reactivity worth and the fraction of delayed neutrons affect (strongly) important parameters like total nuclear power and local power distribution. Thence they have to be set to conservative values as well. Furthermore, the reactivity worth of the ejected control rod should be increased for conservative reasons.

- The clad-to-coolant heat transfer and the heat transfer in the gap affect the fuel enthalpy, hence they should either be decreased or increased depending on whether the safety analysis is either for PCMI or for DNB, respectively. On the one side, a higher fuel enthalpy can lead to more distinct PCMI with increased potential for fuel rod failure (cf. Figure 1) and to higher fuel temperatures potentially inducing fuel melting. On the other side, a lower fuel enthalpy can be caused by a higher heat transfer in the gap [24], which in turn leads to higher heat fluxes to the coolant and might lead to (earlier) onset of film boiling.

To find the limiting scenario, several calculations have to be performed, differing e.g. in initial total nuclear power, and ejected control rod position and reactivity worth. Normally, a control rod inserted in a fresh fuel assembly represents the limiting scenario because of the higher additional reactivity due to greater amount of fissile material [3]. In addition, the pulse amplitude decreases rapidly with distance (see section 1.1). Thence the core-wide limiting fuel rod needs to be located by a search in the neighbourhood of the ejected control rod.

2.4.2 General features of the reactor dynamics code DYN3D

Reactor dynamics codes like DYN3D [88] are adopted in the second step of the core-wide safety analysis for RIA (see subsection 2.4.1). The best estimate code DYN3D is applied by several research centres, nuclear safety authorities, universities and industrial partners for both burn-up calculations (steady-state mode) and reactivity events (transient mode) in LWRs. It was primarily developed for a hexagonal fuel assembly geometry representative for the Russian Vodo-Vodyanoy Energetichesky Reaktor (VVER), and later extended to a quadratic fuel assembly geometry representative for western type reactors.

DYN3D solves the three dimensional neutron diffusion equation based on two or multi neutron energy groups for each axial node of a fuel assembly. The solution relies on the homogenized cross-sections and neutron kinetics data calculated by a lattice physics code before (see subsection 2.4.1). Beside of neutron kinetics, DYN3D includes a four balance equations model describing one and two phase flows in the core [89], hence taking into account the strong coupling between neutron kinetics and thermal hydraulics. The conservation equations of mass, energy and momentum for two phase flow as well as the

conservation equation of mass for vapour phase are solved for each coolant channel, usually representing one fuel assembly. The four balance equations model is closed by a phase slip condition and the assumption that one of the phases is saturated. The source terms in the four equations are the volumetric heat rate, the pressure drop due to friction coefficients and the evaporation/condensation rates. Regarding the volumetric heat rate DYN3D contains a simplified fuel behaviour model like other reactor dynamics codes, i.e. solving the heat conduction equation [94] (see subsection 2.4.3). Beside the four balance equations, the thermal hydraulics modelling contains heat transfer and boiling correlations. In addition, the thermo-physical properties of water and steam are included in DYN3D. Because DYN3D is limited to the core region, several boundary conditions have to be provided in the input for the core inlet and outlet, e.g. coolant inlet temperatures. Furthermore, single friction coefficients are supplied in the input. Concerning hydraulic boundary conditions, either the pressure drop over the core is calculated iteratively for a given coolant core mass flow rate or for the mass flow rates of each channel, or the mass flow rate of each channel is determined iteratively for a given pressure drop. As mentioned one coolant channel represents usually one fuel assembly, hence the thermal hydraulics of all channels are coupled to each other via core inlet, core outlet pressure and core mass flow rate.

2.4.3 Fuel behaviour modelling in the reactor dynamics code DYN3D

The simplified fuel behaviour models in reactor dynamics codes like SIMULATE-3K [87] and DYN3D [88] don't describe the fuel behaviour in great detail like fuel performance codes (cf. Table 4 based on Table 3). Thence these approaches are named as simplified fuel behaviour models, whereas the degree in detail can differ. For example, the cladding is modelled as thin shell in DYN3D. The total changes in fuel radius δR_{fuel} and cladding radius δR_{clad} are defined in DYN3D as following [94]:

$$\delta R_{fuel} = \delta R_{fuel,th} + \delta R_{fuel,el} \quad (8)$$

$$\delta R_{clad} = \delta R_{clad,th} + \delta R_{clad,el} + \delta R_{clad,pl} \quad (9)$$

where the index *el* symbolizes the change in radius due to elastic deformation, the index *th* due to linear thermal expansion, and the index *pl* due to plastic deformation. $\delta R_{clad,pl}$ is limited to cladding creep. For the fuel the plastic deformation isn't taken into account in the

DYN3D fuel rod model at all (cf. eq. (8)). Furthermore, gaseous swelling is neglected, whereas it seems to have an important influence on PCMI observed at highly irradiated fuel rods under RIA (see subsection 2.2.1). The formulation of the fuel elastic deformation ($\delta R_{fuel,el}$) only takes into account the contact pressure between fuel and cladding (Hooke's law). Therefore, the elastic deformation of the fuel is equal zero in DYN3D for open gap conditions. For the cladding, the contact pressure, inner rod pressure and coolant pressure are considered for the elastic deformation ($\delta R_{clad,el}$). However, the increase in inner rod pressure caused by transient fission gas release isn't taken into account because the fission product behaviour is neglected in DYN3D (cf. Table 4). This makes it difficult to model reliably potential transient clad failures due to ballooning (see subsection 2.2.2).

Assuming realistic conditions batches of fuel assemblies are loaded in the core which were pre-irradiated in previous cycle(s). Fuel rod parameters like fuel pellet radius, cladding radius, gap width, released fission gas volume, inner rod pressure, heat transfer coefficient in the gap and radial burn-up profile (power density profile) depend strongly on the pre-irradiation and its conditions (e.g. fuel temperature (see section 4.2)). Some of these parameters can influence largely the neutron kinetics and/or thermal hydraulics (see chapter 6). To ensure reliable results, the reference/initial fuel rod state in DYN3D at BOC must therefore be based on pre-calculations with a fuel performance code like TRANSURANUS [89].

Table 4 – Features of the simplified fuel behaviour model in DYN3D [94] compared to the fuel performance codes TESPAROD [95-97] and TRANSURANUS [60] (according to RIA)

	DYN3D	TESPAROD	TRANSURANUS
Maintaining organization	HZDR, Germany	GRS, Germany	JRC-ITU, Europe
Range of application	Transients (applied also to steady-state)	Transients only	Transients, steady-state
Consideration of pre-irradiation	Provision in the input ¹	Provision in the input ¹	Calculation in the same calculation or via restart
Geometrical representation	1D	1½D	1½D
Fuel compositions ²	UO ₂	UO ₂ , UO ₂ with Gd, MOX	UO ₂ , UO ₂ with Gd, MOX
Burn-up range	Fresh and low burn-up fuel	Fresh, low, medium and high burn-up fuel	Fresh, low, medium and high burn-up fuel
Power density profile	Provision as input (circuitous handling)	Described by simple function of burn-up	Detailed modelling (module TUBRNP [98])
Clad tube representation	Thin shell	Thin shell	Thick wall
Cladding materials	Zry-4	Zry-2, Zry-4, DUPLEX, M5 [®] , ZIRLO [™]	Zry-2, Zry-4, DUPLEX ³ , M5 ^{®3} , ZIRLO ^{™3} , Zr1Nb
Waterside corrosion during normal operation	None	None	Correlations for several cladding materials
High temperature oxidation	Oxidation rate according to Arrhenius law	Leistikov, Cathcart-Pawel, Baker/Just etc.	Leistikov, Cathcart-Pawel, Baker/Just etc.
Hydrogen uptake	None	Yes	None
Pellet-clad contact modelling	Axial sticking	Axial sticking	Frictional sliding
Initial fission gas	Inner rod pressure can be specified	Depending on burn-up or FRAPCON [99]	Detailed modelling (module FISPRO [100])
Fission gas release model	None	Model limited to grains and grain boundaries	NRO-MT (transient under development)
Fuel gaseous swelling model	None	None	NRO-MT (transient under development)
Cladding-coolant heat transfer phases	All	All	All before DNB
Cladding failure criterion for RIA	Hoop stress > yield strength	Hoop stress ≥ hoop burst stress	None (under development)

NRO-MT: Model for normal reactor operation and mild transients.

¹Should be taken from pre-calculations performed with a fuel performance code applicable to pre-irradiations.

²In addition to LWR TRANSURANUS is also validated for different Gen-IV fuel compositions.

³Property of TRANSURANUS users (confidential)

More than one decade ago, the DYN3D fuel behaviour model [94] was developed and validated on RIA experiments performed on fresh fuel in the NSRR [16, 50, 101] and IGR [17] research reactors. Thence today some simplified fuel behaviour models in other reactor dynamics codes describe the fuel behaviour in greater detail than DYN3D. Studsvik's simplified fuel behaviour model INTERPIN [102] applied to CASMO [85] and SIMULATE [87] is validated also for high burn-up conditions and MOX fuel. For example, the implemented fuel thermal conductivity accounts for high burn-up effects. The gap

conductivity (modelled as burn-up dependent) is validated on centreline fuel temperatures measured in the Halden reactor for normal operation [102]. Thence the initial value doesn't have to be provided at the beginning of the transient (cf. Table 4 regarding to DYN3D). Furthermore, the INTERPIN modelling of the corrosion thickness was extended to high burn-up conditions. In comparison with this, DYN3D doesn't take into account the corrosion layer in the thermal and mechanical analysis. In addition INTERPIN determinates the fuel rod power density profile as a function of rod burn-up, while in DYN3D this parameter has to be provided circuitously in the input. Altogether the revised modelling in INTERPIN led to an increase of about 50-60 K in the average fuel temperature at nominal conditions [102]. However, the heat transfer coefficient in the gap, the released fission gas volume, the inner rod pressure and the gaseous swelling may differ (largely) during the transient. These changes are considered in a simplified way or even neglected in the INTERPIN modelling, compared to fuel performance codes. Especially the heat transfer coefficient in the gap is known to be important for the fuel temperatures. This can (strongly) affect the fuel temperature and enthalpy. Furthermore, it's difficult or even impossible to provide reliable heat transfer coefficients in the gap based on pre-calculations due to plasticity effects in the cladding (ballooning) or/and fast kinetics (cf. Figure 36).

2.5 Trend toward coupled code systems with detailed fuel behaviour modelling

Over the last decades multi-physics code systems were developed and applied to reactor safety analysis, simulating in great detail both thermal hydraulics and neutron kinetics (i.e. high resolution of local fluid phenomena) [103, 104]. In addition, these coupled code systems allow the extension of their range of applicability (i.e. simulations including also the secondary circuit of PWR). This trend was taking benefit from the decrease in computational costs.

In the frame of this evolution, the reactor dynamics code DYN3D was already coupled to various codes. For example, to the thermal hydraulics system codes ATHLET and RELAP [105, 106] using external, internal and parallel coupling approaches (cf. Figure 8), to the sub-channel thermal hydraulics code SUBCHANFLOW and to CFD codes [103]. Another example represents Studsvik's reactor dynamics code SIMULATE coupled to RELAP5-3D [107]. Another example is AREVA's reactor analysis system ARCADIA[®] for PWR [108].

Part of this code system is a two-way coupling between the reactor dynamics code ARTEMIS and the sub-channel code COBRA-FLX. Furthermore several reactor dynamics codes, thermal hydraulics system codes, sub-channel thermal hydraulics codes and CFD codes were integrated in the SALOME platform in the frame of the European Commission projects NURESIM (2005-2007) and NURISP (2007-2012) [109]. This platform simplifies the coupling of codes once integrated in SALOME, i.e. for the handling of data transfer and the combination of different discretisations.

Most of the reactor dynamics, thermal hydraulics system, sub-channel thermal hydraulics and CFD codes contain a simplified fuel behaviour model and/or set-up of fuel rod parameters (e.g. heat transfer coefficient in the gap and power density profile) pre-calculated by a fuel rod performance code and provided as input tables [91]. The same holds for coupled code systems consisting of these codes. Nevertheless, the fuel temperature can influence the Doppler coefficient relevant for the neutron kinetics, and the clad temperature the clad-to-coolant heat transfer relevant for the thermal hydraulics. To take further advantage from the decreased computational costs, the benefit and potential has been analysed concerning the online replacement of the simplified fuel behaviour models through coupling approaches to fuel performance codes [109], especially for full two-way coupling approaches.

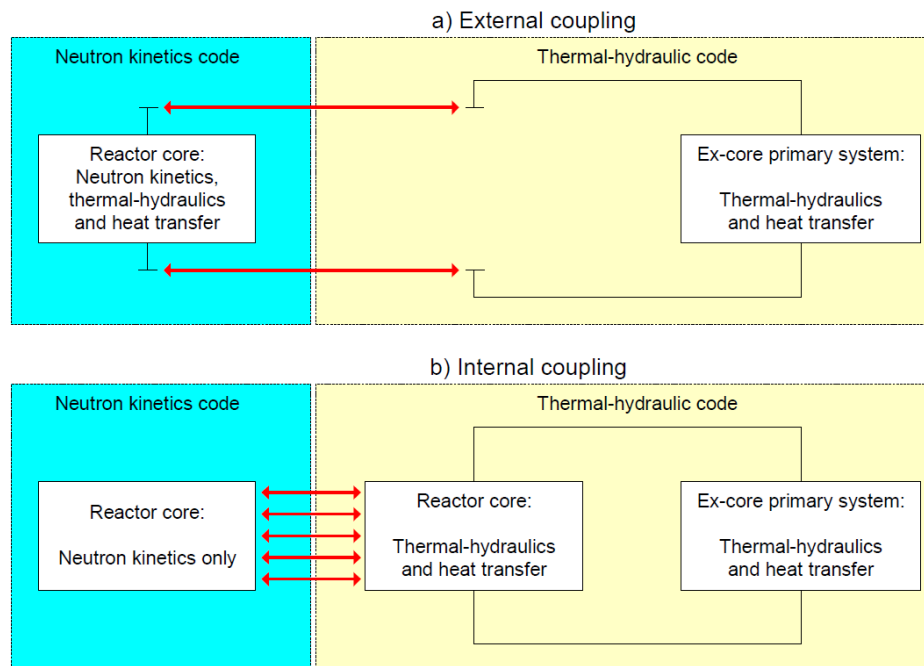


Figure 8: External (a) and internal (b) coupling methodology according to neutron kinetics/reactor dynamics code and thermal hydraulics system code in core wide analysis (red arrows denote data exchange) [3]

So far Rossiter et al. developed a one-way coupling approach to the fuel performance code ENIGMA for full core analysis [110]. In this approach Studsvik's SIMULATE-5 provides its output like pin power history of every rod in the core and power plant operating data to ENIGMA. This new code system named ONUS allows a quick and comfortable integration of the fuel behaviour in core design calculations as well as even online support of the plant operation [111]. Nevertheless SIMULATE-5 still applies the fuel behaviour model INTERPIN [102] for the calculation of the three dimensional power histories (see subsection 2.4.3). Thence the same simulation results would be obtained carrying out SIMULATE-5 and ENIGMA calculations in series.

Similarly VTT coupled its thermal hydraulics model GENFLO to the transient fuel performance code FRAPTRAN (cf. Table 3) in an approximate way [112]. GENFLO provides an axial power profile (coming from a system code) and thermal hydraulics conditions to FRAPTRAN, which in turn transfers back the heat transfer coefficient in the gap and the flow area reduction due to ballooning. At the present stage, this code system contains an overlapping between the fuel rod model in GENFLO and the fuel performance code FRAPTRAN. Nevertheless, GENFLO is only called once by FRAPTRAN in each time-step, regardless of the number of iteration steps in FRAPTRAN.

JNES presented a full online two-way coupling approach between the thermal hydraulics system code TRACE [113] and the fuel performance code FEMAXI [114] during the OECD RIA Fuel Codes Benchmark [24, 25]. The linear heat rate/nodal power were provided in the OECD benchmark specification (see chapter 3). Under this boundary condition FEMAXI transfers its calculated clad surface temperature to TRACE, which determinates the clad-to-coolant heat flux and gives its value back to FEMAXI. Thence, the simulation contains a high degree in detail in thermal hydraulics and fuel behaviour modelling. This coupled code system is designed for a single pin. Therefore, at the beginning of this work no full two-way coupling to a fuel performance code had so far been reported in the open literature for calculating a whole LWR core online with detailed and well validated fuel behaviour correlations. In view of this, the reactor dynamics code DYN3D was coupled in a one-way and a two-way methodology to the fuel performance code TRANSURANUS in this work [115] (see chapters 5 and 6). More than two decades ago TRANSURANUS was already coupled to the European Accident Code EAC-2 for liquid metal fast breeder reactor (LMFBR) [116]. Nevertheless, the presented development isn't based on this previous work.

On the one side, the TRANSURANUS code was extensively developed further in the last decades, hence the versions of the fuel performance code can (strongly) differ in code structure and models. On the other side, it was decided to develop a general TRANSURANUS coupling interface (see chapters 5) and to implement modifications in the TRANSURANUS code that could be generally used for future code couplings. In parallel to the development of the coupling in this work, the high-fidelity multi-physics system TORT-TD/CTF/FRAPTRAN, combining in once the step 2 (transport neutronics code), step 3 (sub-channel thermal hydraulics code) and step 4 (fuel performance code) of the German licensing methodology for RIA (see subsection 2.4.1), was developed [117]. Furthermore, the fuel performance code SCANAIR capable to RIA [82, 118] (cf. Table 3) was integrated into the SALOME platform in the frame of the European Commission project NURESAFE [119]. These different developments all allow analysing the benefit resulting from detailed online fuel behaviour modelling. For example, these approaches may have the advantages of applying more straightforward safety analysis, of performing more easily uncertainty analysis and maybe of reduction of conservatism in safety analysis [110].

3 OECD RIA Fuel Codes Benchmark for highly irradiated fuel rods

In this work the fuel performance code TRANSURANUS was selected to increase the degree in detail in online fuel behaviour modelling in the simulation tools applied by HZDR (see chapters 5 and 6). The RIA version of TRANSURANUS is still under development [120]. Thence intensive verification and validation work have been carried out for applying TRANSURANUS to such conditions (cf. Figure 2). As representative experimental data for RIA are still limited (see section 3.1). Hence the code performance was evaluated by participation in the international OECD RIA Fuel Codes Benchmark for highly irradiated fuel rods in 2011/2012 (see sections 3.1, 3.2 and 3.3). At the beginning this benchmark allowed real blind TRANSURANUS calculations because information was not known about results of other benchmark participants at that time.

To allow recommendations for future work, the results of TRANSURANUS (HZDR) were analysed in detail in this thesis. Some of the conclusions in section 3.3 are tentative and have to be investigated further in future work (e.g. by uncertainty analysis). They are nevertheless aligned with the recommendations of the OECD RIA Fuel Codes Benchmark. More precisely, e.g. “deeper understanding of the differences in modelling of the different codes”, and “clad to coolant heat transfer in case of water boiling is of particular interest because on the one hand large uncertainties exist on the models and on the other hand it makes large differences in the thermal as well as in the mechanical predictions” [24] were recommended for a follow-up of this benchmark.

3.1 Experimental data

RIA tests on highly irradiated fuel rods

For evaluating the performance of TRANSURANUS for RIA conditions and hence in parallel the capability to couple TRANSURANUS to the reactor dynamics code DYN3D (see chapters 5 and 6), a comprehensive experimental data review was conducted. In this regard, the OECD Halden Reactor Project (HRP) represents worldwide the most extensive experimental database for normal operation, for operational transients and for the design basis accident LOCA. This database contains both “in-pile” online measurements and “out-of-pile” data after irradiation (resulting from PIE). Altogether these data are essential to establish

safety limits and margins, material properties, micro- and meso-structural processes, and validation of fuel performance codes [121]. As RIA conditions are not available in the HRP, only the CABRI reactor in France [15] and NSRR in Japan [16] have been performing RIA tests relevant also for highly irradiated fuel rods in western LWR. However these tests concentrated mainly on fresh, low and medium burn-up fuel rods in the last decades [3], hence mainly not considering fuel rod failures due to PCMI (see sections 2.1 and 2.2). Furthermore these RIA tests are sometimes not fully representative for BWR and PWR conditions [24]. More precisely, a pulse width of a few ms in NSRR (instead of 30 ms and larger as typical in German PWR - see section 1.1) or/and sodium as coolant in the past CABRI (hence without occurrence of DNB) has no potential for fuel rod failures in the late phase of RIA (cf. Figure 4). In the future new RIA experiments will be performed in the OECD/NEA CABRI Water Loop Project analysing the highly irradiated fuel rod behaviour during RIA under conditions more representative for PWR, e.g. water as coolant [122]. For this purpose, a pressurized water loop was installed in the CABRI reactor. Due to unexpected challenges this OECD experimental project was delayed by more than one decade. Currently the first RIA test in the water loop is expected in 2016.

While Germany has no direct access to tests performed in the large-scale RIA experimental program in the NSRR in Japan [16], the NSRR tests FK-1, FK-2 and FK-3 are available in the International Fuel Performance Experiments (IFPE) database of the OECD/NEA [123]. These three tests were performed on capsuled BWR fuel with limited burn-ups from 41 to 45 MWd/kgU under stagnant water conditions and initiated from room temperature representing cold zero power (CZP). Furthermore Germany participates as member in the ongoing OECD/NEA CABRI Water Loop Project [122]. However, no CABRI test with water as coolant is available for the time being. Finally, Germany was not part of the out-of-pile PATRICIA experiments in France [3, 51, 54] analysing CHF, critical temperature and film-boiling heat flux for steady-state and RIA conditions (see section 2.2).

OECD RIA Fuel Codes Benchmark (2011/2012)

Therefore the OECD RIA Fuel Codes Benchmark on highly irradiated fuel rods in 2011/2012 [24, 25], organized by the OECD/NEA Working Group on Fuel Safety (WGFS), represented a good basis for the evaluation of the preliminary RIA version of TRANSURANUS.

The RIA tests CIP0-1⁴ (in sodium in the CABRI reactor), VA-1 and VA-3 (both in stagnant water in the NSRR) were evaluated in this benchmark. Furthermore, results were predicted for the future RIA test CIP3-1 (in water in the CABRI reactor). The initial conditions of the belonging four test rodlets were almost identical. On one hand all four corresponding full length rods were fabricated by the vendor ENUSA in Spain with identical fuel rod characteristics (e.g. all have ZIRLO™ as cladding material). On the other hand, these full length rods were pre-irradiated under similar conditions in the PWR Vandellós-2 (up to maximum pellet burn-ups of around 75 MWd/kgU), with almost identical pre-irradiation conditions. After unloading from the reactor core two full length rods were refabricated to short test rodlets for the CABRI tests CIP0-1 and CIP3-1, another two for the NSRR tests VA-1 and VA-3 (see section 3.2). In the benchmark each RIA test was simulated under two/three different boundary conditions (cf. Table 5).

Table 5 – Cases of the OECD RIA Fuel Codes Benchmark [24]

Case #	Reactor	Rod	Coolant	Specific conditions
1	CABRI reactor	CIP0-1	Sodium	No boiling through sodium
2	CABRI reactor	CIP3-1	Water	Hypothetical – Test in water, but boiling must be inhibited in the models
3	CABRI reactor	CIP3-1	Water	Hypothetical – Test in water, but prescribe the clad outer temperature and use a flat axial power profile
4	CABRI reactor	CIP3-1	Water	Test in water, boiling possible
5	NSRR	VA-1	Stagnant water	Hypothetical – Test in water, but boiling must be inhibited in the models
6	NSRR	VA-1	Stagnant water	Test in water, boiling possible
7	NSRR	VA-3	Stagnant water	Hypothetical – Test in water, but boiling must be inhibited in the models
8	NSRR	VA-3	Stagnant water	Test in water, boiling possible

At the benchmark initiation larger differences in calculated results were expected through different thermal hydraulics modelling in the codes (see section 2.2). This was even confirmed by the results for case #1 with sodium as coolant. To allow a pure comparison in fuel behaviour modelling, the thermal hydraulics boundary conditions were varied on purpose with different constraints for the water as coolant (cf. Table 5). For CIP3-1 three types of thermal hydraulic boundary conditions were applied: Firstly, boiling was inhibited (case #2). Secondly, clad outer temperatures determined by the fuel performance code SCANAIR [93]

⁴ Reference test in sodium for the RIA test CIP3-1 performed in water in the future

containing well validated clad-to-coolant heat transfer correlations for RIA conditions were taken (case #3). Thirdly, the thermal hydraulics were calculated by the code applied by each participant (case #4).

In the frame of this work the performed CABRI test CIP0-1 in sodium (case #1) and the planned CABRI test CIP3-1 carried out in the new installed pressurized water loop (case #2 and case #3) were calculated by HZDR (cf. Table 6). For this purpose, the fuel performance code TRANSURANUS was applied in this work. Results of the other benchmark cases (cf. Table 5) were not contributed by HZDR. On the one side the TRANSURANUS thermal hydraulics model is based on a simplified approach covering the phases before DNB only. Thence the simulation of the benchmark cases #4, #6 and #8 with boiling cannot be carried out with TRANSURANUS in standalone mode (without taking the thermal hydraulics conditions from another code). On the other side numerical instabilities occurred in the TRANSURANUS thermal hydraulics regarding to the NSRR capsuled fuel tests performed in stagnant water with inhibition of boiling (cases #5 and #7).

Table 6 – Main characteristics of the CABRI tests determined in the OECD RIA Fuel Codes Benchmark [24]

Rod	Coolant medium	p_{cool} [MPa]	Inlet T_{cool} [°C]	Maximum injected energy* [cal/g]	FWHM [ms]	Failure [-]
CIP0-1	Sodium	~0.3	280	99	32.4	Survived
CIP3-1	Water	15.5	280	115	8.8	Performed in the future

*At peak power node

However, the code system DYN3D-TRANSURANUS (see chapters 5 and 6) developed in this work should allow to calculate all of these cases in the future (as both one-way approach and two-way approach). For this purpose henceforth the 3D neutron kinetics model in DYN3D can be switched off [120], meaning that the linear heat rates have to be provided as input (e.g. given in the specification of the benchmark [24, 25]). Nevertheless, it should be kept in mind that the fuel rod and heat transfer model in DYN3D were validated on earlier RIA experiments performed in the Japanese NSRR and the Russian IGR [94]. In that context, both coolant velocity and subcooling can have a strong influence on the clad-to-coolant heat transfer under RIA [51, 54]. For example, CHF, critical temperature and film-boiling heat flux can differ (largely) between CABRI and NSRR tests (cf. Table 2). This might be the

main reason for the (partly) larger deviations in clad temperature seen in the results of the different TRANSURANUS participants. More precisely, the results of Università di Pisa (UNIPIS⁵) based on thermal hydraulics boundary conditions pre-calculated with RELAP5-3D [124] (cf. Figure 18), the ones of TÜV NORD EnSys Hannover GmbH & Co. KG and HZDR on the simplified TRANSURANUS thermal hydraulics model.

3.2 Generation of TRANSURANUS inputs

Advanced users apply the fuel performance code TRANSURANUS also to complex irradiation experiments, i.e. performed in the OECD Halden Reactor Project in Norway [43], OECD CABRI Water Loop Project in France [15] and NSRR in Japan [16]. In such experiments a fuel rod passes different stages (cf. Figure 9): Firstly, a full length fuel rod is irradiated in a power reactor, secondly it is refabricated to a short test rodlet equipped with measurement devices in the hot cells, thirdly irradiated/tested in a research reactor.

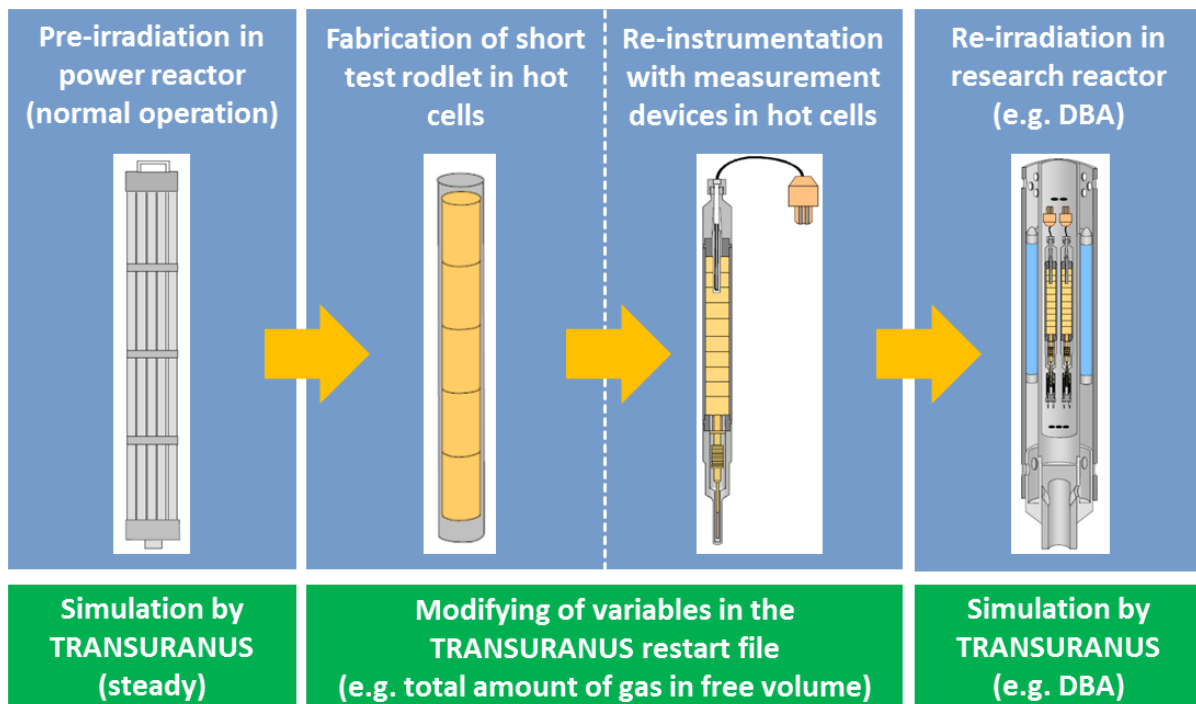


Figure 9: Stages of the fuel rod in a complex irradiation experiment compared to its simulation in TRANSURANUS (individual figures taken from [125])

⁵ Marked as PISA in the figures of the OECD RIA Fuel Codes Benchmark

To ensure a realistic fuel behaviour modelling as best as possible, the whole irradiation history beginning from zero burn-up has always to be given to fuel performance codes like FEMAXI [114], FALCON [62] and TRANSURANUS [60] (see subsection 5.1.4). Therefore, the challenge exists to take into account changes in fuel rod design (cf. Figure 9) and thermal hydraulics conditions (cf. Table 7) in this kind of fuel performance simulations (see subsections 3.2.1 and 3.2.2). More precisely for CIP0-1, thermal hydraulic conditions can differ in coolant (water vs. sodium) and coolant channel geometry (quadratic configuration vs. annular flow channel). In addition the fuel rod design can change e.g. in fuel rod length (full length rod vs. short test rodlet) and gas composition (puncturing and refilling during the refabrication). Finally, different axial resolution of the time-dependent rod power and thermal hydraulics conditions as well as limited application range of models must be accounted for.

Other fuel performance codes like SCANAIR [93], FRAPTRAN [69], RANNS [126] and TESPARD [96] are limited to transient conditions, hence the fuel rod conditions at the beginning of the transient have to be provided in the input of these codes (see section 2.3).

Table 7 – Thermal hydraulics conditions in power reactor vs. research reactor (CIP0-1) [25]

Reactor	Coolant medium	p_{cool} [MPa]	Inlet T_{cool} [°C]	Inlet flow rate [kg/h]	Hydraulic diameter [mm]
PWR Vandellos-2	Water	15.51	290.5 - 292.4	1019 - 1025	11.7 (quadratic)
CABRI	Sodium	~0.3	279.7	1112	14.2 (annular)

3.2.1 Pre-irradiation in power reactor

Fuel rod design

Both the fabricated pellet characteristics (e.g. diameter, dish, chamfer, enrichment, density, densification and grain size) and the fabricated cladding characteristics (e.g. inner diameter, outer diameter and material) are specified in detail in the benchmark specification [25]. Thence the fabricated fuel rod characteristics could be described in detail in the TRANSURANUS input. Concerning the cladding material, the standard TRANSURANUS version does not contain material properties for ZIRLO™ (cf. Table 4), hence the cladding was modelled with the material properties of Zry-4. Advanced cladding materials like ZIRLO™ are characterized by a slower oxide layer build-up [127], compared to Zry-4. As a

second order effect, the clad corrosion layer thickness could therefore be overestimated by TRANSURANUS at the end of the pre-irradiation in the PWR Vandellos-2.

As explained before, the RIA test rodlet was cut from the full length fuel rod, irradiated in a standard fuel assembly in the power reactor (cf. Figure 9 and see subsection 3.2.2). Only the part of the full length fuel rod tested under RIA conditions was calculated by TRANSURANUS for the pre-irradiation. For this purpose, the specified lower and upper plenum volumes of the full length fuel rod were scaled down according to the length ratio of the test rodlet over the full fuel rod. The TRANSURANUS input values of initial fill gas pressure and fill gas temperature are independent on the scaling.

Time-dependent rod power and thermal hydraulics conditions

The linear heat rate, fast neutron flux, coolant flow rate, coolant pressure, coolant temperature and hydraulic diameter have to be provided in the TRANSURANUS input for each time step. The linear heat rate (including their axial distributions) were provided in the benchmark specification for BOC, MOC and EOC of each of the five cycles in the power reactor [25]. The thermal hydraulics parameters were given as constant during each cycle and differed only slightly between the cycles in the Vandellos-2 reactor (cf. Table 7). The fast neutron flux was not given, hence it was assumed to be proportional to the linear heat rate. The factor was taken from one U.S. PWR because the Vandellos-2 reactor is based on a Westinghouse PWR design.

During the simulation by TRANSURANUS, any modification of the discretisation of the fuel rod and any manual introduction of geometrical changes should be avoided. Nevertheless, the axial discretisation depends on several parameters, e.g. time-dependent rod power, (time-dependent) thermal hydraulics conditions, or/and locations of special online measurements in a research reactor (e.g. thermocouples). Furthermore, their suitable discretisation can differ between power reactor and research reactor. Normally the axial distributions are measured with lower resolution in a power reactor than in a research reactor. For example, the linear heat rate is provided at 10 locations in the PWR Vandellos-2 and at 29 locations in the CABRI reactor regarding to CIP0-1 (both values referring to the test rodlet length) [25].

In the following two methodologies are described to specify an identical axial discretisation among the whole simulation. This description refers to the slice version option in

TRANSURANUS. The bottom of a slice/axial zone is defined by the half distance between its value location and the next underneath lying value location, and vice versa for the top of a slice/axial zone. The geometrical representation of TRANSURANUS is based on a 1½D approach, hence a value at the location is assumed as constant over the whole height of the slice/axial zone.

- 1) First methodology: The axial resolution/discretisation of the research reactor is taken for the whole TRANSURANUS simulation including the pre-irradiation (cf. Figure 10). Thence the set of values belonging to the research reactor changes at each boundary of a slice/axial zone. For the power reactor, the values of the new axial resolution/discretisation (based on the research reactor) are calculated through an interpolation/extrapolation of the values of the original axial resolution/discretisation (based on the power reactor). The values belonging to the power reactor changes also at each boundary of a slice/axial zone.

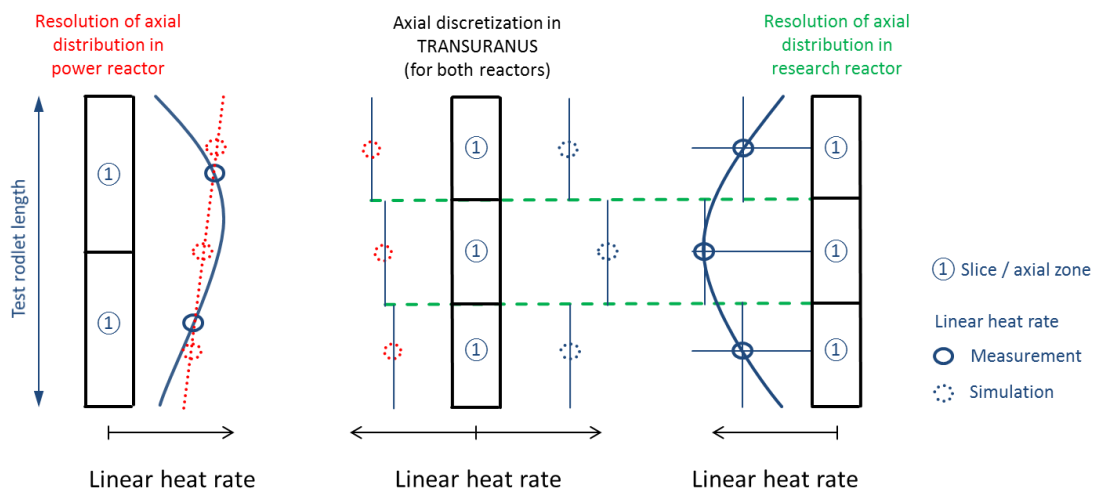


Figure 10: First methodology to combine different axial resolutions/discretisations in power reactors and research reactors (example on linear heat rate with resolution of two locations in power reactor and three locations in research reactor)

- 2) Second methodology: Normally the bottom and top of axial zones/slices of the research reactor distribution do not overlap with the ones of the power reactor distribution. The axial resolution/discretisation of the second methodology combines the ones of both power reactor and research reactor for the whole TRANSURANUS simulation including the pre-irradiation. Therefore, the combined axial resolution/discretisation is normally finer than both axial resolutions/discretisations

alone (cf. Figure 11). At the same time this means that a bottom/top of an axial zone of the power reactor or research reactor defines the bottom/top of the axial zone in the combined axial resolution/discretisation and the top/bottom of the following axial zone. Thence the set of values belonging either to the power reactor or to the research reactor changes at a boundary of an axial zone. Furthermore, both sets of values will change at a boundary of an axial zone, if bottom/top of axial zones of both axial resolutions/discretisations overlap. In the extreme case this second methodology can lead to very small heights for a few axial zones. For example, this was/would be the case for the TRANSURANUS calculations of the NSRR tests VA-1 and VA-3 (benchmark cases #5, #6, #7 and #8; cf. Table 5). For very low zone heights numerical instabilities can occur in the simulation, although TRANSURANUS is known as a very stable fuel performance code. This second methodology was applied in the TRANSURANUS calculations (HZDR) for the OECD RIA Fuel Codes Benchmark [24, 25].

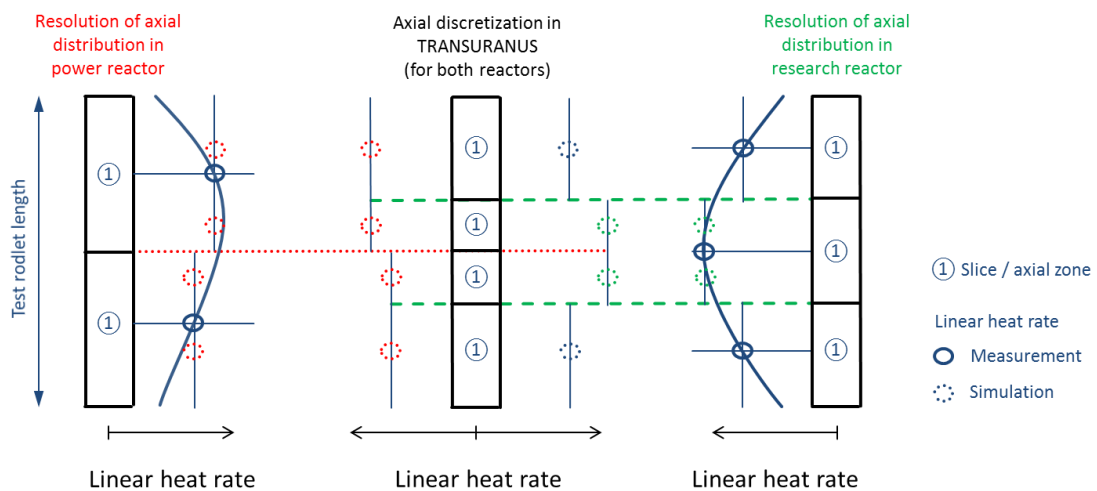


Figure 11: Second methodology to combine different axial resolutions/discretisations in power reactors and research reactors (example on linear heat rate with resolution of two locations in power reactor and three locations in research reactor)

Model options

The required TRANSURANUS model options were applied as in a previous work for several fuel rods irradiated in power reactors [128]: Selection of the kind of thermal and mechanical analysis (either complete thermal-mechanical analysis or only thermal analysis), the kind of mechanical analysis (either explicit technique or visco-elastic approximation), the axial friction force model (either no-slip condition, slip condition or axial friction forces), the heat

transfer coefficient between cladding and coolant (either application of heat transfer correlations, set to infinity in case of providing of clad outer temperatures as outer boundary or providing as input), the plenum temperature model (either low temperature approach, high temperature approach or providing as input), the grain growth model (either no grain growth or model of Ainscough and Olsen [129, 130], the grain boundary fission gas behaviour model (either not treated or treated with one of the existing modelling approaches), the fission gas release model (either not treated or treated with one of the existing modelling approaches), the algorithm solving the diffusion equation for intragranular gas release (either Urgas algorithm [131] or Formas algorithm with selectable number of exponential terms [132]), the threshold burn-up for fission gas release from the HBS (either standard value or specified value for advanced users) and the convergence limits (either standard accuracy or specified value for advanced users).

Of course the selected model option set can influence considerably the simulated fuel rod behaviour/conditions, e.g. gap width and amount of fission gas in the free volume at the beginning of the transient. Therefore, in general the set of model options should be selected with great care.

3.2.2 Refabrication in hot cells and RIA transient in research reactor

Fuel rod design

After the pre-irradiation in the power reactor Vandellos-2 the full length fuel rod underwent PIE in the hot cells (e.g. visual inspection, puncturing of fission gas and γ -scan for the burn-up along the fissile column). Afterwards short fuel test rodlets were refabricated from the full length fuel rod (e.g. including installing of devices for cladding elongation and gas filling). More precisely, e.g. the mother rod fuel fissile height of the CABRI test CIP0-1 amounted to 3657.6 mm, the belonging fuel test rodlet 541 mm [25]. Then this mentioned test rodlet was installed in a test section containing several measurement devices like thermocouples, pressure transducers, flowmeters, void detectors and microphones. Finally, this test section was loaded in the CABRI cell for in-pile RIA testing.

To take into account the fuel rod refabrication prior to the transient simulation, details of the TRANSURANUS restart file generated at the end of the pre-irradiation have to be modified

(cf. Figure 9). For example, the new total amount of gas components has to be specified for the free volume. The fuel rod length does not have to be modified because only this section of the full length fuel rod is simulated by TRANSURANUS regarding the pre-irradiation. Manual geometrical changes should be avoided during the simulation of a complex irradiation experiment with TRANSURANUS (see subsection 3.2.1).

Time-dependent rod power and thermal hydraulics conditions

The discretisation of this data should be identical for both during the pre-irradiation and during the transient (cf. Figure 10 and Figure 11; see subsection 3.2.1). The same data as for the pre-irradiation has to be provided in the TRANSURANUS input for the transient, i.e. linear heat rate, fast neutron flux, coolant flow rate, coolant pressure, coolant temperature and hydraulic diameter (see subsection 3.2.1).

Potentially post-crises heat transfer has to be taken into account during the RIA transient (see subsection 2.2.2). If DNB occurs (as expected in the upcoming CABRI test series), TRANSURANUS will be only capable to model the clad-to-coolant heat transfer before DNB, not the post-critical-heat-flux heat transfer [120]. Therefore, in this case the coolant temperature mentioned above represents the clad outer temperature. Alternatively, the clad-to-coolant heat transfer coefficient can be provided time-dependently in the TRANSURANUS input (see also the below passage “Model options”). Both thermal hydraulics boundary conditions have to be determined before, e.g. carrying out calculations with a thermal hydraulics system code validated for RIA conditions. According to the benchmark case #3 the provided clad outer temperature was calculated by IRSN with its fuel performance code SCANAIR [25]. In the future the lack of a full thermal hydraulics model in TRANSURANUS can be compensated by coupling TRANSURANUS to a code containing a thermal hydraulics model validated for RIA conditions (see section 3.1, chapter 5 and chapter 6).

It is obvious that the linear heat rate will change much more rapidly in a RIA transient than during the pre-irradiation in a power reactor (cf. Figure 12). Thence this kind of data are measured with high frequency in research reactors (e.g. the linear heat rate 1002 times over a period of 2.001 s for the benchmark case #1 (cf. Table 5)). Therefore, the amount of data, which has to be provided in the TRANSURANUS input, is (much) larger compared to the pre-irradiation in the power reactor.

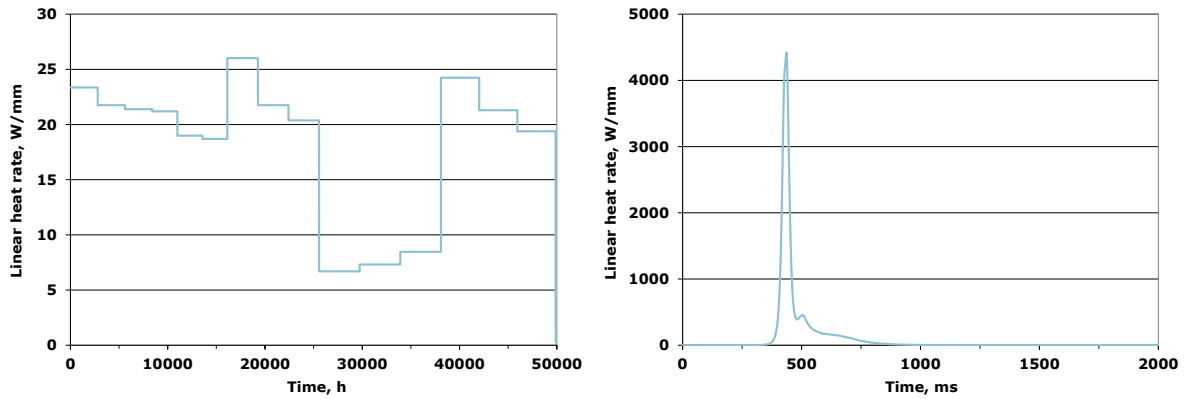


Figure 12: Node linear heat rate over time (benchmark case #1). Left, during pre-irradiation in the power reactor [25]; right, during RIA test CIP0-1 in the research reactor CABRI (extracted from TRANSURANUS (HZDR) results).

Model options

A few model options have to be changed because some selected correlations are either limited to normal operation conditions or to specific geometries. As for the characteristics of the fuel rod design the TRANSURANUS restart file has to be modified. For example, another set of clad properties were selected for transient conditions. This affects the modelling of creep anisotropy coefficients, creep strain, burst stress and crystallographic phase. However, the applied correlations are validated for LOCA, hence in the future clad properties for RIA should be implemented in TRANSURANUS (see subsection 2.3.5). Additionally, the cladding corrosion model was modified. According to benchmark case #1 this included also a coolant change from water to sodium (cf. Table 7). Furthermore, the change in coolant channel geometry has to be taken into account (quadratic configuration vs. annular flow channel). The average plenum temperature has to be calculated by the high temperature approach instead of the low temperature approach chosen for the pre-irradiation. According to the benchmark case #3 the clad outer temperature was given in the benchmark specification [25], pre-calculated by the code SCANAIR [93]. Therefore, the model assuming infinite clad-to-coolant heat transfer was selected.

3.3 Analysis of TRANSURANUS results

3.3.1 Spectrum of fuel performance codes

Results were provided by 17 organizations from 14 countries (cf. Table 8). A wide spectrum of fuel performance codes capable to simulate transient conditions was applied for this task: FALCON [62], FEMAXI [114], FRAPTRAN [69], RANNS [126], RAPTA [133], SCANAIR [93], TESPARD [96] and TRANSURANUS [60]. Among all codes FRAPTRAN and in particular SCANAIR represent the fuel performance codes with the most comprehensive validation on experimental data for RIA. In SCANAIR, the mechanical properties of the cladding were validated on the PROMETRA experimental program [134], the modelling of heat transfer between cladding and coolant on the PATRICIA experiments [55] (see subsection 2.2.2), and the PCMI models on the twelve integral tests REP-Na in the CABRI reactor [15] and on integral tests conducted in NSRR [16] (see subsection 1.1). Thence the modelling in TRANSURANUS could be compared to well validated and state-of-the-art RIA models in this benchmark. In contrast, the Russian code RAPTA was mainly validated on RIA tests performed on VVER annular fuel pellets where the central hole provides additional free volume for fuel expansion in RIA [3]. This might lead to weaker PCMI (see subsection 2.2.1), i.e. no PCMI cladding failure was observed in RIA tests on VVER fuel. Thence it is questionable whether RAPTA is sufficiently validated for the description of pellet-clad contact for solid pellets. It should be noted that an increased number of VVER fuel assemblies feature solid pellets instead of annular pellets [135].

HZDR participated from the beginning of the benchmark. Before the first benchmark meeting each participating institution did not know the results of the other participants. This allowed real blind TRANSURANUS calculations without any information about results of other benchmark participants. The other participating TRANSURANUS users TÜV NORD EnSys Hannover GmbH & Co. KG in Germany, Nuclear Research Institute Řež plc (NRI) in Czech Republic and UNIPI in Italy provided their results in a later stage of the benchmark. In addition to these results HZDR provided a filled questionnaire summarizing the TRANSURANUS code features and together with JRC-ITU both short and long TRANSURANUS code description for the OECD benchmark report [24, 25].

Table 8 – Codes applied by participants in OECD RIA Fuel Codes Benchmark [24]

Contributor	Country	Computer Code	
		Pre-irradiation	RIA transient
BOCHVAR	Russia	RAPTA 5.2	RAPTA 5.2
CIEMAT	Spain	FRAPCON 3.4a	SCANAIR 7.1
		FRAPCON 3.4a	FRAPTRAN 1.4
GRS	Germany	FRAPCON 3.3	TESPAROD
HZDR	Germany	TRANSURANUS	TRANSURANUS
IRSN	France	FRAPCON 3.4a	SCANAIR 7.2
JAEA	Japan	FEMAXI	RANNS
JNES	Japan	FEMAXI	FEMAXI/TRACE
KINS	South Korea	FRAPCON 3.4	FRAPTRAN 1.4/TRACE
MTA EK ⁶	Hungary	FUROM	FRAPTRAN 1.3/TRABCO
NRC	United States	FRAPCON 3.4a	FRAPTRAN 1.4
NRI	Czech Republic	TRANSURANUS	FRAPTRAN 1.4
		TRANSURANUS	TRANSURANUS
PSI	Switzerland	FALCON-PSI	FALCON-PSI
SSM	Sweden	FRAPCON 3.3	SCANAIR 3.2
		FRAPCON 3.3	SCANAIR 7.1
TRACTEBEL	Belgium	FRAPCON 3.4a	FRAPTRAN 1.4
TÜV NORD	Germany	TRANSURANUS	TRANSURANUS
UNIPI ⁷	Italy	TRANSURANUS	TRANSURANUS/RELAP5
VTT	Finland	ENIGMA	SCANAIR 6.6

3.3.2 Use of input data (comparison to other fuel performance codes)

Linear heat rate

The time-dependent linear heat rate was provided in the benchmark specification [25]. Therefore, identical code results were expected for the injected energy. Nevertheless, the lower bound and upper bound of all predictions differ around 10 cal/g in the case #1 (cf. Figure 13). For all benchmark cases simulated by HZDR, the injected energy calculated by

⁶ Marked as EK in the figures of the OECD RIA Fuel Codes Benchmark

⁷ Marked as PISA in the figures of the OECD RIA Fuel Codes Benchmark

TRANSURANUS (HZDR) is in very good agreement with SCANAIR (IRSN), see Figure 13 for case #1. This is important because small derivations in injected energy can be sensitive to important fuel parameters, e.g. fuel enthalpy and fuel temperature.

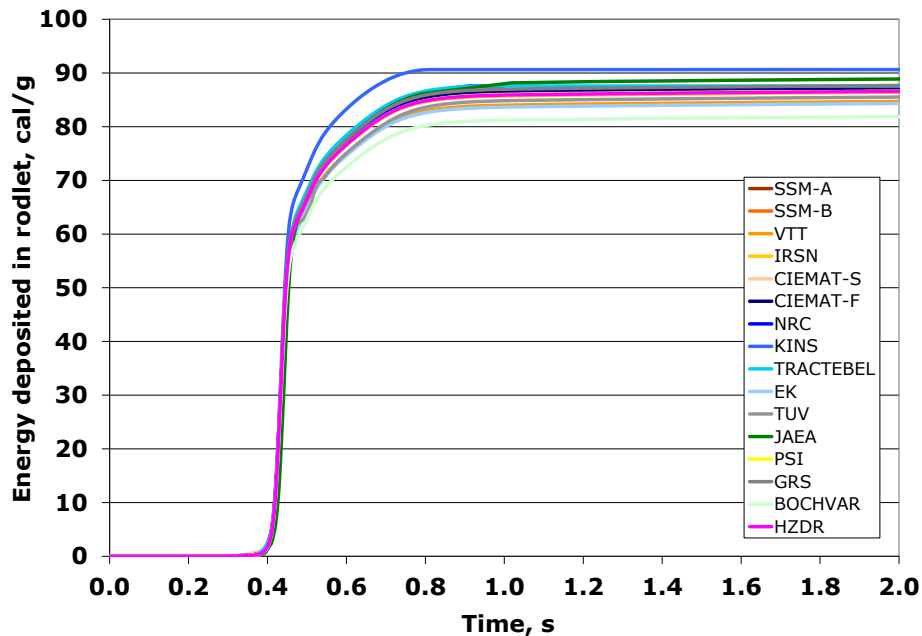


Figure 13: Energy deposited over time in the whole rodlet (benchmark case #1) [25]

Clad temperature

For case #3 the clad outer temperature was given in the benchmark specification [25]. Thence very good agreement in this parameter could be observed (with exception of the results from JNES and UNIP). Nevertheless, differences in clad inner temperature (impact on e.g. fuel temperature and fuel enthalpy) may still occur because of different clad tube representation. Some fuel performance codes like FRAPTRAN (cf. Table 3) and TESPARD (cf. Table 4) model the clad tube only as thin shell. This approach assumes constant/uniform temperature, stress, strain and material properties over the clad thickness (see subsection 2.3.3). However, the clad temperature can differ considerably over the clad thickness during RIA (cf. Figure 7).

Initial conditions (e.g. gap width)

Ideally, fuel rod parameters during pre-irradiation and during the RIA transient are determined by the same fuel performance code (e.g. FEMAXI, FALCON and TRANSURANUS). As an alternative, a steady-state fuel performance code (e.g. FRAPCON) and a transient fuel performance code (e.g. SCANAIR and FRAPTRAN) can be applied in series (see section 3.2). As the number of calculated variables can be (very) high in fuel performance codes (e.g. in case of TRANSURANUS), it might not be possible to transfer all

of them between the steady-state code and the transient code for the characterization of the initial conditions of the RIA transient.

If the initial conditions are not identical, differences between both simulation methodologies can occur easily in the results of the RIA transient. For example, the (initial) gap width is sensitive to the local temperature (cf. Figure 14). Hence, (initial) differences in gap width influence the heat transport out of the pellet, and can strongly influence the fuel behaviour during the late phase during RIA, even more under post crisis conditions (cf. Figure 4 and see subsection 2.2.2). In the early phase of RIA, initial differences in gap width may not have a large impact on the fuel behaviour with regard to PCMI because gap closure takes place at the same time of energy injection (depending on the burn-up conditions and the characteristics of the power pulse).

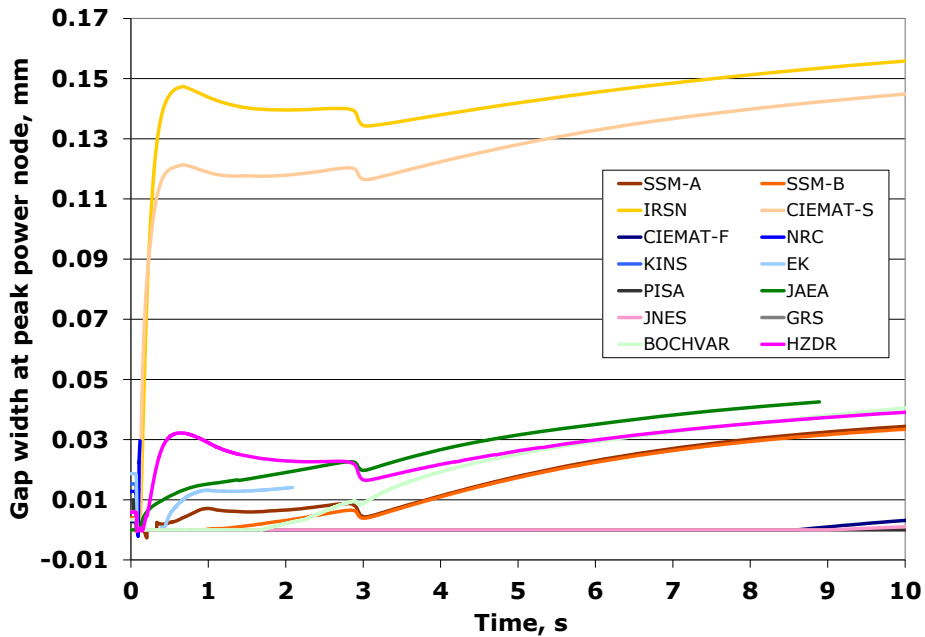


Figure 14: Gap width over time at peak power node (benchmark case #3) [25]

3.3.3 Thermal behaviour (comparison to other fuel performance codes)

For the work presented in chapters 5 and 6 a good prediction of the thermal behaviour in TRANSURANUS is essential because fuel temperature and clad temperature are transferred back to the reactor dynamics code DYN3D in the two-way coupling approach (see chapter 6). The fuel temperature affects directly the neutron kinetics through the Doppler temperature.

The clad temperature affects the thermal hydraulics through clad-to-coolant heat transfer in DYN3D.

Rodlet enthalpy

The evolution of the rodlet enthalpy is a key parameter for comparison because it is affected considerably by the injected energy (cf. Figure 13), the power density profile / the heat release distribution, the fuel thermal conductivity, the heat transfer in the gap and the clad-to-coolant heat transfer. The impact of the power density profile, fuel thermal conductivity and heat transfer in the gap can be seen in the analysis with the coupled code system DYN3D-TRANSURANUS presented in chapter 6 and in Ref. [10].

In the three simulated benchmark cases, the rodlet enthalpy of TRANSURANUS (HZDR) agrees well in maximum value and shape to almost all other codes. Figure 15 illustrates the situation for case #3 with prescribed clad outer temperatures, i.e. excluding the differences caused by clad-to-coolant heat transfer modelling. However, for TRANSURANUS (HZDR) the enthalpy decreases more rapidly than for SCANAIR (IRSN). One main reason can be the gap width (cf. Figure 14) being a sensitive parameter with regard to the heat transfer in the fuel rod. A larger gap width entails a decrease in the gap heat transfer coefficient, hence a slower reduction in rodlet enthalpy.

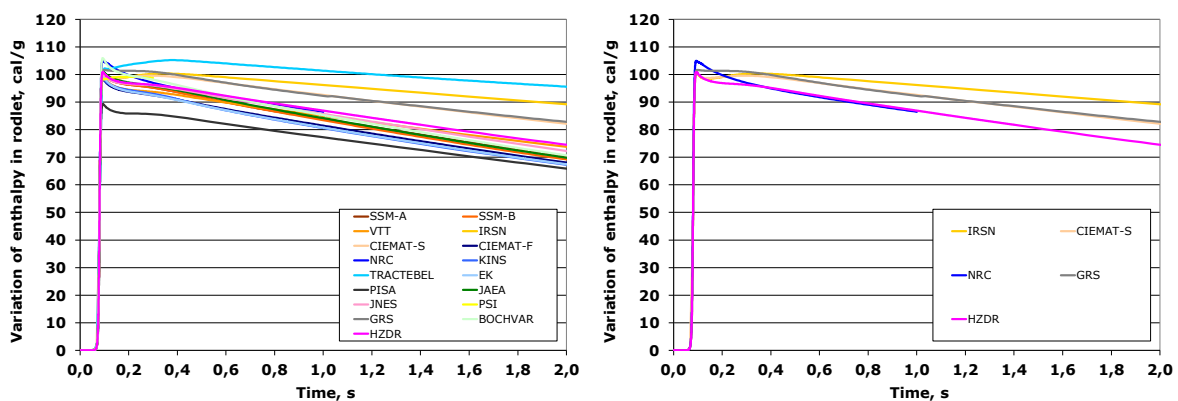


Figure 15: Variation of enthalpy over time in the whole rodlet with respect to initial conditions of the transient (benchmark case #3). Left, results provided by all participants of the benchmark; right, selected results from the left side. [25]

Fuel temperature

Other reasons for the differences in benchmark case #3 (Figure 15) can be the power density profile and the fuel thermal conductivity. To understand the impact, the temperature profile

and its time evolution should be discussed. At the beginning of a RIA transient, high burn-up fuel is heated almost adiabatically according to the radial power density profile [3]. This leads to a temperature profile peaked in the pellet periphery [3]. The maximum fuel temperature of the whole transient occurs at the time of energy injection, meaning at the beginning of the RIA transient (cf. Figure 16). TRANSURANUS (HZDR) predicted a 50 K higher maximum fuel temperature compared to SCANAIR (IRSN) at the beginning, before the maximum fuel temperature decreases in the course of the transient (cf. Figure 16). This results from a higher maximum rodlet enthalpy in TRANSURANUS at the beginning (cf. Figure 15). However, this difference is still in the range of the uncertainty of fuel performance codes. At the same time the radial location of the maximum temperature is almost identical between TRANSURANUS (HZDR) and SCANAIR (IRSN) in Figure 17, meaning the modelling of the power density profile is similar in both codes. In the course of the RIA transient this location moves towards the fuel pellet centre (cf. Figure 17). This is influenced strongly by the fuel thermal conductivity. The location of maximum fuel temperature calculated by TRANSURANUS (HZDR) is in good agreement with SCANAIR (CIEMAT-S). SCANAIR (IRSN) predicts a slightly slower shifting of this maximum toward the pellet centre over the time. Nevertheless, only TESPAROD (GRS) shows a better agreement in the radial location predicted by SCANAIR (IRSN) than TRANSURANUS (HZDR). If the radial peak temperature stays longer in the outer part of the pellet, the average distance to the gap and the cladding is shorter and a steeper decrease in average fuel temperature and average fuel enthalpy can be expected from this. However, it is the opposite in Figure 15, potentially due to a higher impact of the gap width (cf. Figure 14) and (maybe) a lower fuel thermal conductivity.

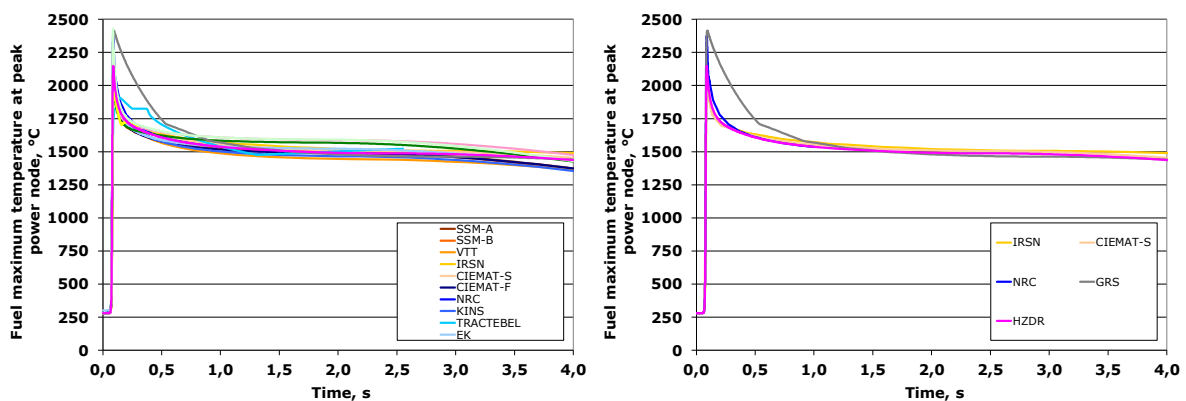


Figure 16: Fuel maximum temperature over time at peak power node (benchmark case #3). Left, results provided by all participants of the benchmark; right, selected results from the left side. [25]

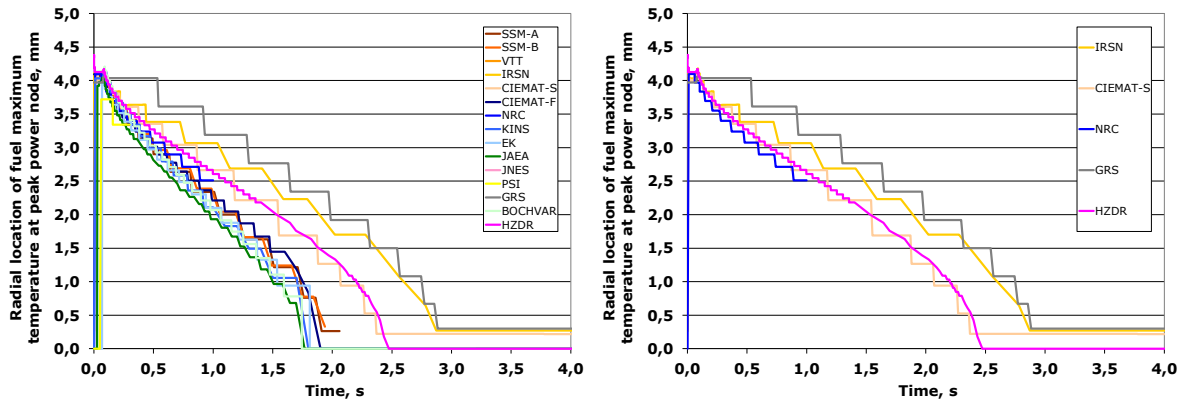


Figure 17: Radial location of the maximum of the fuel temperature over time at peak power node defined as distance from the centre of the pellet (benchmark case #3). Left, results provided by all participants of the benchmark; right, selected results from the left side. [25]

Clad outer temperature

The clad outer temperature as a function of time was provided in the benchmark specification for case #3. For the other cases the clad outer temperature depends on the modelling of the clad-to-coolant heat transfer in the used codes. Larger discrepancies were expected at least beyond DNB due to different modelling in the codes, e.g. in critical heat flux, critical temperature and clad-to-coolant heat transfer coefficients in the heat transfer regimes for transition, film boiling and rewetting (see subsection 2.2.2). This is caused by two main reasons: On the one hand, thermal hydraulic models in fuel performance codes and thermal hydraulics system codes (e.g. RELAP5 [124] was applied by UNIPI to calculate the thermal hydraulics conditions for TRANSURANUS) might not always take into account high kinetics effects occurring under RIA (cf. Figure 6). On the other hand, the thermal hydraulic models and codes are difficult to validate on RIA experiments representative for BWR and PWR conditions because of lack in experimental data. For example, the thermal hydraulics model in DYN3D [94] was validated on NSRR and IGR tests (see section 1.1).

For the case #2, assuming inhibition of boiling, differences larger than 500 K occurred already in maximum clad outer temperature (cf. Figure 18). Nevertheless, the clad outer temperatures of TRANSURANUS (HZDR) and SCANAIR (IRSN) differ less than 50 K over the whole time range. Unexpected differences among all codes were also observed in the case #1 performed in sodium (between lower and upper bound) where the maximum outer clad temperatures differ by more than ~350 K. Thence, the differences in this parameter are not limited to the coolant water.

Because the thermal hydraulics conditions can have a large impact on the fuel rod behaviour in the late phase of a RIA transient (cf. Figure 4) the modelling of clad-to-coolant heat transfer should be improved in both a) fuel performance codes (including transient thermal hydraulics modelling) and b) computer codes providing thermal hydraulics conditions to fuel performance codes (not including transient thermal hydraulics modelling). However, several institutions may not have access to data of thermal hydraulics experiments carried out for RIA, e.g. the out-of-pile PATRICIA experiments in France (see subsection 2.2.2).

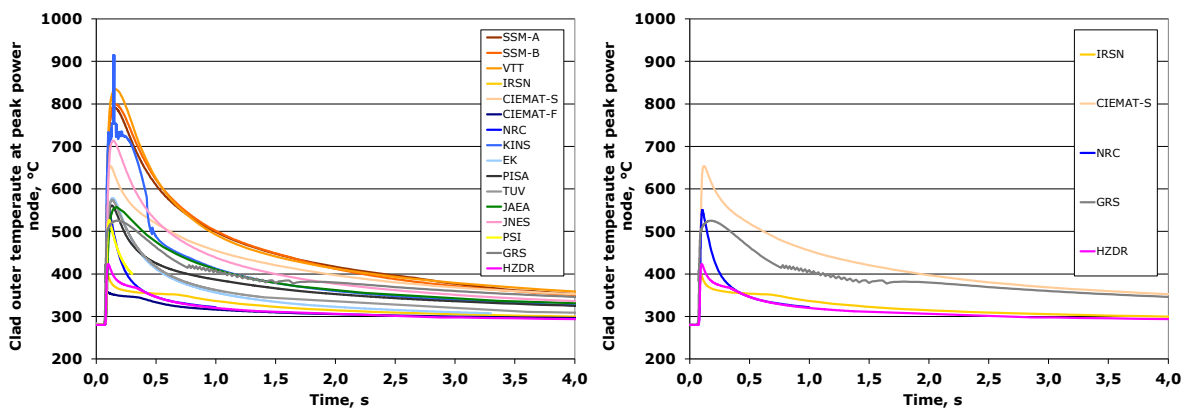


Figure 18: Clad outer temperature over time at peak power node (benchmark case #2). Left, results provided by all participants of the benchmark; right, selected results from the left side. [25]

3.3.4 Mechanical behaviour (comparison to other fuel performance codes)

Because of the obvious strong coupling between thermal and mechanical fuel rod behaviour, the TRANSURANUS capabilities to accurately model the mechanical behaviour during RIA are discussed in more detail.

Gap width

For case #3, the gap width predicted by TRANSURANUS (HZDR) shows the best agreement (among all participating codes) to SCANAIR (IRSN) and SCANAIR (CIEMAT-S). More precisely, this means the shape of the curve, the rapid increase after energy injection and the rapid decrease at the same time of quenching (cf. Figure 14). Note that, in spite of provided clad outer temperatures, SCANAIR (IRSN) determined a gap width of more than one order of magnitude higher than all other participating codes. As the gap width has a sensitive impact

on the heat transfer, the difference in gap width can have a larger feedback on the thermal fuel rod behaviour (see chapter 6 and subsection 3.3.3).

Outer fuel radius and inner clad radius

Both inner clad and outer fuel radius should be studied to analyse the differences in gap width. In case #3, the outer fuel radius will agree well between TRANSURANUS (HZDR) and SCANAIR (IRSN), if the initial radius at time 0 s (meaning at the beginning of the transient) takes on identical values (cf. Figure 19). Nevertheless, SCANAIR (IRSN) calculated still slightly greater values, presumably because the fuel gaseous swelling model in TRANSURANUS is developed for steady-state conditions (cf. Table 3 and see subsection 2.3.5). In case #1 TRANSURANUS (HZDR) underestimated more the outer fuel radius calculated by SCANAIR (IRSN) as might be expected from the case #3 (cf. Ref. [25]). At the same time the injected energy in the rodlet took on lower values for case #1 [25], hence the difference in the fuel gaseous swelling model cannot be the only reason for the discrepancy in the outer fuel radius. In contrary to case #3 the gap did not re-open in the TRANSURANUS (HZDR) calculation for case #1 until the end time of 2 s (in consistent to SCANAIR (IRSN)). Therefore, the outer fuel radius was influenced additionally by the cladding behaviour, whereas TRANSURANUS does not contain clad properties validated for RIA (see subsection 2.3.5).

For case #3, quantity and evolution of the inner clad radius calculated by TRANSURANUS (HZDR) are closest to the (systematically higher) values of SCANAIR (IRSN) and SCANAIR (CIEMAT-S), cf. Figure 20. These differences are larger than for the outer fuel radius (cf. Figure 19). The situation is similar for the inner clad radius in case #1, underlining the need for RIA-specific clad properties to be implemented in TRANSURANUS (see subsection 2.3.5).

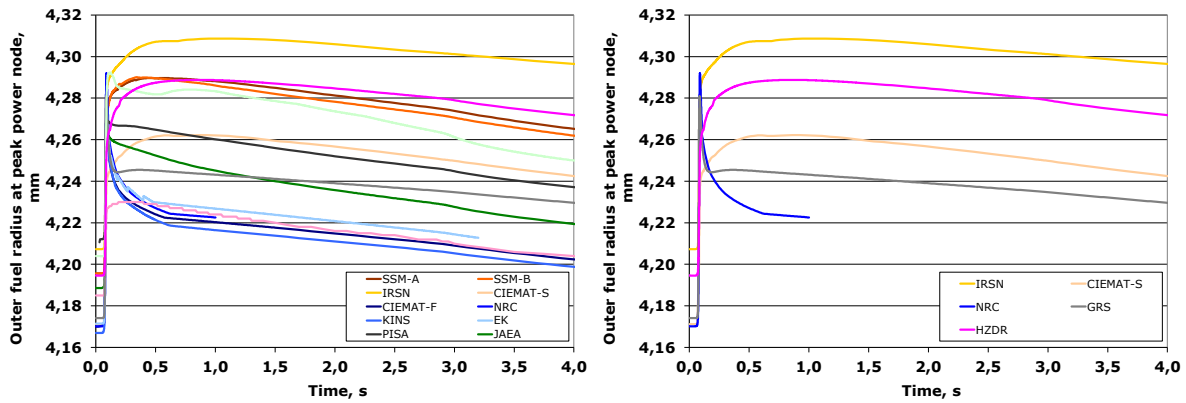


Figure 19: Outer fuel radius over time at peak power node (benchmark case #3). Left, results provided by all participants of the benchmark; right, selected results from the left side. [25]

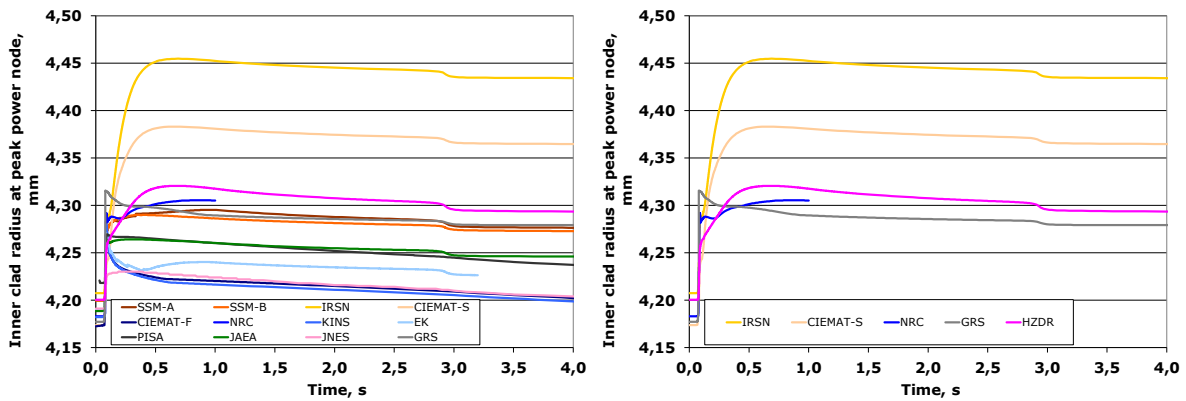


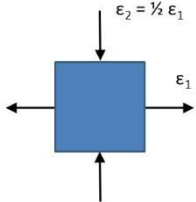
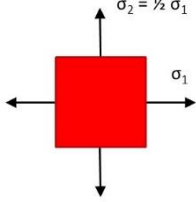
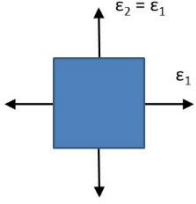
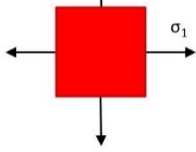
Figure 20: Inner clad radius over time at peak power node (benchmark case #3). Left, results provided by all participants of the benchmark; right, selected results from the left side. [25]

Outer clad permanent hoop strain

Several previous Figures in this chapter refer to the power peak node. Nevertheless many parameters vary along the test rodlet length, i.e. due to the axial power profile in the CABRI reactor [25]. The post-RIA outer clad permanent hoop strain represents one of the varying parameters. For this parameter good agreement can be seen between the experimental data and TRANSURANUS (HZDR) in the middle region of the test rodlet in case #1 (cf. Figure 21). However, TRANSURANUS (HZDR) overestimated considerably the clad permanent hoop strain profile at both the bottom of the rodlet and the top of the rodlet. This might be caused by the applied clad properties in TRANSURANUS. The implementation of clad properties for RIA is planned in the future (see subsection 2.3.5). Thence the best choice was to select material properties in TRANSURANUS for internal pressure loading under LOCA conditions [26]. In general, internal pressure loading refers to plane-strain tension conditions

with hoop strain of $\varepsilon_1 \neq 0$ and axial strain of $\varepsilon_2 = 0$ assuming isotropic plasticity [13] (cf. Table 9). However, especially case #1 is distinguished by PCMI (see subsection 2.2.1). The reason is the performing in sodium, hence without onset of film boiling in the late phase. If PCMI with perfect fuel-cladding bonding occurs as loading, the stress state will be characterized by equal-biaxial tension referring to $\varepsilon_2 = \varepsilon_1$ (cf. Table 9). As conclusion the clad permanent hoop strain was simulated assuming internal pressure loading instead of equal-biaxial tension, hence TRANSURANUS (HZDR) had to calculate too high values for the strain in the direction of ε_1 because $\varepsilon_2 = 0$ instead of $\varepsilon_2 = \varepsilon_1$.

Table 9 – States of stress relevant to the mechanical testing for RIA (assuming isotropic plasticity) [13]

State of stress	Strain	Stress
Uniaxial tension		
Plane-strain tension		
Equal-biaxial tension		

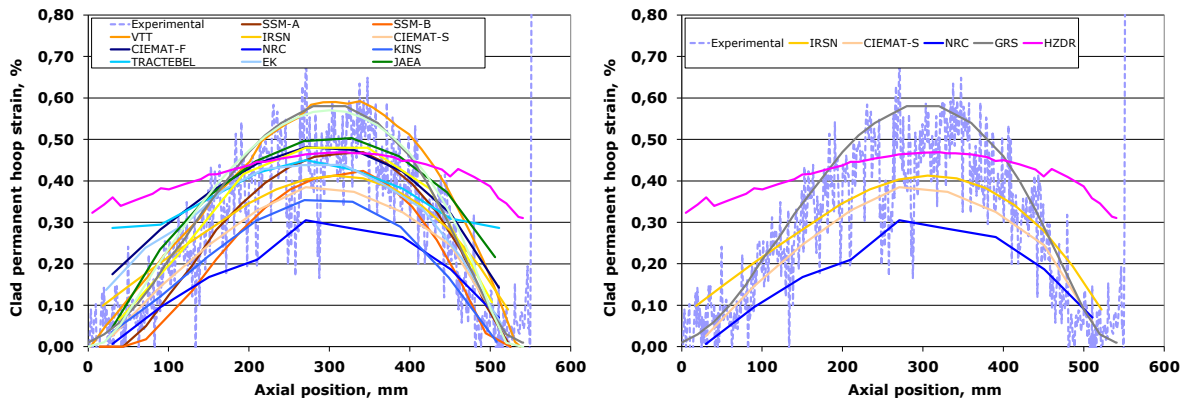


Figure 21: Outer clad permanent hoop strain at the end of the transient as a function of height with respect to the bottom of fissile column (benchmark case #1). Left, experimental data and results provided by all participants of the benchmark; right, experimental data and selected results from the left side. [25]

The explanation for the overestimation in Figure 21 is confirmed by the clad permanent hoop strain calculated for case #2. More precisely, the cladding of this case is mostly forced by internal pressure loading due to onset of film boiling (see subsection 2.2.2). Thence the clad is forced by plane-strain tension as stress state (cf. Table 9). Material properties exist in TRANSURANUS for this kind of loading (validated for LOCA conditions), and were taken for this benchmark case. Therefore, TRANSURANUS (HZDR) determined a clad permanent hoop strain profile close to the one of SCANAIR (IRSN) for case #2, but underestimated it slightly (cf. Figure 22). One reason for this difference to SCANAIR might be the lack of a transient fission gas release model in TRANSURANUS (cf. Table 3). This can lead to a lower internal pressure loading than in SCANAIR (IRSN). A second reason might be again the applied clad properties in TRANSURANUS validated for internal pressure loading, but for the conditions occurring during LOCA (see subsection 2.3.5). More precisely, the flow behaviour of cladding depends on strain, strain rate and stress rate [13]. Nevertheless, the results of TRANSURANUS (HZDR) closely match the one of SCANAIR (IRSN) in Figure 22, compared to the results of the other benchmark participants.

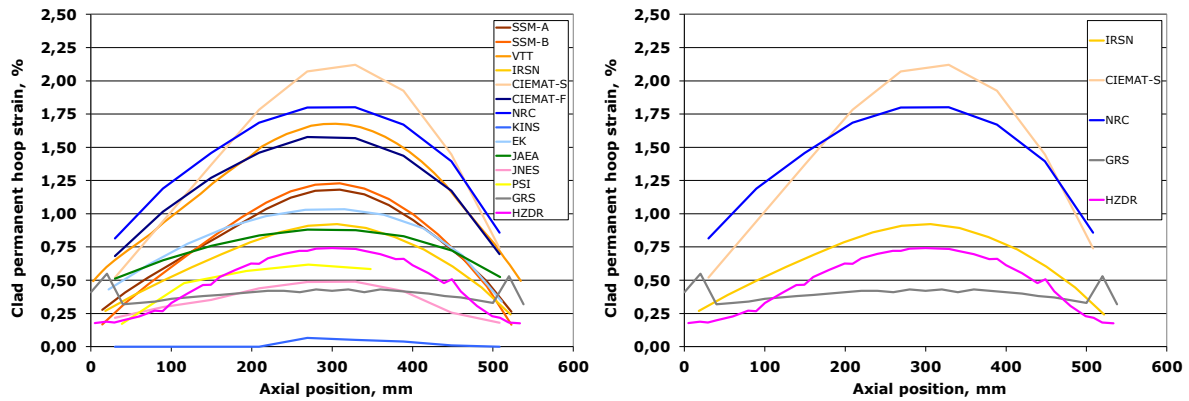


Figure 22: Outer clad permanent hoop strain at the end of the transient as a function of height with respect to the bottom of fissile column (benchmark case #2). Left, results provided by all participants of the benchmark; right, selected results from the left side. [25]

Total axial cladding elongation

The total axial clad elongation in the case #1 (caused by PCMI meaning stress state equal-biaxial tension, cf. Table 9) was underestimated by TRANSURANUS (HZDR). More precisely, TRANSURANUS (HZDR) determined around half of the online measured values (cf. Figure 23). In contrary, SCANAIR (IRSN) predicted values close to the experimental data. According to the case #2 the total axial clad elongation (mostly caused by internal pressure loading meaning stress state plane-strain tension) was also underestimated by TRANSURANUS (HZDR). Furthermore, this underestimation in case #2 was more pronounced than for the clad permanent hoop strain.

Referring to Table 9 the underestimations in total axial cladding elongation can be explained by the thin shell theory (see subsection 2.3.3) and Levy-Mises theory [136] of plasticity in isotropic models. Analysing it theoretically on behalf of this theories, the ratio of plastic axial strain to plastic hoop strain amounts the value zero for plane-strain tension (internal pressure loading during opened gap conditions) and the value one for equal-biaxial tension (PCMI with perfect bonding during closed gap conditions) [13]. As already mentioned the transient clad properties in TRANSURANUS are limited to plane-strain tension, hence the ratio is always – considered theoretically – zero (meaning plastic axial strain equal zero). Therefore, the axial strain component was underestimated by TRANSURANUS for PCMI conditions. Because case #2 is characterized by both stress states (gap re-opening at 1.5 s [25]), there was observed also an underestimation in case #2.

If clad properties for RIA were implemented in TRANSURANUS, gap re-opening should be taken into account. On the one side, this means TRANSURANUS should be capable to model two different stress states during the devolution of one RIA transient (see previous paragraph). On the other side, this gap re-opening indirectly influences the internal pressure loading. More precisely, gap re-opening allows transient fission gas release/burst release into the free volume [137].

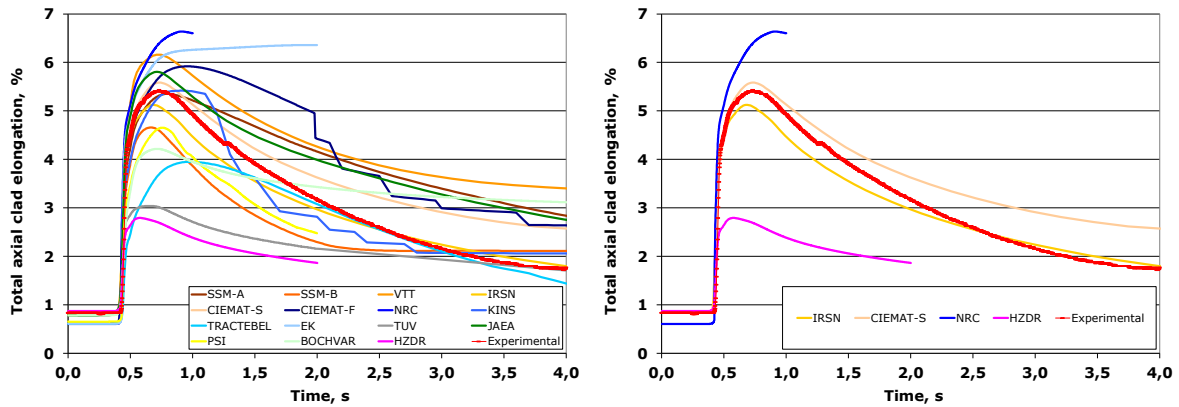


Figure 23: Total axial clad elongation containing thermal, elastic and plastic components with respect to cold state conditions over time (benchmark case #1). Left, experimental data and results provided by all participants of the benchmark; right, experimental data and selected results from the left side. [25]

3.4 Summary and recommendations for future work

As so far only a limited number of RIA tests were performed on highly irradiated fuel rods. Thence, the participation in the OECD RIA Fuel Codes Benchmark (2011/2012) represented a good opportunity to evaluate the performance of the RIA version of TRANSURANUS that is still under development. RIA tests more representative for PWR conditions will be performed in the OECD CABRI Water Loop Project in the future.

According to the benchmark the TRANSURANUS results showed a very good agreement in injected energy, variation of enthalpy, central fuel temperature, maximum fuel temperature and location of the maximum fuel temperature. An accurate prediction of the thermal fuel rod behaviour during RIA is essential for successful replacement of a simplified fuel behaviour model in a reactor dynamics code through a two-way coupling to a state-of-the-art fuel performance code. At the end this will allow great degree in detail in online fuel behaviour

modelling in this coupled code system (see chapter 6). Furthermore, TRANSURANUS possesses a stable numerical behaviour which is an important requirement for simulating very narrow but high power pulses occurring in RIA.

Nevertheless, the modelling of the mechanical behaviour for RIA conditions should be improved in TRANSURANUS. While axial elongations of fuel stack and cladding were underestimated, TRANSURANUS showed a better agreement for the stress state plane-strain tension (typical for internal pressure loading). This is caused by a lack of clad properties for the stress state equal-biaxial tension (typical for highly irradiated fuel rods in the early RIA phase). Therefore, the applied clad properties are validated on internal pressure loading, even only validated for LOCA conditions. Furthermore, TRANSURANUS does not contain a transient fission gas release model what might lead to lower internal pressure loading.

A transient fission gas release model and a more detailed plenum temperature model for TRANSURANUS are currently under development. The gaseous swelling model has to be extended to the more rapid conditions under RIA. Finally, clad properties including a failure criterion should be implemented in the RIA version of TRANSURANUS (see subsection 2.3.5). Regarding computer programmes providing the thermal hydraulics conditions to TRANSURANUS, their thermal hydraulics modelling should be improved further. In parallel to this development work, TRANSURANUS can be further evaluated when it will be applied in upcoming international benchmarks. This can give valuable information for defining future development tasks.

4 Improved modelling of high burnup structure in the TRANSURANUS code

Over the last few decades there has been a tendency to increase the discharge burn-up of nuclear fuels. After extended residence times in a reactor, the nuclear fuel develops a so-called HBS that is characterised by the depletion of fission gas in the fuel matrix and the development of micron-sized porosity surrounded by sub-micron-sized grains [27, 33] (see section 2.1). The HBS is of special interest because it may limit the productive life of fuel [31, 35] and has an important potential effect on fuel behaviour during DBA such as RIA. The RIA stress state and the related cladding response depend strongly on the fuel burn-up [13]. For example, PCMI becomes more important with higher burn-up [24] as the fission gas filled pores in the HBS extend rapidly due to a sharp temperature increase and peaked radial temperature profile at the fuel periphery during a RIA.

It is important to properly account for the increase of the discharge burn-up of commercial nuclear fuel in fuel performance codes like TRANSURANUS [60], which is used in the EU by research organisations, safety authorities and industry. Despite the many publications about the HBS made until now, there are still open questions about its formation mechanisms [39], as well as its consequences on the fuel behaviour such as fission gas release [138], e.g., during DBA (cf. Figure 2). More precisely, there remains uncertainty about the exact conditions under which the HBS forms [27, 28]. Ref. [27] was cited in different models that describe the HBS formation at an engineering level, i.e., in fuel performance codes, as a function of the local burn-up alone. The scatter in local burn-up values at which the HBS starts to form is expected to be affected by the local temperature [139], since defect annealing is supposed to inhibit HBS formation. In line with this idea, Khvostov et al. [140, 141] recently proposed a model for describing both the formation, development and behaviour (fission gas release and swelling) of the HBS in a fuel performance code as a function of the so-called ‘effective burn-up’. The latter was defined as a temperature dependent burn-up value, considering that when the local temperature exceeds a given threshold, there is no further accumulation of defects that could contribute to the HBS formation, hence there is no further increase in the effective local burn-up value that is used in a HBS model. Nevertheless, as will be pointed out in this chapter, the predicted upper threshold temperature of 800 °C is in disagreement with the experimental temperature threshold of Kinoshita et al. [142], and can be overcome by the model presented in this chapter.

In this chapter, the experimental data of high burn-up fuel in the section 4.1 (not measured in the frame of this work) are complemented by a multi-physics simulation. More precisely, the fission product behaviour was simulated by means of a sub module of TRANSURANUS fuel performance code. Based on the in-pile temperature measurements and radial Xe profiles obtained from post-irradiation examinations, a model could be created for fuel performance codes to assess the threshold burn-up and temperature for the formation of the HBS on the basis of the Xe depletion, as described in the section 4.2. The subsequent section 4.3 discusses the effect of parameters such as the temperature and Xe yield on this threshold burn-up. In the last section 4.4, we summarise our findings and suggest refinements to future experiments and to modelling of the HBS formation. This chapter 4 is taken from Ref. [20].

4.1 Experimental data of high burn-up fuel (High Burnup Rim Project)

In the frame of the HBRP⁸, the formation of the HBS was studied in greater detail for a better understanding of the threshold conditions and the processes and mechanisms involved. The experiment also allowed the investigation of physical and chemical properties of the fuel after restructuring. Given the large gradients of radial burn-up and temperature distributions in fuel rods [39], the fuel was fabricated in discs that were separated by molybdenum discs from each other in the stack. The UO₂ discs of diameter 5 mm, thickness 1 mm, ²³⁵U enrichment 25.8 wt.% and fabricated grain size of 9.7 µm were irradiated in a gas flow rig in the Halden Boiling Water Reactor. The test rig contained four rods each comprising four fuel stacks. The fuel stacks of each rod were irradiated to different final burn-ups under temperatures nearly identical and constant over time [142]. The fuel temperature was held nearly constant over the irradiation and was controlled by a change in fill gas composition (He/Ar ratio). The achieved burn-up, measured by chemical and γ-spectroscopy analyses, and calculated average disc temperature (based on thermocouples) of each fuel stack are summarised in Figure 24 and in Table 10 for all fuel stacks. The UO₂ discs containing no Gd or additives are subject of this chapter.

⁸ HBRP was initiated by CRIEPI, TEPCO and JRC-ITU, and was co-sponsored by CRIEPI, Japanese utilities, Mitsubishi Heavy Industries, Nippon Nuclear Fuel Development Corporation, Nuclear Fuel Industries, Electricite de France, ABB Atom AB, Swedish Nuclear Power Inspectorate and Swedish utilities, Electric Power Research Institute of USA, IFE of Norway, and was carried out in co-operation with IFE and JRC-ITU Karlsruhe.

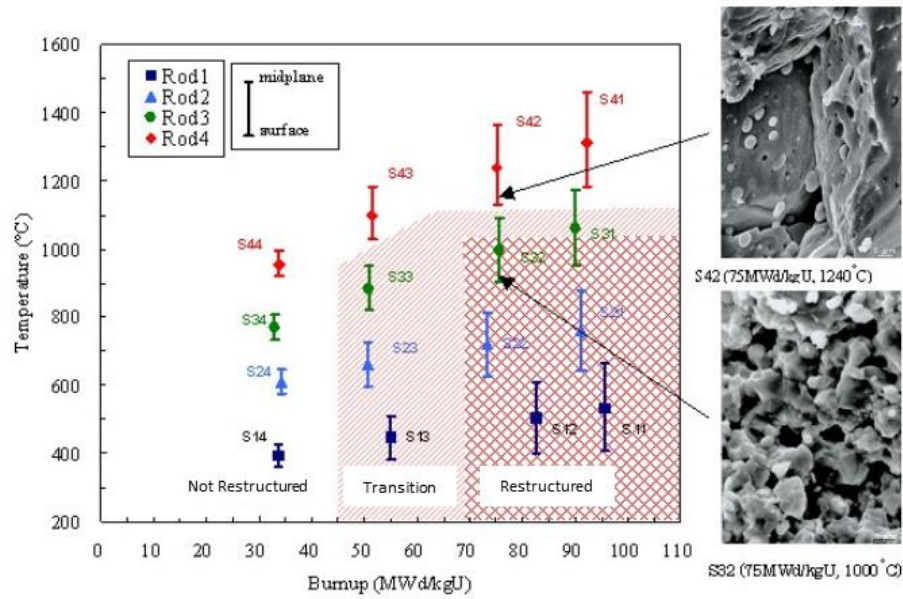


Figure 24: Burn-up and average irradiation temperature of the 16 stacks of HBRP. The extremes represent the temperature difference between the surface and the centre of the discs, obtained by a finite element calculation [142]

Table 10 – Burn-up and calculated temperature at end of life (EOL) reached for the 16 stacks [142]

	Rod 1	Rod 2	Rod 3	Rod 4
Stack 1	S11	S21	S31	S41
Burn-up [MWd/kgU]	96	91	90	92
U1~U2 [°C]	666~604	877~832	1175~1118	1460~1378
U3~U4 [°C]	459~408	693~643	996~949	1227~1182
Average Temp. [°C]	530	760	1060	1310
Stack 2	S12	S22	S32	S42
Burn-up [MWd/kgU]	82	73	75	75
U1~U2 [°C]	609~565	811~776	1089~1043	1365~1294
U3~U4 [°C]	446~401	664~626	942~905	1167~1131
Average Temp. [°C]	510	720	1000	1240
Stack 3	S13	S23	S33	S43
Burn-up [MWd/kgU]	55	51	51	51
U1~U2 [°C]	512~488	728~702	951~917	1183~1134
U3~U4 [°C]	414~382	625~599	845~820	1053~1029
Average Temp. [°C]	450	660	880	1100
Stack 4	S14	S24	S34	S44
Burn-up [MWd/kgU]	34	34	33	34
U1~U2 [°C]	425~414	647~631	808~788	995~969
U3~U4 [°C]	380~360	590~574	750~734	935~920
Average Temp. [°C]	400	610	770	950

4.2 Temperature dependent modelling of the Xe depletion

4.2.1 New standalone Xe depletion model

In the TRANSURANUS fuel performance code, the formation of the HBS is simulated as part of the TUBRNP model [27], which describes the evolution of the major fuel constituents. As far as Xe is concerned, a rate equation is implemented, assuming the depletion from the fuel matrix to be dependent on the local burn-up [27]:

$$\frac{dXe}{dbu} = -a * Xe + \dot{c}_{Xe} \quad (10)$$

where Xe is the local xenon concentration, \dot{c}_{Xe} is the xenon creation rate and a is a fitting constant. An integration of this equation [27] yields to:

$$Xe(bu) = \dot{c}_{Xe} \left[\frac{1}{a} + \left(bu_0 - \frac{1}{a} \right) e^{-a(bu-bu_0)} \right] \quad (11)$$

For the onset of the depletion mechanism, TUBRNP applies a local threshold burn-up (bu_0) between 60 and 75 GWd/tU. After fitting to experimental data, the above equation leads for an infinite local burn-up to an asymptotic Xe concentration of 0.25 wt.%. Depending on \dot{c}_{Xe} the fitting constant a in the TUBRNP model was calculated to be 7.0×10^{-5} t/(MWd).

According to a recent review of Baron et al. [39], the HBS transformation mainly depends on the local burn-up, while secondary effects arise from local temperature, instantaneous fission density, local density of fission products, initial grain size, local fuel constraint, initial additives and local oxygen potential. The influence of the restraint pressure has been separately studied by Une et al. [143] comparing discs irradiated without any restraint pressure in the JRR-3 test reactor to Halden Boiling Water Reactor pellets with large PCI restraint. The study found no significant influence of the restraint pressure on the Xe depletion. In this context the chosen HBRP discs represent an appropriate database (similar initial grain size, no initial additives) that allows the influence of the fuel temperature on the onset of the Xe depletion to be studied over a wider range of burn-up values and temperatures.

In order to account for the effect of the temperature on the restructuring, an approach has been proposed by Khvostov et al. [140, 141], expressing the restructuring based on the Kolmogorov-Johnson-Mehl-Avrami (KJMA) [144-147] generic correlation in dependence of the effective burn-up. His approach was inspired by that of Kinoshita [148], who also suggested the KJMA correlation, although he formulated it in dependence of the burn-up:

$$\varepsilon_s = 1 - \exp \left[-k_d \left(\frac{bu_{eff}(t)}{bu_{eff0}} \right)^3 \right] \quad (12)$$

where ε_s is volumetric ratio of the restructured domain, k_d is the factor taking into account the effects of the initial fuel structure ($k_d = 1.0$ for normal fuel or $k_d \approx 0.5$ for large-grained fuel [140]), bu_{eff} is the effective burn-up, bu_{eff0} is a reference value of the effective burn-up ($bu_{eff0} = 7.3\%$ FIMA [140]). The increment of the effective burn-up bu_{eff} is defined as [140]:

$$\Delta bu_{eff} = \begin{cases} \Delta bu, T \leq T_1 \\ f(T) * \Delta bu, T_1 < T < T_2 \\ 0, T \geq T_2 \end{cases} \quad (13)$$

where T is the local fuel temperature expressed in $^{\circ}C$, Δbu is the considered burn-up increment and $f(T)$ is a factor specifying the temperature influence in the range of partial defect healing in Khvostov's model:

$$f(T) = \frac{T_2 - T}{T_2 - T_1} \quad (14)$$

T_2 marks the temperature limit for complete healing of defects, and T_1 is the onset-temperature for partial healing. In Ref. [140], these limits were set to $T_1 = 380^{\circ}C$ and $T_2 = 800^{\circ}C$.

The temperature thresholds of Khostov et al. are fairly low with respect to the temperatures for point defect annealing in UO_2 obtained from differential scanning calorimetry that indicates defect annealing until temperatures around 1300 K [149]. One also notices a clear discrepancy between the value of T_2 and the threshold temperature of $1100^{\circ}C$ from HBRP [142]. In view of this and because of the limited number of temperature levels considered in HBRP (see Figure 24), the definition of the effective burn-up was further simplified in this

paper by applying a ‘Heaviside step function’ without any temperature transition zone in the factor $f(T)$ in Eq. (13):

$$f(T) = \begin{cases} 0, & T > T_{thres} \\ 1, & T \leq T_{thres} \end{cases} \quad (15)$$

where T_{thres} is the temperature threshold in °C and T is the local fuel temperature in °C.

Khvostov et al. introduced the idea of applying the effective burn-up in order to explain both the experimental scatter in the matrix Xe concentration as function of the local burn-up by the local fuel temperature, and the influence of the temperature on the high burn-up restructuring. To that end, they compared the effective burn-up and its temperature thresholds T_1 and T_2 to the experimental data used earlier for deriving Eq. (11) [27], experimental data of standard LWR high burn-up fuel [19], a few experimental points from discs of the HBRP [142], experimental data about the influence of grain size on Xe matrix depletion in HBS [150] and specific fuel porosity in the pellet rim-zone [151]. However, the value of 800 °C for T_2 is in disagreement with the temperature threshold of 1100 °C from HBRP [142].

4.2.2 Implementation of the Xe depletion model in TRANSURANUS

For a quantitative analysis of the influence of the fuel temperature on Xe depletion, the TRANSURANUS fuel performance code was reduced to a ‘point version’ that is run separately for each location in radial and axial direction. The local values of burn-up and fuel temperature are input as a function of time. The model thus accounts for the creation of the fission products and actinides via TUBRNP (adapted to the experimental conditions of the HBRP), and the matrix Xe depletion in the HBS described above. The TRANSURANUS ‘point version’ was integrated in a fitting environment that allows analysis of the matrix Xe depletion and its dependence on the temperature thresholds in Eqs. (14) and (15).

The best-fit parameters were found iteratively by minimization of the merit function χ^2 :

$$\chi^2(a) = \sum_{k=1}^N \left[\frac{y_k - y(x_k, a)}{\sigma_k} \right]^2 \quad (16)$$

where N is the number of data points, x_k and y_k define the data point with index k , σ_k is the related experimental uncertainty (e.g., the standard deviation), and a summarises all fitted parameters of the correlation $y(x_k, a)$. In the present work we thus obtain a nonlinear model with two unknown parameters arising from the Xe depletion model: the effective burn-up threshold bu_{eff0} and the temperature threshold T_{thres} (as part of the definition of the effective burn-up). For the fitting procedure, the Levenberg–Marquardt method [152] was used.

4.3 Results of the sensitivity analysis

4.3.1 Impact of threshold burn-up

The experimental data used to infer the dependence of the retained Xe on the local burn-up according to Eqs. (10) and (11) came from fuel samples from different reactors, vendors and fuel designs [27]. This variety of conditions was assumed to cause the scatter in measured Xe concentration. A pronounced scatter occurs at the beginning of depletion and makes it difficult to find a precise value for the threshold burn-up.

Figure 25 shows the Xe concentrations measured in the HBRP discs as a function of the local burn-up. The data of Figure 25 can be satisfactorily described by the existing Xe depletion model [27], apart from the fact that the threshold burn-up (bu_0) is considerably lower – between 45 and 60 GWd/tU, and that the Xe yield is overestimated. It should be noted that for some discs in the restructured zone the measured fuel fragments could not be attributed to their original radial locations during the irradiation, as the discs had broken into pieces or disintegrated to powder. Moreover, the discs with high burn-up and high temperatures showed partial fragmentation, and in such cases a radially averaged burn-up was used. This approach is justified because the measured radial Nd profiles across the discs are nearly flat and are directly linked to the radial burn-up profiles (e.g., for a disc of the fuel stack S13 with an average disc burn-up of 55 GWd/tU: the ratio of the local burn-up over the average disc burn-up is 0.93 in the centre and 1.15 in the periphery), implying a very small radial gradient of the fission rate density (power profile). Conversely, the standard fuel rod geometry in previously analysed datasets leads to a considerable radial gradient of the fission rate density in the rim zone (e.g., for a PWR fuel pellet with an ^{235}U enrichment of 4.1 wt.% and average pellet burn-

up 50 GWd/tU: the ratio of the local burn-up over the average pellet burn-up is 0.90 in the centre and 2.05 in the periphery), implying a larger uncertainty of the local burn-up and of the Xe content [39].

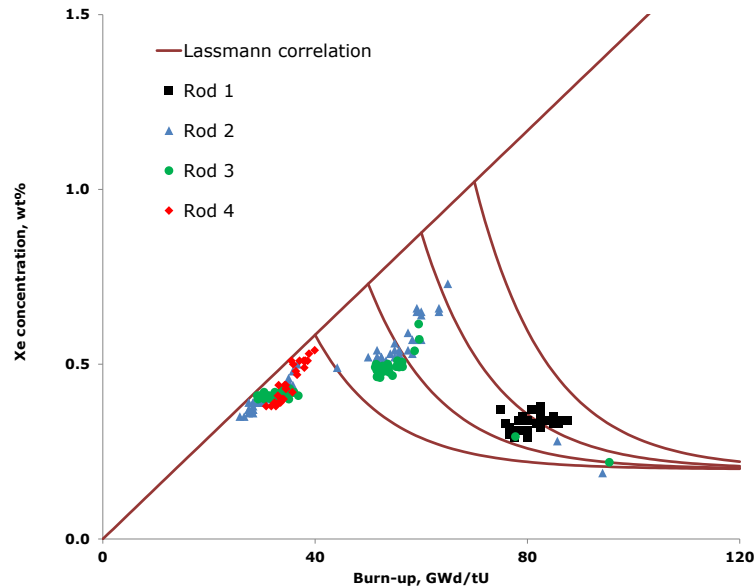


Figure 25: Comparison between predicted and measured local xenon concentrations as a function of the local burn-up for data from HBRP. The prediction is based on the depletion model in Ref. [27] with the threshold burn-up varied between 40 and 70 GWd/tU in steps of 10 GWd/tU. Rod numbering corresponds to the numbering in Figure 24.

A preliminary analysis of HBS formation in heavy water reactor (HWR) UO_2 fuel by Walker et al. [28] confirms that the restructuring appears at a local burn-up above 70 GWd/tU and requires a local temperature below 1200 °C, i.e., in line with the temperature threshold of 1100 °C found from the HBRP discs [142]. However, Une et al. [143] reported burn-up thresholds similar to those revealed in Figure 25. They were derived from discs with enrichments of 10.0 and 19.8 wt.% ^{235}U , irradiated in the JRR-3 test reactor in Japan. There is thus a difference between the burn-up threshold for Xe depletion found by Lassmann et al. [27] (60–75 GWd/tU), and the range seen from the HBRP data in Figure 24 (45–70 GWd/tU), as well as for the onset of depletion around 51 GWd/t reported by Une et al. [143].

4.3.2 Impact of threshold temperature

Regarding the influence of the fuel temperature on the threshold burn-up for the HBS formation, only rough quantitative estimates are available so far. Spino et al. [29] mentioned a temperature threshold around 1200 °C. No HBS formation was seen above this temperature, and the threshold should also affect the Xe depletion. We have therefore refined the quantitative analysis of the temperature threshold for HBS formation, by applying the TRANSURANUS ‘point version’ described in subsection 4.2.2 to the experimental conditions of the HBRP.

As a first step in the sensitivity analysis, the (fixed) temperature thresholds T_1 and T_2 as suggested by Khvostov et al. [140] were tested in combination with various fixed values for the effective burn-up threshold (Table 11). The parameter a in Eqs. (10) and (11) was also fixed because, together with the Xe creation rate \dot{c}_{Xe} , it defines the asymptotic value of Xe [27]. The resulting values of the merit function χ^2 (Eq. (16)) are compiled in Table 11, assuming a standard deviation σ_k of 10% for all Xe measurements of the HBRP.

Table 11 – Values of the merit function χ^2 for temperature values given in Ref. [140]

bu_{eff0} [GWd/tU]	T_1 [°C]	T_2 [°C]	χ^2 [-]
40.00	380	800	7784
50.00	380	800	7838
60.00	380	800	10903

In the next step, the above described new Xe depletion model was used to minimize the merit function by fitting the temperature threshold together with the effective burn-up threshold – again applying a fixed constant a . For the temperature factor $f(T)$ a Heaviside step function was applied (Eq. (15)) instead of the linear function in Ref. [140]. The standard deviation σ_k was again set to 10% of the measured value for each datapoint. The resulting fitted parameters (Table 12) lead to a considerable improvement of the merit function (i.e., reduction). The error band σ_{stand} given for each fitted parameter is related to a 68% confidence interval.

Table 12 – Values of the fitted parameters bu_{eff0} and T_{thres} with 68% confidence intervals.

bu_{eff0} [GWd/tU]	$\sigma_{stand}(bu_{eff0})$ [GWd/tU]	T_{thres} [°C]	$\sigma_{stand}(T_{thres})$ [°C]	χ^2 [-]
49.22	± 0.21	1049	± 17	535

The fitted temperature threshold is in good agreement with the range $(1100 \pm 100)^\circ\text{C}$ derived from the experiment [142]. It is also consistent with Walker's work [28], which pointed out that the HBS may form in a pellet up to a local fuel temperature of 1200°C – albeit for average cross-sectional burn-up values between 70 and 80 GWd/tU.

The fitted effective burn-up threshold lies in the experimentally observed range (cf. Figure 24 and Figure 25). According to Ref. [142], restructuring in the HBRP discs starts at local burn-up between 51 and 55 GWd/tU and is in agreement with the observations of Une et al. [143] on other discs. Because in most of the discs the above fitted temperature threshold was not exceeded, the burn-up values in Figure 25 (x-axis) would hardly be modified when transforming them to the effective burn-up, and the threshold values for burn-up and effective burn-up are very similar. It is obvious that the effective burn-up defined in Eq. (13) will only affect (improve) the modelling of HBS formation for local temperatures higher than approximately 1100°C .

Attention is drawn to the scarcity of available Xe measurements in the 'sensitive' region of the burn-up and temperature threshold (cf. Figure 24). Therefore, the effective burn-up was formulated as a Heaviside step function of the local temperature. However, the high burn-up restructuring and the Xe matrix depletion are characterized by a transition zone that should eventually lead to a small temperature impact persisting below 1100°C , for which more experimental data are required.

4.3.3 Impact of Xe yield

The experimental uncertainty of the EPMA signal and the temperature impact on the HBS cannot fully explain the onset of Xe depletion at different burn-ups in Figure 25. A closer analysis of the low burn-up range in this figure reveals a different average value of the slope of the Xe production before the onset of depletion, i.e., when fission products only

accumulate in the matrix (at low temperature). This over prediction points to the need to analyse the influence of the Xe creation rate itself. This idea is corroborated by the observation that the above mentioned highly enriched disc irradiations induce local variations in the neutron spectrum, which in turn affect the fission product yields.

In order to assess the effect of the Xe yield, the original value used in TUBRNP for a fuel rod in the Halden Boiling Water Reactor (not adapted to HBRP, hence differing from the value used for Table 12) was decreased by a constant factor. The results are summarized in Table 13, showing that on the one side the temperature threshold is almost constant; on the other side the (effective) burn-up is sensitive to the Xe yield. A 20% reduction of the Xe yield for fitting of the Xe data in the HBRP discs leads to local (effective) burn-up threshold values that are in line with those reported in the open literature for LWR fuel rods.

Table 13 – Values of the fitted parameters bu_{eff0} and T_{thres} with their standard errors (dependence on Xe creation rate).

Xe yield [%]	bu_{eff0} [GWd/tU]	$\sigma_{stand}(bu_{eff0})$ [GWd/tU]	T_{thres} [°C]	$\sigma_{stand}(T_{thres})$ [°C]	χ^2 [-]
100	48.45	±0.22	1067	±71	552
90	57.13	±0.34	1067	±53	661
80	62.95	±0.38	1072	±46	411

4.4 Summary and recommendations for future work

In this chapter experimental data from HBRP (not measured in the frame of this work) are presented providing a basis for a sensitivity study aimed at characterizing the burn-up threshold and temperature limit as main parameters controlling the formation and extension of the HBS observed in nuclear fuels. In HBRP, discs of UO₂ enriched to 25.8% ²³⁵U were irradiated in the Halden Boiling Water Reactor at nearly constant and uniform temperatures between 400 and 1310 °C up to burn-up levels ranging from 35 to 100 GWd/tU, and subjected to extensive PIE. The results presented here focus on measurements of retained Xe by EPMA.

The experimental study is complemented by a multi-physics analysis. The Xe measurements have been re-analysed on the basis of the model for Xe depletion of Lassmann et al. [27] the TRANSURANUS code, which only considers the local burn-up value as a threshold parameter, and by means of the model of Khvostov et al. [140, 141], that uses the effective burn-up. Comparing both models with the EPMA data presented in this study revealed that the temperature levels applied in the model of Khvostov et al. are in disagreement with experimental observations, whereas the model of Lassmann et al. [27] was successfully extended to account for both temperature and burn-up following the idea of Khvostov [140, 141]. More precisely, the effect of both parameters was introduced in this model by means of a Heaviside step function. The fitting of the model on the basis of the HBRP data showed that the HBS forms at a local burn-up level exceeding 49 ± 0.2 GWd/tU and at temperatures below 1049 ± 17 °C. The temperature threshold is in agreement with the value reported in the open literature [28]. The local burn-up value is consistent with the observations of Une et al. [143] on highly enriched UO₂ discs, but is in disagreement with those on the basis of commercial fuel rods, according to which the HBS forms at local burn-up levels between 70 and 80 GWd/tU [28]. These differences cannot be attributed to experimental uncertainties alone.

Since HBS formation occurs gradually, it is expected that instead of applying Heaviside step functions for the burn-up and temperature levels, transition functions based on the KJMA approach could provide a refinement of the models for HBS formation implemented in fuel performance codes. Nevertheless, this would require more accurate experimental data from discs irradiated under conditions close to the transition.

5 Development of the general TRANSURANUS coupling interface

More than two decades ago TRANSURANUS was coupled to the European Accident Code EAC-2 for LMFBR [116] (see section 2.5). Nevertheless, at the beginning of this work no full two-way coupling approach has so far been reported in the open literature for calculating a whole LWR core online with detailed and well validated fuel behaviour correlations. TRANSURANUS is well suited for the requirements for a successful coupling also in case of challenging transient conditions: high numerical stability, numerical robustness, low computation time, applicable time scales from milliseconds to years in the same simulation, and the feasibility to simulate complex fuel behaviour scenarios and irradiation experiments (see chapter 3). Thence recently, the coupling of various thermal hydraulics codes and reactor dynamics codes containing simplified fuel behaviour models to TRANSURANUS has been discussed e.g. by Gesellschaft für Anlagen- und Reaktorsicherheit (GRS) for its thermal hydraulics system code ATHLET [153], by Karlsruhe Institute of Technology (KIT) for its sub-channel thermal hydraulics code KTF [154], and by Helmholtz-Zentrum Dresden-Rossendorf (HZDR) for its reactor dynamics code DYN3D (cf. Figure 2). Each of these planned couplings is based on TRANSURANUS as underlying fuel performance engine in the coupled code system (cf. Figure 26).

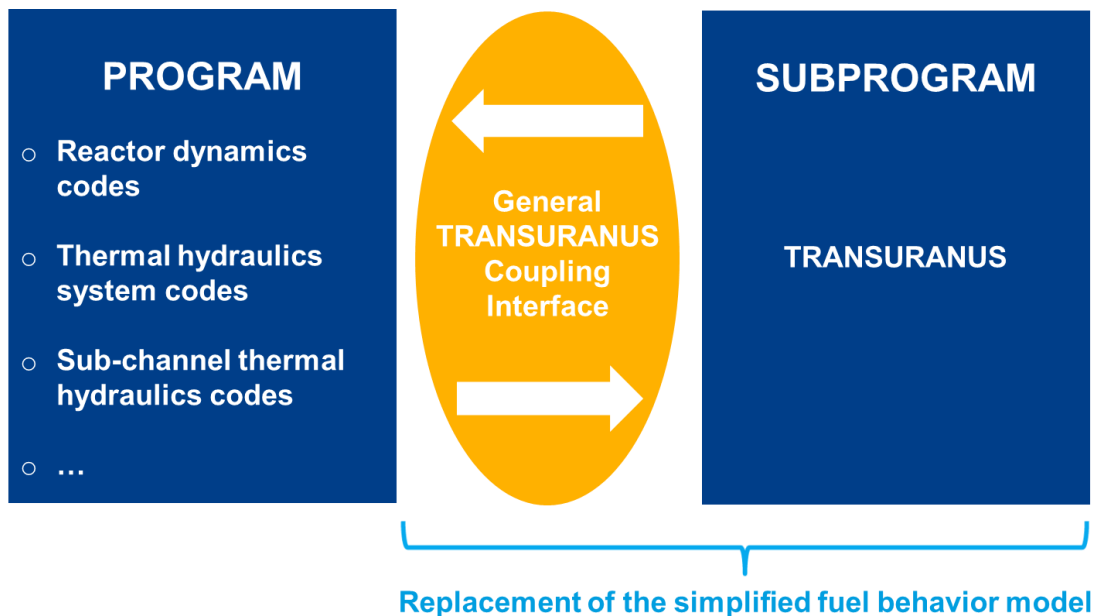


Figure 26: Main principle of the general TRANSURANUS coupling interface, whereas one fuel rod is calculated per call of the interface.

On this basis and in close cooperation between HZDR and the TRANSURANUS developers group at JRC-ITU, it was decided to develop a general TRANSURANUS coupling interface and to implement modifications in the TRANSURANUS code that could be generally used for future code couplings. For example, DYN3D should be easily replaceable by any other code in the coupled code system DYN3D-TRANSURANUS (cf. Figure 26). The behaviour of one fuel rod is calculated per call of the coupling interface. Both integral parts (in Figure 26) are often named together as “general TRANSURANUS coupling interface” in this thesis. The sections 5.1 and 5.2 are (partly) taken from Ref. [10, 120].

5.1 Main features

5.1.1 One-way and two-way coupling

State-of-the-art safety analyses are still often performed by means of step-by-step standalone simulations using a reactor dynamics code/thermal hydraulics code for calculation and providing time-dependent boundary conditions to the fuel performance code and then performing offline the fuel behaviour analysis (see section 2.4). The objective of the developed one-way and two-way coupling approaches was to create a closer connection between neutron kinetics and thermal hydraulics codes on the one hand and fuel performance codes on the other hand. The coupled neutronics/thermal hydraulics code provides process time, time-dependent rod power and thermal hydraulics conditions to TRANSURANUS, which in turn transfers user selected parameters (e.g. fuel temperature) back in case of the two-way coupling approach (cf. Figure 29 and Figure 30). This means that TRANSURANUS replaces the call of the simplified fuel behaviour model in the coupled neutronics/thermal hydraulics code, and is part of the iteration process in each time step.

For the one-way coupling, TRANSURANUS has no impact on the simulation carried out by the code it is coupled to. Nevertheless, thence the main advantage of the one-way coupling is the automatic data transfer between the two codes. In case of the two-way coupling, TRANSURANUS obviously influences the entire simulation. For example, a transfer of the fuel temperature to a reactor dynamics code has direct feedback on the Doppler reactivity effect simulated by the neutronics. Both approaches can be implemented by means of the general TRANSURANUS coupling interface.

5.1.2 Flexibility in time-step length and numerical stability

One-way coupling can be performed by subsequent calling of TRANSURANUS by the leading code without iteration steps. Two-way coupling can also be performed by a simple explicit calling of TRANSURANUS without iterations, providing the updated coupling parameters for the next time-step, or can be accomplished by an iterative call of both codes for each time-step. In the first case, the time-steps must be chosen sufficiently small, while in the second case a truncation criterion for the interruption of the iteration has to be defined.

Depending on the TRANSURANUS time-step criteria (e.g. for creep strain or fuel temperature), intermediate time-steps are – if necessary – automatically introduced by TRANSURANUS in the time-step interval provided to TRANSURANUS for the fuel behaviour calculation (not affecting the time-step control algorithm of the code coupled to TRANSURANUS). For this purpose, transferred quantities such as rod power and thermal hydraulics conditions are linearly interpolated between beginning and end of given time-step. In this way, the code calling TRANSURANUS can use its own time-step control algorithm. The TRANSURANUS time-step determination was restructured for the coupling, but doesn't affect the results. Furthermore, the wide range of existing time-step criteria results in a stable numerical convergence of TRANSURANUS.

5.1.3 Freely selectable level of detail in fuel behaviour modelling

The TRANSURANUS input provides the capability to select the level of detail in fuel behaviour modelling, for example from complete thermal-mechanical analysis to thermal analysis with given heat transfer coefficient in the gap, from taking into account axial friction forces to neglecting them, from calculated heat transfer coefficient in the gap/between cladding and coolant to given heat transfer coefficient, or from radial distribution of the power density form factor to flat distribution, etc. as will be illustrated further (see chapter 6). The level of detail can be adapted in a coupled code system via the TRANSURANUS input. This gives the opportunity to neglect phenomena with low impact on the simulation and to save computational costs on a case-by-case basis.

5.1.4 Pre- and post-calculations with TRANSURANUS standalone

To ensure a realistic fuel behaviour modelling, the whole irradiation history has always to be given to TRANSURANUS. Under realistic conditions, at least several fuel assemblies in the reactor core are pre-irradiated due to reactor operation in previous fuel cycles. If the code coupled to TRANSURANUS doesn't determinate the pre-irradiation, the general TRANSURANUS coupling interface will be able to handle this issue through TRANSURANUS standalone producing a binary file for each fuel rod containing the status at the end of the pre-irradiation. Then these so-called "TRANSURANUS restart files" are provided to the coupled code system before performing the transient calculation. This allows even the modelling of complex irradiation experiments consisting of pre-irradiation in a power reactor, re-fabrication in hot cells and subsequent testing under DBA conditions in a research reactor (cf. Figure 9). At the end of the code system simulation, further analysis can be carried out with TRANSURANUS standalone for continued irradiation.

5.1.5 Automatic switch from steady-state to transient conditions

Some of the TRANSURANUS models need an input parameter to indicate the reactor state during the simulation with the coupled code system. For example, cladding material properties modelling in TRANSURANUS has to be changed from normal operation to DBA conditions. In addition to the LOCA specific section in the TRANSURANUS input, an additional small separate coupling input file is used for each fuel rod in the general interface. The user can select the kind of model modifications in this input because fuel rod behaviour models often depend on reactor design, cladding material or fuel composition. Furthermore, any variable of the TRANSURANUS restart file can be adapted in this input if required. Altogether, this additional input allows a code system simulation without interruption for switching the TRANSURANUS models.

5.1.6 Parallelization

Although the coupling approach DYN3D-TRANSURANUS applied at assembly level for a full core requires computation times already acceptable for industrial applications (cf. Table

19), the general coupling interface was designed to be prepared for parallelization. One main principle of the coupling shown in Figure 26 is the calculation of one fuel rod per call of the general TRANSURANUS coupling interface, hence in each iteration step the fuel rods are treated sequentially one by one. Normally, there should be no interaction between the fuel behaviour calculations of different rods in the same iteration step, at least e.g. if the architecture of the thermal hydraulics coupled code bases on 1D vertical and hence parallel cooling channels. The implementation of the capability for parallelization is a future task enabling a significant reduction in computation costs per simulation.

5.1.7 Further features

Using the general TRANSURANUS coupling interface, a coupling at pin level, at assembly level as well as a mixture of both can be carried out. Each coupled fuel rod is identified through fuel assembly number and fuel rod number. This specification defines the name of the folder existing for each coupled fuel rod. At the beginning of the simulation each folder contains a TRANSURANUS input file. In case of a pre-irradiated fuel rod the folder contains also a restart file and output files from a pre-calculation with TRANSURANUS (see subsection 5.1.4). If necessary, it even comprises a small additional coupling input for the automatic switch, e.g. from steady-state to transient conditions (see subsection 5.1.5). During the simulation all normal TRANSURANUS output files including a restart file will be written to each fuel rod folder, if convergence is reached in the actual time-step of the coupled code system. The content of output files can be controlled by the TRANSURANUS input as usual. Finally, the standard TRANSURANUS post-processing tools can be applied to the output files.

As the synchronization of TRANSURANUS code versions is required for reducing and simplifying software maintenance, a new input variable and a few new control variables were introduced in the source code, allowing the use of identical software in both standalone as well as in coupled mode (see subsection 5.3.1).

5.2 Applicability for various scenarios

The general TRANSURANUS coupling interface together with the modified TRANSURANUS version can be used for the simulation of several scenarios in various reactor designs:

- Different fuel compositions and cladding materials for the reactor types BWR, PWR, VVER, HWR, and FR with sodium as well as lead(-bismuth) coolant [155-157],
- Normal operation, operational transients and DBA like LOCA [26, 158],
- Time scales from milliseconds/seconds (e.g. RIA) over seconds/minutes (e.g. LOCA) to years (e.g. normal operation or latterly also dry fuel storage) in the same simulation run.

In addition, many of the phenomena modelled by TRANSURANUS can be switched off to simplify the analysis and to save computational costs. For instance, a complete thermal-mechanical analysis can be reduced to a thermal analysis with given heat transfer coefficient in the gap. As a result, the TRANSURANUS code itself offers a good base for a wide application range of the general coupling interface.

The version of TRANSURANUS for RIA simulations is still under development and its performance is evaluated, e.g. by participation in international benchmarks organized for instance by OECD/NEA [24, 25] (see chapter 3) or IAEA [57]. In the RIA Fuel Codes Benchmark of the OECD/NEA, TRANSURANUS already showed a good agreement in injected energy, variation of enthalpy, central fuel temperature, maximum fuel temperature and location of the maximum fuel temperature, in comparison to codes like SCANAIR [93], which is well validated for RIA. As for the current coupling stage of DYN3D-TRANSURANUS only an accurate determination of the transferred fuel temperature, its radial distribution and its influence on the clad temperature is necessary (cf. Figure 30), and thence fulfilled.

5.3 General guidelines for applications

5.3.1 TRANSURANUS input

For coupling purposes, the standard TRANSURANUS version maintained by the JRC-ITU includes the new input variable ICOUPL (beginning from version v1m1j12, April 2012):

- ICOUPL = 0: TRANSURANUS is applied in standalone mode.
- ICOUPL = 1: TRANSURANUS is applied as part of a coupled code system.

Both the modified TRANSURANUS version (also applicable in standalone mode, see subsection 5.1.7) and the general TRANSURANUS coupling interface applies this control variable ICOUPL. However, today this new input variable doesn't control anything in the standard TRANSURANUS version of JRC-ITU because the implementations done in the frame of this coupling work will be integrated in the standard version in a later stage. Furthermore, TRANSURANUS will automatically set the value of ICOUPL to zero, if an input of a previous code version is read in (downward compatibility).

The first part of the TRANSURANUS input can be prepared as in the case for the standalone mode. More precisely, fuel rod design specifications given in reports/documents and model options based on former experiences (e.g. due to participation in international benchmarks organized by IAEA [57] and OECD/NEA [24, 25]). The model options may differ slightly compared to the standalone mode, e.g. ICOUPL (see above) and IALPHA defining the determination of the clad-to-coolant heat transfer coefficient. Furthermore, if the standard equidistant radial discretisation in TRANSURANUS isn't compatible to the discretisation applied in the code coupled to TRANSURANUS, the fuel rod will be discretised with the help of manually calculated values. Normally the cladding modelling isn't affected by different radial discretisations due to the thin shell approach (see subsection 2.3.3) applied by many reactor dynamics codes, thermal hydraulics system codes and sub-channel thermal hydraulics codes. To take into account high temperature gradients along the cladding thickness (cf. Figure 7) and separate processes on the inner and outer cladding surface (see subsection 2.3.3), the cladding should be represented at minimum with two coarse zones in TRANSURANUS. The second input part (named as macro input part) containing time dependent linear heat rate, fast neutron flux and thermal hydraulics conditions (e.g. coolant

pressure, coolant temperature, coolant flow rate) hasn't to be provided. During the simulation these parameters are transferred directly from the code coupled to TRANSURANUS [120].

For pre-irradiated fuel rods the whole pre-irradiation history has always to be given to TRANSURANUS [120] (see section 3.2). If the code coupled to TRANSURANUS doesn't take into account the whole irradiation history, the general TRANSURANUS coupling interface is designed to handle this issue through pre-calculations with TRANSURANUS standalone (see subsection 5.1.4). The macro input part has to be set for this standalone calculation.

5.3.2 Modifications in the code coupled to TRANSURANUS

The code coupled to TRANSURANUS has to be prepared for the “docking” to the general TRANSURANUS coupling interface. For example, several modification steps were conducted in case of DYN3D (see chapter 6). All modifications were carried out under the restriction that no variable of TRANSURANUS and its general coupling interface would be used in DYN3D as well as vice versa. Only the transfer variables of the interface call are applied in both parts (cf. Figure 26), whereas these variables were declared two times in the code system, once in DYN3D as well as once in the general TRANSURANUS coupling interface and TRANSURANUS. The following modification steps in DYN3D embed many small details and have to be repeated at least partly in codes planned to couple to TRANSURANUS:

- 1) *New input variable:* Implementation of a new input option to select either the standard simplified fuel behaviour model of the code coupled to TRANSURANUS, the one-way coupling approach not affecting the results of the code coupled to TRANSURANUS or the two-way coupling approach affecting the results of the coupled code system. Depending on the coupled code this input variable will define the fuel behaviour modelling either core-wide, at assembly level or at pin level.
- 2) *Restructuring of the source code:* The fuel behaviour of a complete fuel rod is simulated at once per execution of a 1.5 dimensional fuel performance code, enabling to take into account friction forces (i.e. important for PCMI and hence fuel stack

elongation) and inner rod pressure (i.e. important for ballooning). On the other side several reactor dynamics codes and thermal hydraulics codes calculate node by node at least parts of the thermal hydraulics due to highly limited random access memory in the past. For example, before the coupling development started the DYN3D code structure contained a large loop calculating node by node the metal water reaction, the fuel behaviour with known heat flux density, the heat transfer regime and the heat flux density with known clad temperature for the considered coolant channel (cf. Figure 27 on the left). To determine the fuel behaviour of a complete rod, i.e. consider all axial nodes at once to allow coupling to TRANSURANUS, this loop was split in three loops (cf. Figure 27 on the right). At the same time several variables weren't declared node dependent but their values needed to be stored nodewise for calculating the heat transfer regime and the heat flux density in the loop after fuel behaviour determination. Thence larger modifications of the DYN3D code structure were necessary for the coupling to TRANSURANUS.

- 3) *Specification of transferred data arrays:* Regarding the call of the general coupling interface through the coupled code, an unambiguous definition of the transferred data variables including their dimensions and units is important for both one-way approach (cf. Figure 29) and two-way approach (cf. Figure 30). Normally the data provided by the thermal hydraulics system codes, sub-channel thermal hydraulics codes or reactor dynamics codes represent the variables of the TRANSURANUS macro input part (see subsection 5.3.1). Vice versa the fuel performance code can transfer back e.g. fuel temperature for the neutronics and/or clad temperature for the thermal hydraulics (only in the two-way approach). According to both directions the list of transferred data variables can be extended, e.g. to take into account the fuel rod geometry calculated by TRANSURANUS in the coupled code system. Furthermore, the transferred data variables were assembled in data arrays, sorted by type of variable and direction. These data arrays were only adopted in DYN3D and the general TRANSURANUS coupling interface (not in TRANSURANUS).
- 4) *Embedding of interface call:* The source code part simulating the fuel rod behaviour based on simplified modelling (cf. Figure 27 on the right, middle loop over axial nodes) should be replaced by a new subroutine call. Its task is the control of degree of detail in fuel behaviour modelling, hence the call of the fuel behaviour model and/or

the coupled fuel performance code depending on the newly introduced input variable (cf. Point 1). Possible artificial reflector nodes in reactor dynamics codes should still be handled by the simplified model. It might be difficult to integrate them into the analysis performed by the coupled fuel performance code. In addition the impact of detailed modelling should be negligible, i.e. due to no appearance of burn-up effects. Finally, if the code part embedding the fuel behaviour modelling is separated for steady-state and transient conditions (as the thermal hydraulics in DYN3D), two calls referring to the coupling interface will be introduced.

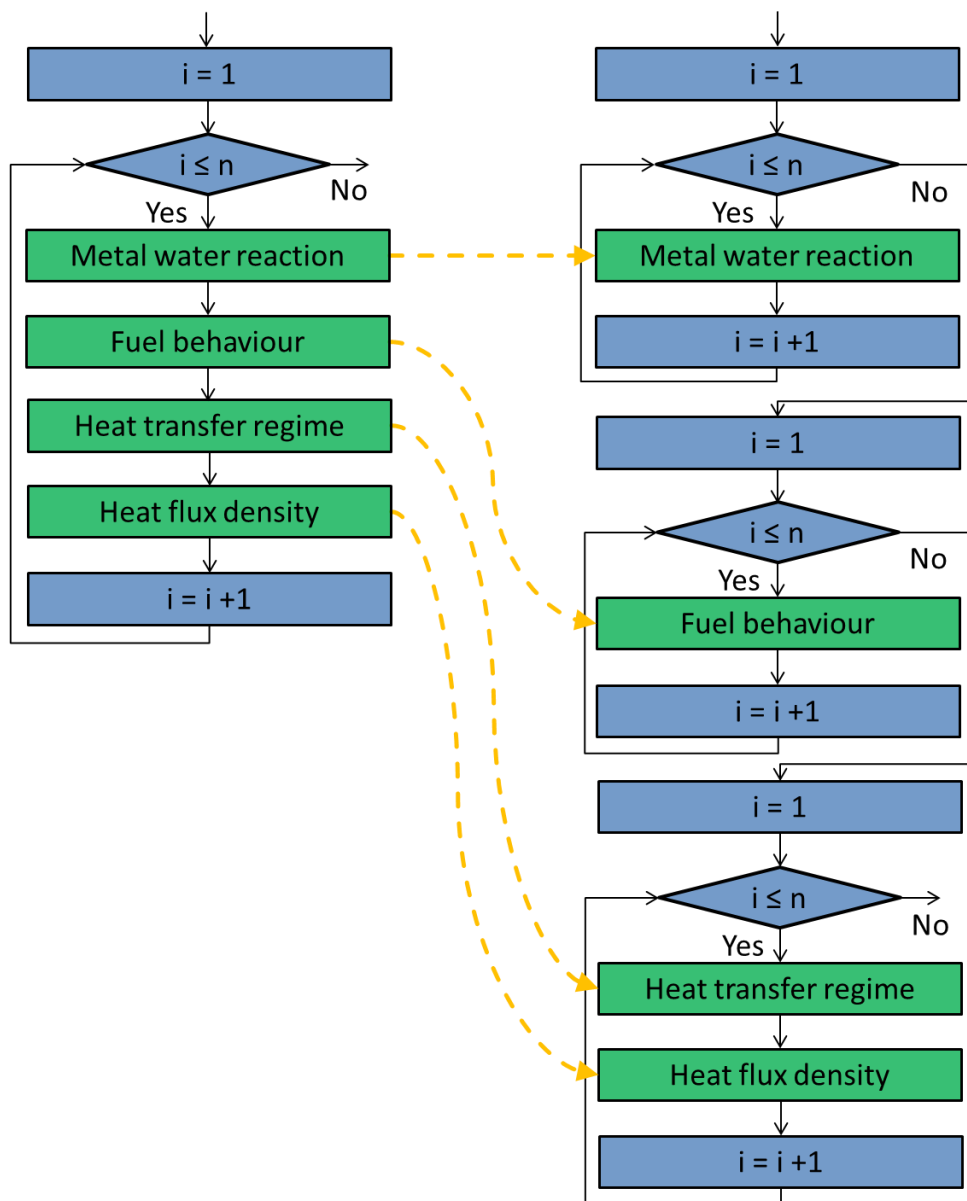


Figure 27: Local restructuring of DYN3D to allow determination of the whole fuel rod behaviour at once (i : count variable; n : total number of axial nodes in the coolant channel). Left, previous local DYN3D code structure; right, new local DYN3D code structure after restructuring.

- 5) *Definition/Set of transferred control variables in the source code:* Several control variables are transferred to the general coupling interface beside the data arrays (cf. Point 3). For example fuel assembly number, fuel rod number, status of the iteration process and writing/updating of output files are controlled by them to guarantee successful working including high flexibility. The values of these control variables are set in the source code, partly close to the call of the general coupling interface. Further control variables, which are not transferred to the general coupling interface, may be implemented in the source code additionally. For example, one control variable in DYN3D ensures that the coupling can be only applied to the two neutron energy groups version of DYN3D in this development stage.

5.3.3 Maintenance of the code system

On the one side the TRANSURANUS code and the general TRANSURANUS coupling interface have to be maintained, on the other side the code coupled to the fuel performance code needs maintenance, too (cf. Figure 26). All code system parts are developed permanently and separately and are applied by several institutions. These maintenance needs will increase, if once the modified TRANSURANUS version is integrated in the standard version at JRC-ITU (see subsection 5.1.7) and the belonging general coupling interface is released to the TRANSURANUS user group. For example, if TRANSURANUS has to provide a variable parameter to a coupled code which wasn't yet foreseen. Thence the fuel performance code has to be extended/be modified. Another example represents the integration of a confidential TRANSURANUS version in a coupled code system, i.e. embedding the 80% methodology [128].

For limiting the maintenance, the new coupling interface should be released to users for the first time, when the general coupling interface will be parallelized enabling fuel behaviour determination of several fuel rods at the same time (see subsection 5.1.6). Furthermore, before it is provided to a larger number of users the interface should be tested and improved with the coupling to a second code (besides DYN3D). This should ensure that most of the control variables of the interface call haven't to be modified, hence guaranteeing and preserving the generality itself. Of course it is difficult to fix the transferred data arrays in dimensions and containing variables (see subsection 5.3.2, Point 3). To limit further the maintenance work, no

variable of the code coupled to TRANSURANUS should reside in the fuel performance code and its general coupling interface as well as vice versa (like for DYN3D-TRANSURANUS).

According to confidential TRANSURANUS versions, for the coupling the TRANSURANUS source code was modified in subroutines normally not touched by other code developments. Thence for the coupling modified TRANSURANUS subroutines can be integrated with low effort in special versions.

5.4 Summary and recommendations for future work

Most of the reactor dynamics, thermal hydraulics system, sub-channel thermal hydraulics, CFD codes and their code systems contain a simplified fuel behaviour modelling and/or set-up of fuel rod parameters (e.g. heat transfer coefficient in the gap and power density profile) pre-calculated by a fuel rod performance code and provided as input tables [91] (see section 2.5). Thence recently a worldwide trend occurred to replace simplified fuel behaviour models by coupling to fuel performance codes.

A coupling of two computer codes requires modifications in two source codes and moreover development of a coupling interface (i.e. organizing the data transfer), hence experts of both codes are needed. Therefore, a general TRANSURANUS coupling interface together with modifications in TRANSURANUS was developed, limiting this development work almost completely to modifications in the code coupled to the fuel performance code (see subsection 5.3.2). To ensure this the general coupling interface provides many features, e.g. one-way and two-way coupling, flexibility in time-step length, coupling at pin level or assembly level, and automatic switch from steady-state to transient conditions (see section 5.1). Furthermore, this computer tool can be applied to several scenarios in various reactor designs including different fuel compositions (see section 5.2). Because the generalized character of the developed interface limits work and costs, the replacement of simplified fuel behaviour models in neutronics and thermal hydraulics codes becomes more attractive.

The feedback on neutron kinetics and thermal hydraulics from great degree in detail in online fuel behaviour modelling isn't reported so far in the open literature for calculating a full LWR core [120]. Thence the assumed feedback has to be analysed, e.g. on the new coupled code

system DYN3D-TRANSURANUS (see chapter 6). This coupled code system can be applied to RIA scenarios. A future coupling with a thermal hydraulics system code is moreover of interest, i.e. for the analysis of LOCA scenarios, but also for complex RIA scenarios like anticipated transient without scram (ATWS) or boron dilution transients. The analysis of a boron dilution scenario is presented in chapter 6 of this work. However, the boundary conditions at the reactor pressure vessel inlet are provided as input in this analysis. The development of a coupling between the thermal hydraulics code RELAP and TRANSURANUS was proposed in the frame of the international benchmark on fuel modelling in accident conditions (FUMAC), organized by IAEA.

6 Application of the new code system DYN3D-TRANSURANUS for RIA

Most of the reactor dynamics, thermal hydraulics system, sub-channel thermal hydraulics and CFD codes contain a simplified fuel behaviour and/or set-up of fuel rod parameters (e.g. heat transfer coefficient in the gap and power density profile) pre-calculated by a fuel rod performance code and provided as input tables [91]. The same holds for coupled code systems consisting of these codes. Therefore, traditionally licensing calculations concerning fuel rod performance are done in a conservative manner [10] (see subsection 2.4.1).

The overall interaction between neutron kinetics, thermal hydraulics and detailed fuel behaviour modelling has been rarely analysed in the open literature so far (see subsection 2.5). Thence, one trend in advanced safety analysis is to quantify the benefit resulting from replacement of simplified fuel behaviour models by a two-way coupling approach to a fuel performance code. Such a two-way coupling approach allows detailed fuel behaviour modelling coupled online with neutron kinetics and/or thermal hydraulics. One of the first full online two-way couplings to a fuel performance code for a whole LWR core was developed in the frame of this thesis [10, 115, 120, 159]. This new coupled code system DYN3D-TRANSURANUS is described in this chapter (cf. Figure 2). Furthermore, DYN3D-TRANSURANUS results are presented for two RIA scenarios: Firstly, a CR ejection event and secondly a boron dilution transient as extreme RIA scenario. This chapter is taken from Ref. [10, 159].

6.1 Description of the new code system DYN3D-TRANSURANUS

The reactor dynamics code DYN3D consists of the 3D neutron kinetics core model and its own thermal hydraulics model [88]. Taking benefit from the decreased costs of computational power, DYN3D was coupled to thermal hydraulics system codes [106, 160], sub-channel thermal hydraulics code and CFD codes [103] in the last two decades (cf. Figure 28). These coupled code systems allow greater detail in thermal hydraulics modelling (i.e. high resolution of local fluid phenomena) and extension of the capability range (i.e. for simulations including also the secondary circuit of a PWR).

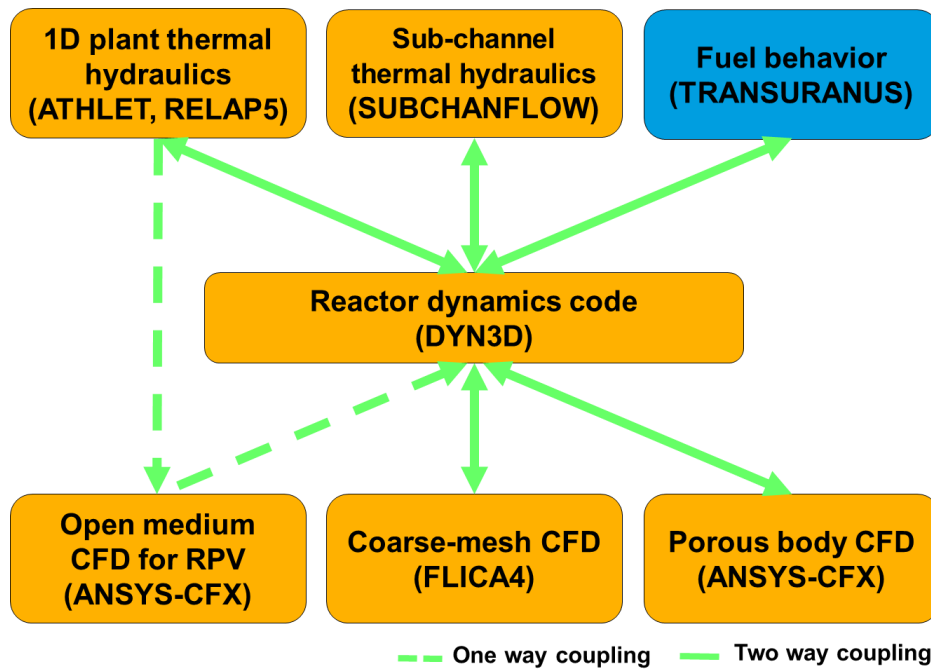


Figure 28: Coupling approaches with the reactor dynamics code DYN3D

Nevertheless, all coupling approaches contain a simplified fuel behaviour modelling so far. For example, the internal DYN3D fuel rod model [94] is embedded in the DYN3D thermal hydraulics part and belongs also to the category of simplified fuel behaviour models (see subsection 2.4.3 and cf. Table 4). More precisely, it takes into account the thermo-mechanical interaction between fuel and cladding after gap closure in a simplified way. Neither fission gas release nor the HBS phenomena are explicitly taken into account [94]. The DYN3D thermal hydraulics model comprises a full heat transfer regime map ranging from one-phase convection to post-CHF film boiling or dispersed flow conditions. In contrast, the thermal hydraulics model in the fuel performance code TRANSURANUS covers the phases for normal operating conditions only. The thermal hydraulics conditions have to be provided as input to TRANSURANUS for accident simulations.

According to the different degree in detail in fuel behaviour modelling in both models, its influence on the heat transfer conduction solution is analysed in Ref. [10] (see subsection 6.4.2): “For all burn-up levels DYN3D-TRANSURANUS [(fuel behaviour was modelled by TRANSURANUS)] systematically calculated higher maximum values for the node centreline fuel temperature (max. difference of 180.7 K) compared to DYN3D standalone [(fuel behaviour was modelled by the internal DYN3D fuel rod model)]. These differences were analysed with respect to the influence of the modelling of fuel thermal conductivity, radial

power density profile and heat transfer in the gap. For the individual impact of these three components of simplified modelling in DYN3D the following main trends were observed: The simulated fuel centreline temperature decreased due to the simplified fuel thermal conductivity, decreased due to the simplified heat transfer in the gap, and increased due to the simplified power density profile. It is important to note that the temperature differences could be completely explained by a combination of the three factors.”

Both the one-way and the two-way approaches of the general TRANSURANUS coupling interface (see chapter 5) are applied to DYN3D-TRANSURANUS [10]. DYN3D provides the reference time step (Δt), time-dependent linear heat rate of the rod (LHR) and thermal hydraulics conditions like heat transfer coefficient between clad to coolant ($\alpha_{\text{clad, sf}}$), coolant temperature (T_{cool}) and coolant pressure (p_{cool}) to TRANSURANUS (cf. Figure 29 and Figure 30). For the two-way coupling, TRANSURANUS replaces the call of the simplified DYN3D fuel behaviour model, and is part of the iteration process in each time-step in DYN3D. Thence, TRANSURANUS in turn transfers parameters like radial fuel temperature distributions (T_{fuel}) and clad surface temperature ($T_{\text{clad, sf}}$) back to DYN3D. It is worth noting that TRANSURANUS takes into account gamma heating in both the cladding and coolant, hence the gamma heatings are also considered in the call of TRANSURANUS in the one-way coupling and two-way coupling. T_{fuel} affects directly the neutron kinetics through the Doppler temperature, and $T_{\text{clad, sf}}$ the thermal hydraulics through clad-to-coolant heat transfer in DYN3D. This set of transferred parameters can be easily extended, e.g. to include the fuel rod geometry from TRANSURANUS in DYN3D in the future. It should be pointed out that the coupling was developed at fuel assembly level due to the DYN3D thermal hydraulics architecture, based on 1D vertical cooling channels which represents one or more fuel assemblies each (one fuel assembly in the calculations presented in this chapter). This means that, identical to DYN3D, one representative/average fuel rod is calculated in the coupled code system for each 1D vertical cooling channel. Although DYN3D and TRANSURANUS are best estimate codes, every user is free to choose conservative input data and to implement conservative models in the codes.

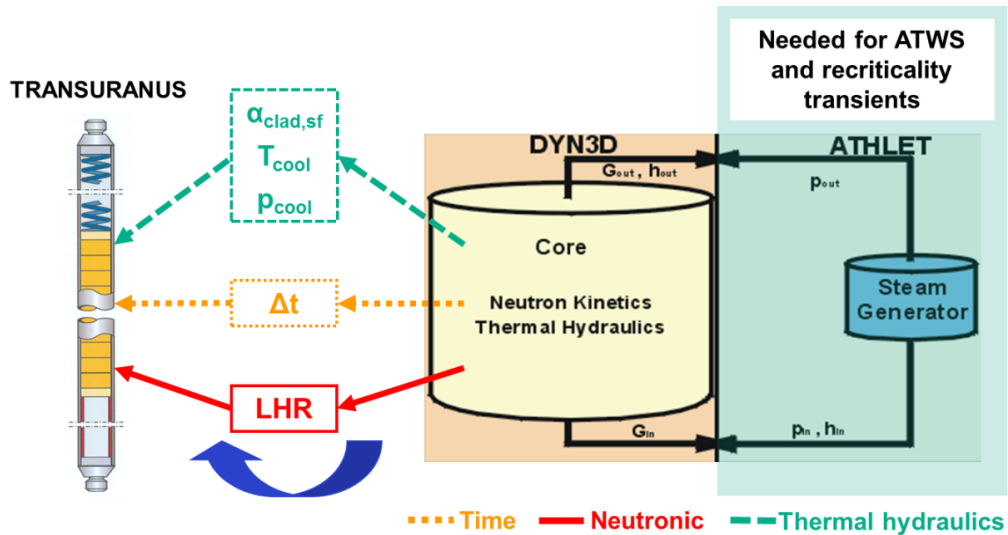


Figure 29: Data transfer between DYN3D and TRANSURANUS via the general TRANSURANUS coupling interface for one-way coupling (prospective in combination with the thermal hydraulics system code ATHLET) [10]. As shown, a later planned extension to DYN3D-ATHLET-TRANSURANUS was already taken into account, e.g. applicable to ATWS in the future (G_{in} : coolant mass flow density at the core inlet; G_{out} : coolant mass flow density at the core outlet; h_{in} : coolant specific enthalpy at the core inlet; h_{out} : coolant specific enthalpy at the core outlet; p_{in} : coolant pressure at the core inlet; p_{out} : coolant pressure at the core outlet).

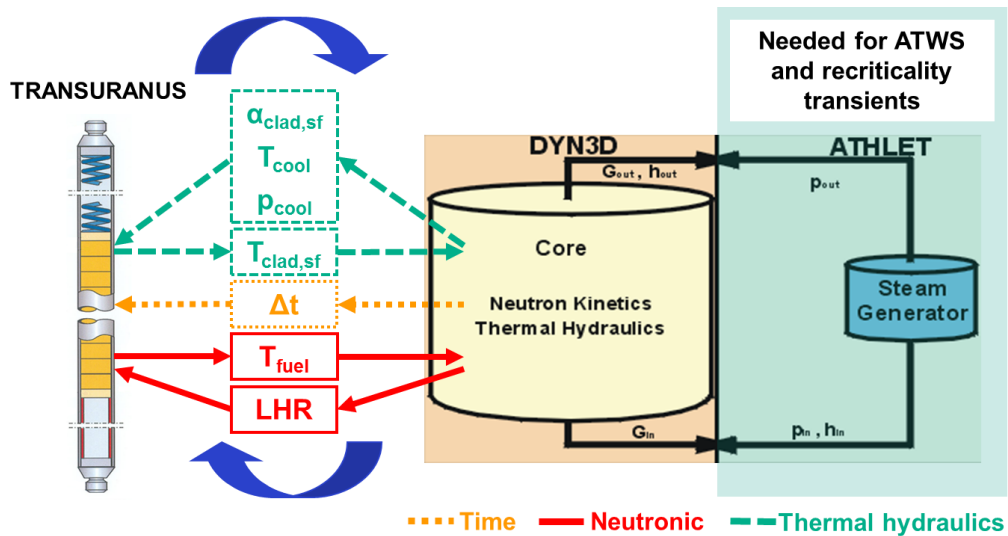


Figure 30: Data transfer between DYN3D and TRANSURANUS via the general TRANSURANUS coupling interface for two-way coupling (prospective in combination with the thermal hydraulics system code ATHLET) [10]. As shown, a later planned extension to DYN3D-ATHLET-TRANSURANUS was already taken into account, e.g. applicable to ATWS in the future (G_{in} : coolant mass flow density at the core inlet; G_{out} : coolant mass flow density at the core outlet; h_{in} : coolant specific enthalpy at the core inlet; h_{out} : coolant specific enthalpy at the core outlet; p_{in} : coolant pressure at the core inlet; p_{out} : coolant pressure at the core outlet).

6.2 Variants of the code system differing in detail of fuel behaviour modelling

The TRANSURANUS input provides the capability to reduce the level of detail in fuel behaviour modelling, for example from complete thermal-mechanical analysis to thermal analysis with given heat transfer coefficient in the gap (see subsection 5.1.3). Furthermore, the clear and well defined structure of the TRANSURANUS code allows easily the introduction of new correlations for material properties of fuel, cladding and/or coolant, e.g. thermal conductivity, heat of melting, density and elasticity constant. The so-called realistic variant is applied for the scenarios in this chapter. This variant is based on the TRANSURANUS inputs generated in the frame of the OECD RIA Fuel Codes Benchmark for highly irradiated fuel rods (see chapter 3), which gave good and reliable results for the parameter transferred back from TRANSURANUS to DYN3D (cf. Figure 30). As in the OECD benchmark the material properties content of the standard TRANSURANUS version of JRC-ITU were applied also in this realistic version of the coupled code system.

For analysing differences between DYN3D and the two-way approach of DYN3D-TRANSURANUS, the level of detail in fuel behaviour modelling was reduced from the realistic one in order to align to DYN3D in different ways. Beside the realistic one these modified versions (named as variants I, II, III and IV) are additionally applied in subsections 6.4.1 and 6.4.2 for the control rod (CR) ejection event.

Variant I (fuel thermal conductivity)

DYN3D comprises its own transient fuel behaviour model, which was developed and validated for fresh and low burn-up fuel [94]. The TRANSURANUS correlation is well validated up to high burn-ups, i.e. the fuel thermal conductivity depends besides of temperature on porosity, Gd concentration and burn-up. For aligning and analysis of the impact, the DYN3D fuel thermal conductivity correlation was applied in the TRANSURANUS code.

Variant II (power density profile)

The power density profile over the fuel pellet radius can be given as input to DYN3D. In this case, pre-calculations by a fuel performance or a neutron transport code such as the Monte Carlo code MCNP [161] have to be performed. Thence, a flat power density profile is usually used as standard in DYN3D. In contrary, TRANSURANUS contains several approaches for

calculating the radial power density form factor. The standard TUBRNP model [27] is used in this work. For investigating the influence of the radial form factor, a flat profile was set in the TRANSURANUS input in variant II.

Variant III (heat transfer in the gap)

For each fuel rod, the heat transfer coefficient in the gap is provided in the DYN3D input for its own fuel behaviour model. Alternatively, the change of the heat transfer coefficient in the gap during a transient can be calculated by DYN3D in a simplified way. In the realistic version of the code system, the URGAP model in TRANSURANUS was chosen taking into account gas bonding, thermal conductivity of mixture according to Lindsay and Bromley, and accommodation coefficients [162]. The modelling of the heat transfer in the gap is sensitive. Only advanced fuel performance codes can consider the heat transfer in the gap in an accurate manner. For analysing the impact of the heat transfer coefficient in the gap, the corresponding TRANSURANUS input was set to the DYN3D input value. In this mode, TRANSURANUS carried out a thermal analysis only.

Variant IV (combination of variants I, II, III)

An aligning was introduced for fuel thermal conductivity, power density profile and heat transfer coefficient in the gap.

6.3 Specification of simulated RIA scenarios for German PWR

Two RIA scenarios were calculated: Firstly, a CR ejection event (see subsection 6.4.2) and secondly a boron dilution transient as extreme RIA scenario (see subsection 6.4.3). The differences between DYN3D standalone and the two-way coupling approach of DYN3D-TRANSURANUS are analysed in the first scenario. For this purpose, several variants of the code system differing in level of detail in fuel behaviour modelling were used. In addition, the differences between one-way and two-way coupling approach are discussed in the second scenario. According to both scenarios, a German PWR Konvoi design characterized by thermal power of 3750 MW, four loops and 193 fuel assemblies of the type 18x18-24 was selected. The core map is shown in Ref. [163] and refers to a generic input distinguished by low leakage core loading pattern with UO₂, Gd doped UO₂ and MOX fuel at begin of cycle at Xe equilibrium. Neutron kinetics as well as thermal hydraulics were modelled 1:1 for all 193

fuel assemblies, and both in DYN3D and in DYN3D-TRANSURANUS one representative fuel rod of each fuel assembly was used. The internal DYN3D fuel behaviour model provides only fuel correlations for UO_2 , Gd and MOX correlations have not yet been implemented. A two group neutronic cross section library, generated by the lattice code HELIOS [86], was used to calculate the macroscopic cross sections taking into account burn-up state, poisoning, thermal hydraulics feedback and fuel assembly reshuffling.

In this reactor design, a number of 61 CRs regulate the reactor power; each CR combines 24 CR fingers, which fit into the 24 guide tubes in the 18x18-24 assembly type. The CRs are assigned either in the one CR bank L or the six CR banks D. The CR banks D are used for the control of reactivity in operation including fast operational transients. In analogy, the CR bank L is designed to supply the necessary shut down reactivity for a scram, to handle the control of the axial power density distribution over the core, and to support the CR bank D in case of a fast operational power transient.

For analysing the pure effect resulting from a two-way coupling approach in comparison with DYN3D standalone (with its internal UO_2 fuel behaviour model) and with one-way coupling approach (with its internal UO_2 fuel behaviour model), only UO_2 fuel properties correlations were activated in TRANSURANUS in the coupled calculations. Otherwise this effect would be additionally influenced by the in DYN3D not modelled fuel compositions Gd doped UO_2 and MOX.

6.3.1 Control rod ejection

For hot full power (HFP) conditions, all CRs in a German type PWR are practically out of core or inserted only partially. Thence the effect of a reactivity insertion due to a CR ejection is limited under HFP conditions. According to reactor operation rules, four CR banks D can be inserted fully in the power range between HZP and 30% of nominal reactor power. Thence, a typical ejection of one CR (core position N11 in Figure 32 and Figure 33) belonging to one of the four CR banks D was calculated starting from HZP as well as from power level 30% of nominal. The ejection time was set conservatively to 0.1 s [7], whereas the real ejection time is affected by the severity of the CR mechanical failure and coolant pressure [3]. The activation of the scram signal isn't considered during the simulations. Film

boiling did not occur during this scenario. The time 0.1 s corresponds to the onset of the CR ejection in all figures regarding this scenario.

6.3.2 Boron dilution transient

The background of this scenario is the following. In the initial state, all CR are fully inserted into the core excluding the most effective CR, which is fully withdrawn assuming a single failure for the boron dilution transient. If a steam generator tube leaks and the secondary side pressure is higher than in the primary circuit (e.g. during an outage), unborated feed water will enter the affected primary loop forming a slug of - conservatively - unborated coolant in the affected loop. A slug volume of 36 m³ is considered for this scenario. This volume represents the maximum volume of a slug that can be accumulated in the selected scenario. Assuming that the reactor operator doesn't recognize the leakage and starts up as first main coolant pump the one in the affected circuit after the outage, the slug of unborated coolant will move towards the downcomer and the lower plenum of the reactor pressure vessel. There it mixes with the highly borated coolant. As a result, under-borated coolant with a heterogeneous boron concentration pattern at 30 bar and 192 °C is considered to be introduced in this scenario into the core, leading immediately to excess reactivity insertion values of around 2\$ in this case [164]. The ultimate core power rise initiated by this reactivity insertion is limited by the Doppler reactivity feedback. Secondary core power peaks can occur during the movement of the under-borated moderator front through the core (cf. Figure 37 (a) and (b)). The first power peak is cut off in Figure 37 (b) to zoom into the details of the secondary power peaks.

The coolant mixing after entrance of the unborated coolant into the downcomer is a highly complex fluid dynamics process. Thence, it cannot be modelled by the DYN3D thermal hydraulics model that is restricted to the reactor core. Therefore boric acid concentrations as a function over time, measured in the experimental facility Rossendorf Coolant Mixing model (ROCOM) [165], were provided as input to DYN3D for the boron concentration at the inlet of each vertical cooling channel. Alternatively, the mixing of boric acid concentration and coolant temperature can be calculated by a fast-running coolant mixing model named as semi-analytical perturbation reconstruction model (SAPR) coupled to DYN3D [164]. In reality, back flow would appear into the three loops with switched off main coolant pumps. This

effect is inherently considered in the provided boron input to DYN3D as far it also occurred during the corresponding ROCOM experiments. The beginning time (0 s) corresponds to the main coolant pump start in all figures regarding this scenario.

6.4 Results and discussion

6.4.1 Pre-calculations for critical boron concentration

The results from DYN3D, the code system with fully realistic modelling and its variants containing simplifications in modelling (see section 6.2) differ in critical boron concentration. This is caused by different fuel temperature levels due to varying degree in fuel behaviour modelling and/or different modelling in DYN3D and TRANSURANUS. Thence for the scenario CR ejection, the critical initial state of the reactor and the corresponding critical boron concentration had to be pre-calculated in separate runs. If the fuel assembly was irradiated in a previous cycle, the pre-irradiation would be calculated with TRANSURANUS standalone for the input of DYN3D-TRANSURANUS. In that case typical time-dependent rod power and thermal hydraulics conditions were assumed.

For HZP, fuel temperatures are low and thence differences are (almost) not visible in the calculated critical boron concentration (cf. Table 14). In contrast differences occur for 30% of nominal reactor power. A priori it is clear that the value from the one-way coupling approach must be identical to DYN3D, as it can be seen from Figure 29. As it can be seen from Table 14, the variant IV of the two-way coupling approach provides the critical boron concentration value closest to the DYN3D standalone result. That means that the differences between DYN3D standalone and the realistic two-way coupling approach are indeed caused by the simplifying assumptions implied in variants I, II and III concerning fuel thermal conductivity, radial power density profile in the fuel pellet and heat transfer in the gap.

Table 14 – Critical boron concentration of the initial reactor state for CR ejection transient

Code (system)	Critical boron concentration [ppm]	
	HZP	30% of nominal reactor power
DYN3D standalone	1608.92	1225.27
Two-way coupling approach DYN3D-TRANSURANUS (realistic)	1608.87	1198.98
Two-way coupling approach DYN3D-TRANSURANUS (variant I)	1608.87	1219.59
Two-way coupling approach DYN3D-TRANSURANUS (variant II)	1608.87	1163.93
Two-way coupling approach DYN3D-TRANSURANUS (variant III)	1608.87	1212.38
Two-way coupling approach DYN3D-TRANSURANUS (variant IV)	1608.87	1223.68

6.4.2 Comparison of DYN3D standalone and two-way coupling approach

6.4.2.1 Analysis of differences in global and local parameters

Global parameters

For the CR ejection transient, the maximum total nuclear power in the peak is almost identical between the two-way approach of DYN3D-TRANSURANUS (1839 MW) and DYN3D standalone (1835 MW), cf. Figure 31 (left). In the coupled system the power decreases slightly steeper after reaching the maximum value. After 20 s the value of DYN3D standalone is 47 MW higher. No onset of DNB occurred locally. Furthermore, the global average fuel temperature is shown in Figure 31 (right). A difference of 43 K between both results can be seen from the beginning. The difference increases slightly over the time (max. increase of 1.4 K). Obviously, for moderate RIA cases the difference in global average fuel temperature depends strongly on the initial state of the fuel rod, and less on the modelling of the change in e.g. heat transfer in the gap and fuel conductivity during the transient with fixed burn-up. This fact is important because the core loading contains fuel from zero burn-up up to high burn-up.

The TRANSURANUS code and thence also DYN3D-TRANSURANUS simulate the initial fuel state in greater detail because they take into account the whole pre-irradiation history beginning at zero burn-up. In addition, TRANSURANUS takes the thermal conductivity of high burn-up fuel with HBS porosity into account while DYN3D is only validated until medium burn-ups.

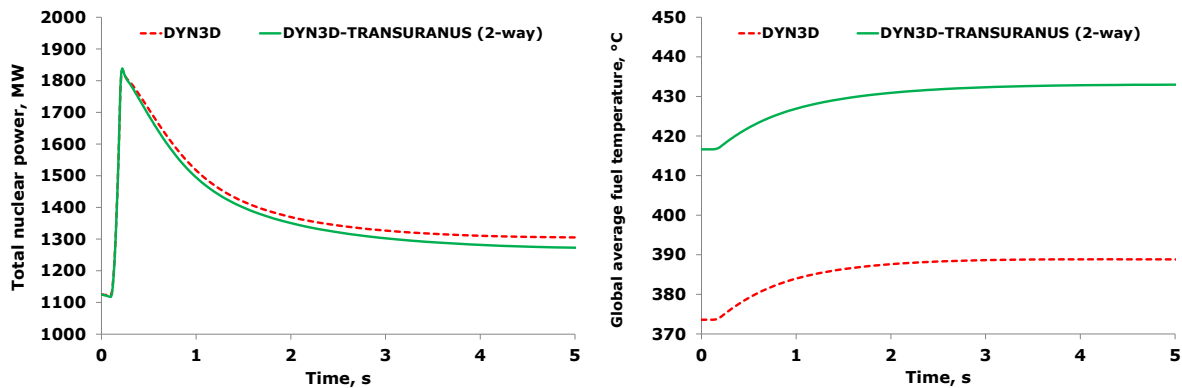


Figure 31: Total nuclear power over time (left) and global average fuel temperature over time (right) for CR ejection at 30% of nominal reactor power.

Local parameters

For better understanding, these global differences were analysed in more detail on fuel assembly and node-wise level for the CR ejection transient. As known from other calculations [3], the magnitude of power increase represents a local parameter over the core, and thence the values of enthalpy insertion strongly differ among the fuel assemblies. The enthalpy increase is influenced by position in the core and burn-up of the fuel assembly, reactivity worth and insertion level of the ejected CR, and axial power distribution. In the calculated scenario, the ejected CR is located in a fresh fuel assembly, marked in Figure 32. As expected, the maximum fuel enthalpy increase occurs with 47.7 J/g in this fresh fuel assembly. While the neighbouring fuel assemblies in Figure 32 also show higher than average enthalpy increases, this effect decreases with distance from the ejected CR. To analyse the effect of the coupling in more detail, the relative difference $\Delta(\Delta h)_{rel}$ between the maximum assembly-average fuel enthalpy increase simulated by DYN3D standalone on one hand and by DYN3D-TRANSURANUS on the other hand is quantified in Figure 33. The relative differences range between -156.8 % and 10.4 %, positive values meaning that DYN3D calculates a larger value than the coupled code system or vice versa.

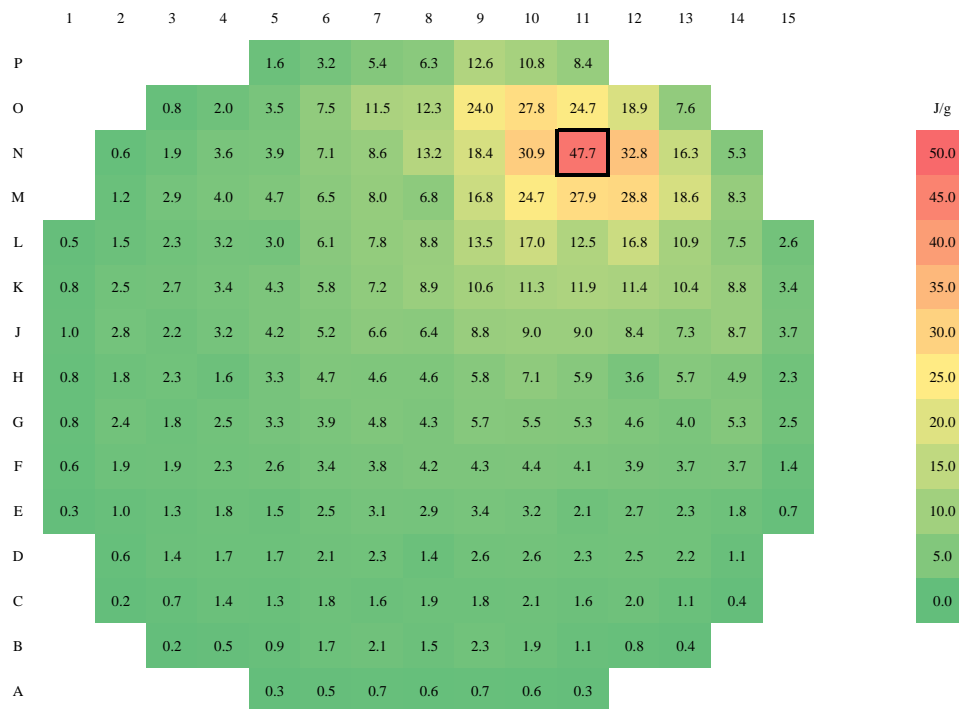


Figure 32: Maximum assembly-average fuel enthalpy increase Δh calculated by DYN3D-TRANSURANUS for CR ejection at 30% of nominal reactor power (bordered fuel assembly represents the location of the ejected CR)

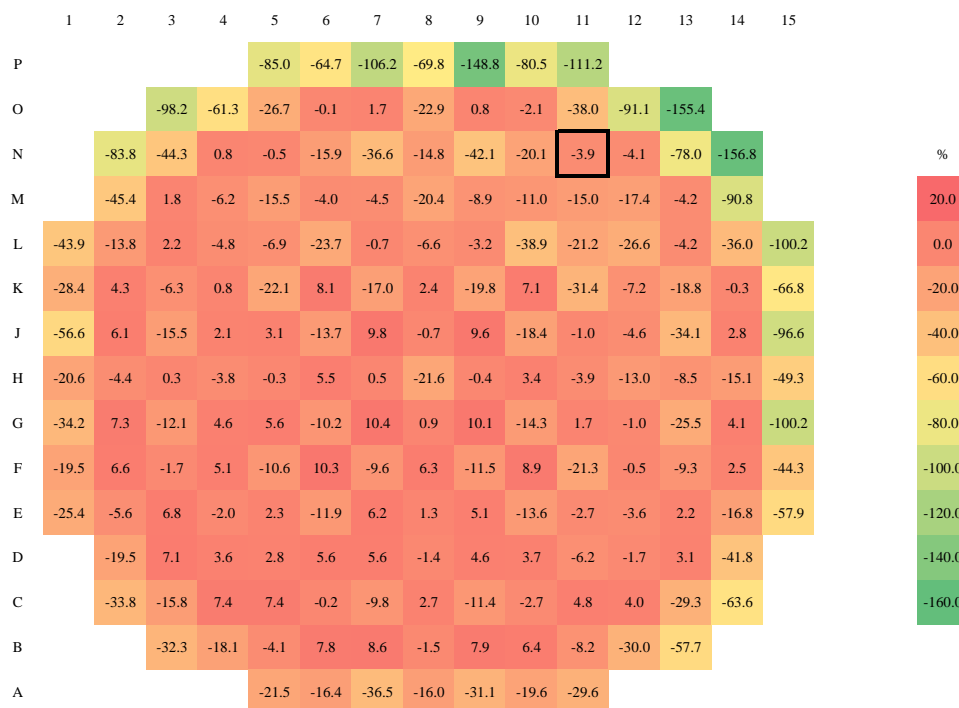


Figure 33: For CR ejection with no onset of DNB, relative difference $\Delta(\Delta h)_{rel}$ in maximum assembly-average fuel enthalpy increase Δh between DYN3D and DYN3D-TRANSURANUS at 30% of nominal reactor power ($> 0\%$: value of DYN3D is larger; $< 0\%$: value of DYN3D is lower; bordered fuel assembly represents the location of the ejected CR)

For all fuel assemblies with an enthalpy increase beyond 5J/g in Figure 32 and a relative difference of $|\Delta(\Delta h)_{\text{rel}}| > 50\%$ in Figure 33, the values are shown in Table 15 in relation to the burn-up. The relative differences increase from fresh fuel to a burn-up of 40 MWd/kgHM. Beyond this burn-up threshold, the difference can rise sharply. Absolute relative differences of 50 % and more only occur for burn-up values higher than 40 MWd/kgHM, of 100 % and more for burn-up values higher than 55 MWd/kgHM. However, no conclusion can be drawn about the conservatism of the simplified intrinsic fuel behaviour model in DYN3D with respect to reactor safety because there are two contrarious trends. On the one side, a higher fuel enthalpy can lead to more distinct PCMI with the increased potential for fuel rod failure, or to higher temperatures inducing fuel melting. On the other side, a lower fuel enthalpy might be caused by higher heat transfer in the gap [24], which in turn leads to higher heat fluxes and might cause earlier DNB onset. This ambiguity points out the benefits of the coupled code system which can model the fuel behaviour in a great degree of detail until high burn-ups.

Table 15 – Relative difference $\Delta(\Delta h)_{\text{rel}}$ in maximum assembly-average fuel enthalpy increase Δh in relation to the fuel assembly burn-up for CR ejection transient

Relative difference $\Delta(\Delta h)_{\text{rel}}$ [%]	Δh calculated by the code system [J/g]	Burn-up [MWd/kgHM]
-69.8	6.3	46.3
-78.0	16.3	45.1
-80.5	10.8	50.2
-90.8	8.3	43.8
-91.1	18.9	43.8
-106.2	5.4	59.2
-111.2	8.4	55.2
-148.8	12.6	59.9
-155.4	7.6	64.9
-156.8	5.3	64.4

For analysing the main parameters causing the differences in Δh , node-wise differences in maximum centreline fuel temperature were analysed with respect to the influence of the fuel thermal conductivity, radial power density profile in the fuel pellet and heat transfer in the gap. Contrary to the node average fuel enthalpy, the centreline fuel temperature also contains local information, i.e. the radial temperature distribution can be peaked at the periphery due to

adiabatic heating at the beginning of a CR ejection [24]. For all burn-up levels, DYN3D-TRANSURANUS systematically calculates higher maximum values for the node centreline fuel temperature (max. difference of 180.7 K) compared to DYN3D standalone in case of a CR ejection (cf. Figure 34 (left) and Table 16). Larger differences are already observed for low burn-up fuel, although in the case of a CR ejection initiated from HZP conditions, the differences in Figure 34 (right) are negligible and are in the uncertainty range of a fuel performance code.

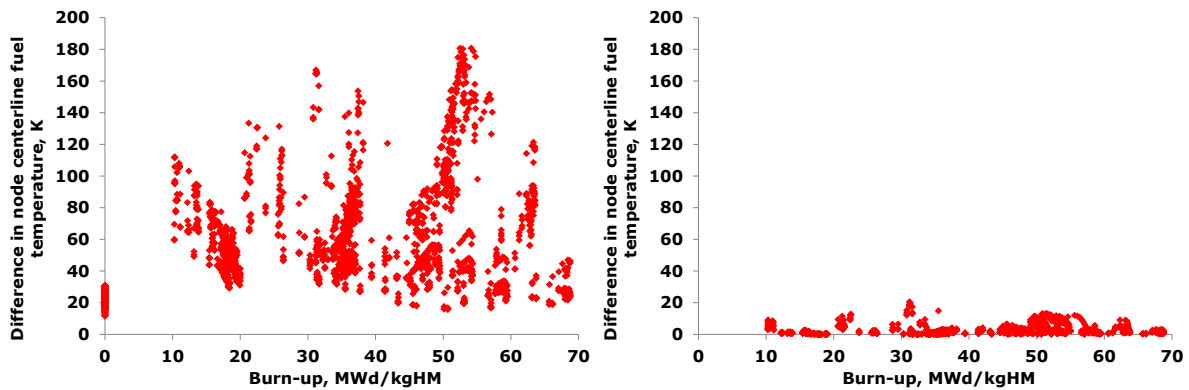


Figure 34: Node-wise differences in maximum centreline fuel temperature over node burn-up for CR ejection without DNB. Differences are defined as two-way coupling approach DYN3D-TRANSURANUS (realistic) minus DYN3D. Left, at 30 % of nominal reactor power; right, at HZP conditions.

Table 16 – Differences in maximum values of the node centreline fuel temperature for CR ejection transient (defined as DYN3D-TRANSURANUS minus DYN3D standalone)

Code system	Differences in max. values of node centreline fuel temperature [K]	
	minimum	maximum
Two-way coupling approach DYN3D-TRANSURANUS (realistic)	11.7	180.7
Two-way coupling approach DYN3D-TRANSURANUS (variant I)	-77.1	100.1
Two-way coupling approach DYN3D-TRANSURANUS (variant II)	14.4	580.0
Two-way coupling approach DYN3D-TRANSURANUS (variant III)	-11.8	119.6
Two-way coupling approach DYN3D-TRANSURANUS (variant IV)	-4.2	3.7

It should be pointed out that the differences in the calculated quantities could be minimized by adopting input values e.g. for the radial power density profile in the DYN3D internal fuel rod model, which is not the standard approach. In this case, pre-calculations by a fuel performance code like TRANSURANUS must be performed to obtain these values. However, the direct coupling is the more consistent way to achieve best estimate results.

6.4.2.2 Impact of fuel thermal conductivity

Firstly, the influence from different models for fuel thermal conductivity λ_{fuel} was analyzed. DYN3D describes $\lambda_{fuel} \left[\frac{W}{mK} \right]$ in a simplified approach as usual in thermal hydraulics system, sub-channel thermal hydraulics and reactor dynamics codes:

$$\lambda_{fuel} = \frac{3800}{T_{fuel} + 130} + 3400 \times 10^{-17} \cdot T_{fuel}^4 \quad (17)$$

where T_{fuel} is the local fuel temperature in K . In contrary, TRANSURANUS models the thermal conductivity $\lambda_{fuel} \left[\frac{W}{mK} \right]$ of LWR UO_2 fuel in greater detail, i.e. also accounting for the burn-up degradation, Gd content and porosity [166]:

$$\lambda_{fuel} = \left(\frac{1}{a+a_1bu+a_2Gd+b_1buT_p+b_2GdT_p+bT_{fuel}} + \frac{c}{T_{fuel}^2} e^{\frac{d}{T_{fuel}}} \right) (1 - P)^{2.5} \quad (18)$$

T_{fuel} is again the local fuel temperature in K , T_p is the local absolute temperature defined as $T_p = \min(1923, T_{fuel})$ in K , bu is the local burn-up in $\left[\frac{MWd}{kgU} \right]$, Gd is the local gadolinium concentration in $wt\%$, and P is the local porosity. In particular, the porosity has an impact because of the restructured periphery in high burn-up fuel. The remaining parameters in eq. (18) are fitting constants [166].

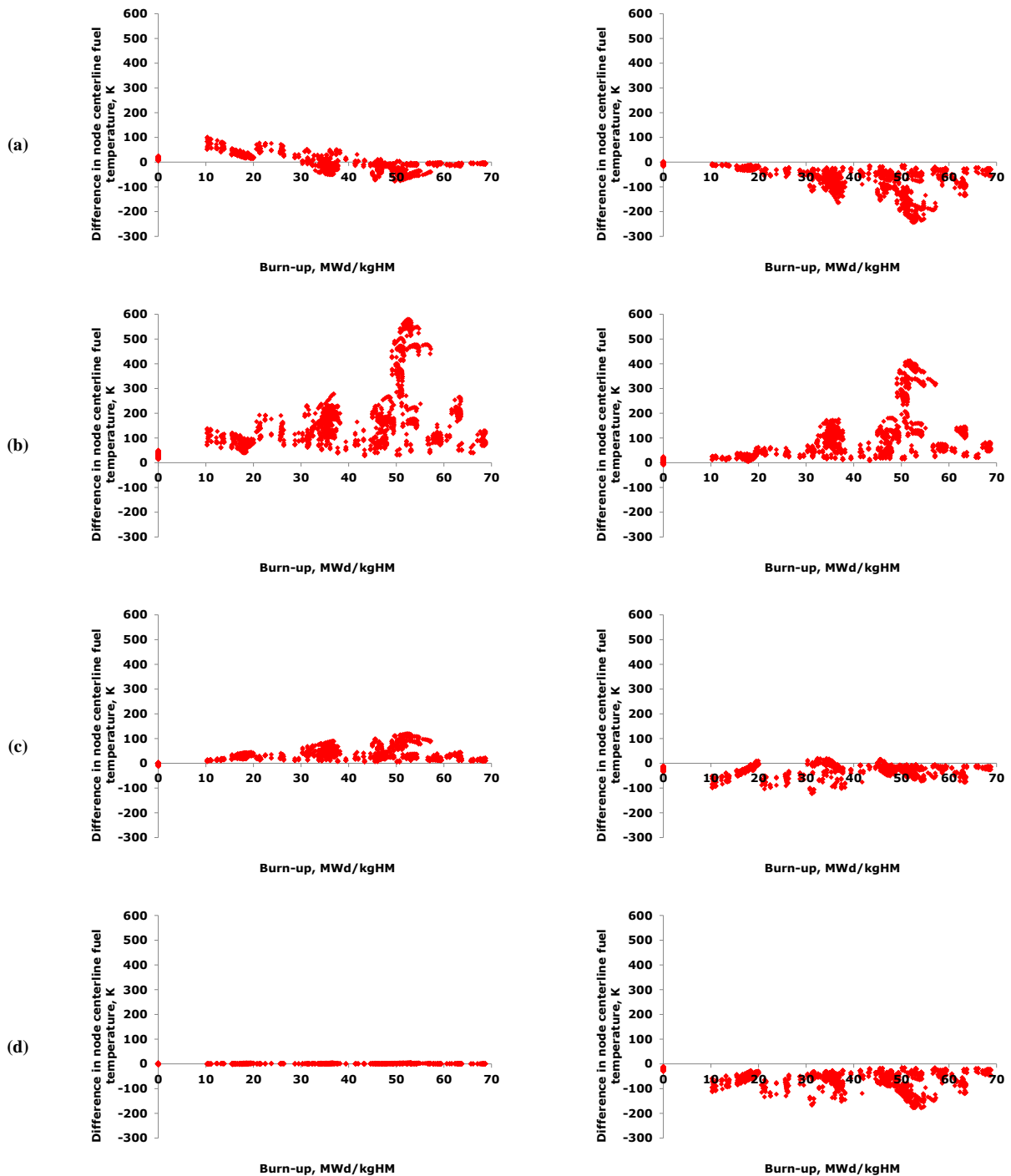


Figure 35: Node-wise differences in maximum centreline fuel temperature over node burn-up for CR ejection at 30% of nominal reactor power for (a) variant I with identical fuel thermal conductivity, (b) variant II with identical power density profile, (c) variant III with identical heat transfer coefficient in gap, and (d) variant IV as combination of (a), (b) and (c). Left, difference defined as two-way coupling approach DYN3D-TRANSURANUS (variant I, II, III or IV) minus DYN3D (standalone); right, differences defined as two-way coupling approach DYN3D-TRANSURANUS (variant I, II, III or IV) minus DYN3D-TRANSURANUS (realistic).

Eq. (17) was implemented in the code system as a first simplification, and will be referred to as variant I (see section 6.2). The variant I leads to node-wise differences in maximum centreline fuel temperature ranging between -244 K and 2 K (cf. Figure 35 (a) on the right). The differences up to 20 MWd/kgHM lie in the range of a fuel performance code uncertainty; beyond this burn-up value the DYN3D correlation leads to lower temperatures with increasing tendency up to 50 - 55 MWd/kgHM. This is mainly attributed to the so-called thermal conductivity degradation with increasing burn-up. At even higher burn-up, the differences decrease due to the lower injected energy in these nodes. On the one side the importance of the fuel thermal conductivity can be clearly seen, on the other side eq. (18) shows the complexity to provide all necessary information for integrating it into a thermal hydraulics system, sub-channel thermal hydraulics and reactor dynamics codes. For example, the porosity depends on densification, fission gas swelling and HBS porosity development. Nevertheless, the results in Figure 35 also show that the thermal conductivity cannot completely explain the differences.

6.4.2.3 Impact of power density profile

For increased burn-ups, the radial power density profile is not flat anymore [98]. The exact modelling of this phenomenon is important at least for fast reactivity transients because the high amount of injected energy during a few milliseconds can first result in a radial temperature profile peaked at the periphery [3, 24]. To analyse the influence on the differences in Figure 34 (left), DYN3D-TRANSURANUS was aligned to DYN3D imposing a flat profile in TRANSURANUS for all fuel rods, described in more detail as variant II in section 6.2. The differences with this modification lie between -9 K and 413 K compared to the realistic version of the code system (cf. Figure 35 (b) on the right). Above 30 MWd/kg HM the differences show a rapid increase to almost 200 K. Furthermore, a peak in the differences up to 413 K occurs between 50 - 55 MWd/kgHM. The fuel performance code uncertainty is much lower than the observed differences (cf. Figure 35 (b) on the right). As expected, the assumption of a flat profile in DYN3D represents a conservative approach for the centreline fuel temperature due to an overestimated power density factor in the centre.

To simulate the radial power density profile in DYN3D as an appropriate function of burn-up and composition, two alternative approaches exist beside a coupling approach to a fuel

performance code. Firstly, the TRANSURANUS burn-up model (TUBRNP) [98] can be integrated as standalone model to a code like DYN3D. A second alternative represents the supply of form factors as input table. In this case, pre-calculations by a fuel performance code must be performed for different burn-up levels. Furthermore, the transferred form factors should account for the dependences on neutron flux spectra and fuel rod design (e.g. fuel composition). However, the direct coupling is again the more consistent way to achieve best estimate results.

6.4.2.4 Impact of heat transfer in gap

The value of the gap heat transfer coefficient is influenced by the gap width as well as the gas mixture depending on initial fill gas conditions and released fission gas. For the variant III described in section 6.2, the heat transfer coefficient in the gap in DYN3D-TRANSURANUS was set to the one of DYN3D standalone. Additional tests showed that neglecting the mechanic analysis has almost no effect on the differences in Figure 35 (c) in comparison with the influence resulting from the heat transfer coefficient in the gap. Most of the calculated maximum node centreline fuel temperatures (cf. Table 16) are higher (max. 120 K) in the realistic version of DYN3D-TRANSURANUS than in DYN3D. It seems that for the majority of considered fuel rods the heat transfer coefficient used in the DYN3D input is higher than in TRANSURANUS.

Due to the complexity and sensitivity of the heat transfer in the gap, only fuel performance codes usually consider all its relevant parameters. In current state-of-the-art transient safety analysis with coupled code systems, the heat transfer coefficient in the gap is often provided as burn-up and/or linear heat rate dependent input table. For example, the AREVA core thermal hydraulics analysis code system COBRA-FLX [91] offers this as one option. Results of DYN3D-TRANSURANUS confirm the possibility of input tables for accurate simulations of CR ejection without onset of DNB. However, for the heat transfer coefficient a unique solution does not exist for a given linear heat rate (cf. Figure 36 (a) on the left). The node average fuel enthalpy is likely a better indicator for the heat transfer coefficient rather than the linear heat rate.

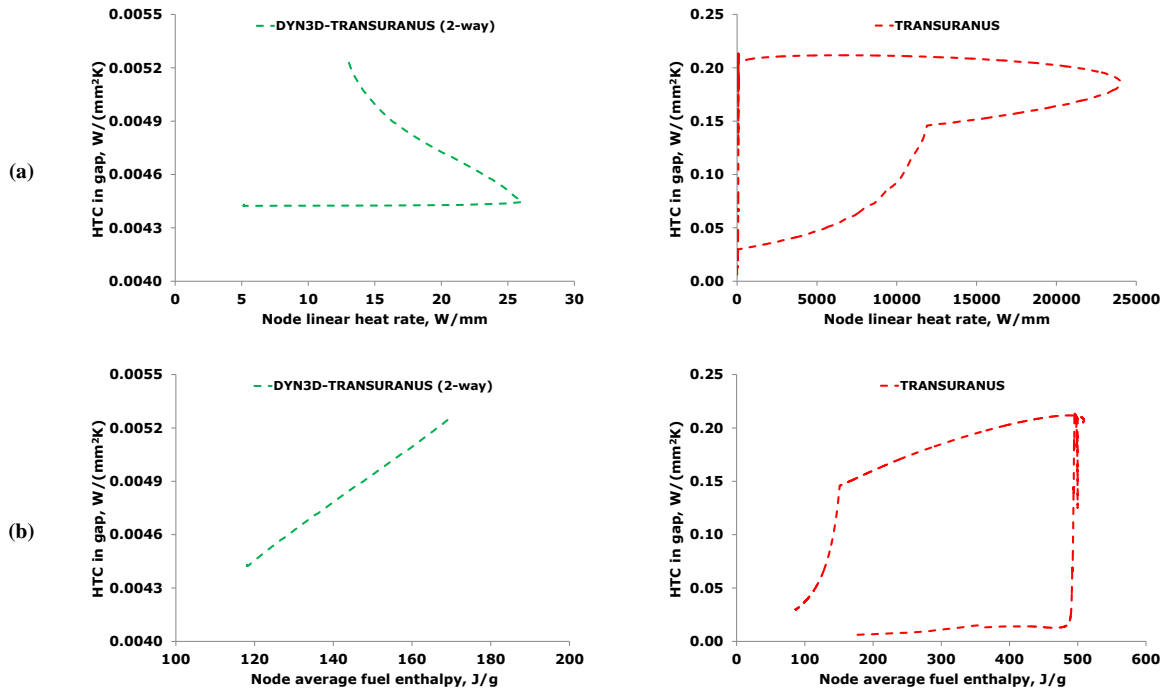


Figure 36: Heat transfer coefficient (HTC) in gap as function of (a) node linear heat rate and (b) node average fuel enthalpy. Left, two-way coupling approach of DYN3D-TRANSURANUS (realistic) for CR ejection with no onset of DNB initiated at 30 % of nominal reactor power (slice with maximum linear heat rate of the fuel assembly containing the ejected CR, cf. Figure 32); right, TRANSURANUS standalone for CR ejection case #3 of OECD RIA Fuel Codes Benchmark with onset of DNB [24] (slice in the middle of the test rodlet).

In a later stage of a RIA ballooning can occur due plasticity of the cladding material at high temperature after onset of DNB and/or fission gas release. This can lead to differences higher than the shown in Figure 35 (c) and will influence the above relation between fuel enthalpy and heat transfer coefficient. The heat transfer coefficient in Figure 36 on the right confirms this by a TRANSURANUS standalone simulation for case #3 of the OECD RIA Fuel Codes Benchmark with onset of DNB [24]. Case #3 represents the CIP3-1 experiment to be performed at the CABRI water loop facility characterized by PWR fuel closely burned up to 75 MWd/kgHM (sectional average burn-up), initiated from HZP, injected energy at peak power node of 115 cal/g, coolant temperature of 280 °C, coolant pressure of 15.5 MPa (all planned values) and a hypothetical boundary condition assuming a flat axial power profile. Because the relationship also depends on heat regimes and their durations, the generation of an input table is very complex. Furthermore, if a feedback on neutronics and thermal hydraulics is considered from detailed fuel behaviour modelling, this may require a manual iteration process between the code system using such an input table and the generation of this

input table by a fuel performance code. Altogether, the direct coupling is again the more consistent way to achieve best estimate results.

6.4.2.5 Impact of all three factors

In variant IV all three previous influences were taken into account. By combining all three factors, negligible differences in maximum node centreline fuel temperature compared to DYN3D standalone (cf. Table 16 and Figure 35 (d) on the left) are observed, which indicates that they account for the differences brought about by the code coupling in the case under consideration.

6.4.3 Comparison of one-way and two-way coupling approach

6.4.3.1 Analysis of differences in feedback on neutron kinetics

Global feedback: reactivity, thermal power and fuel temperature

For the boron dilution transient, the evolutions of total reactivity over time are almost identical comparing the DYN3D-TRANSURANUS one-way approach (identical to DYN3D standalone for this parameter) and the DYN3D-TRANSURANUS two-way approach, cf. Figure 37 (a). The first rise in total reactivity reached peak values of 2.11 \$ (one-way approach) and 2.07 \$ (two-way approach), both greater than 1 \$ meaning prompt criticality. The corresponding peak values of total nuclear power amounted 32,090 MW (one-way approach) and 32,144 MW (two-way approach). In the initial phase of the transient, the reactor is still sub-critical with zero power. Therefore, all temperatures, including the fuel temperatures, are more or less equal to the coolant temperature at the core inlet. So differences can't be expected applying DYN3D-TRANSURANUS (two-way approach) and DYN3D, before under-borated coolant entered the core. When the reactor becomes critical and later super-critical, the power starts to rise very quickly and in parallel the fuel temperature increases. The delay, caused by heat transfer time constant, leads to the situation that the heat-up of the fuel immediately after reactivity insertion is practically adiabatic. This means that it isn't affected by heat conduction in the fuel rod. If the adiabatic condition would

be fulfilled exactly, this should lead to identical results. Therefore, the difference in the first peak of total nuclear power amounted only 0.17 %, hence is negligible.

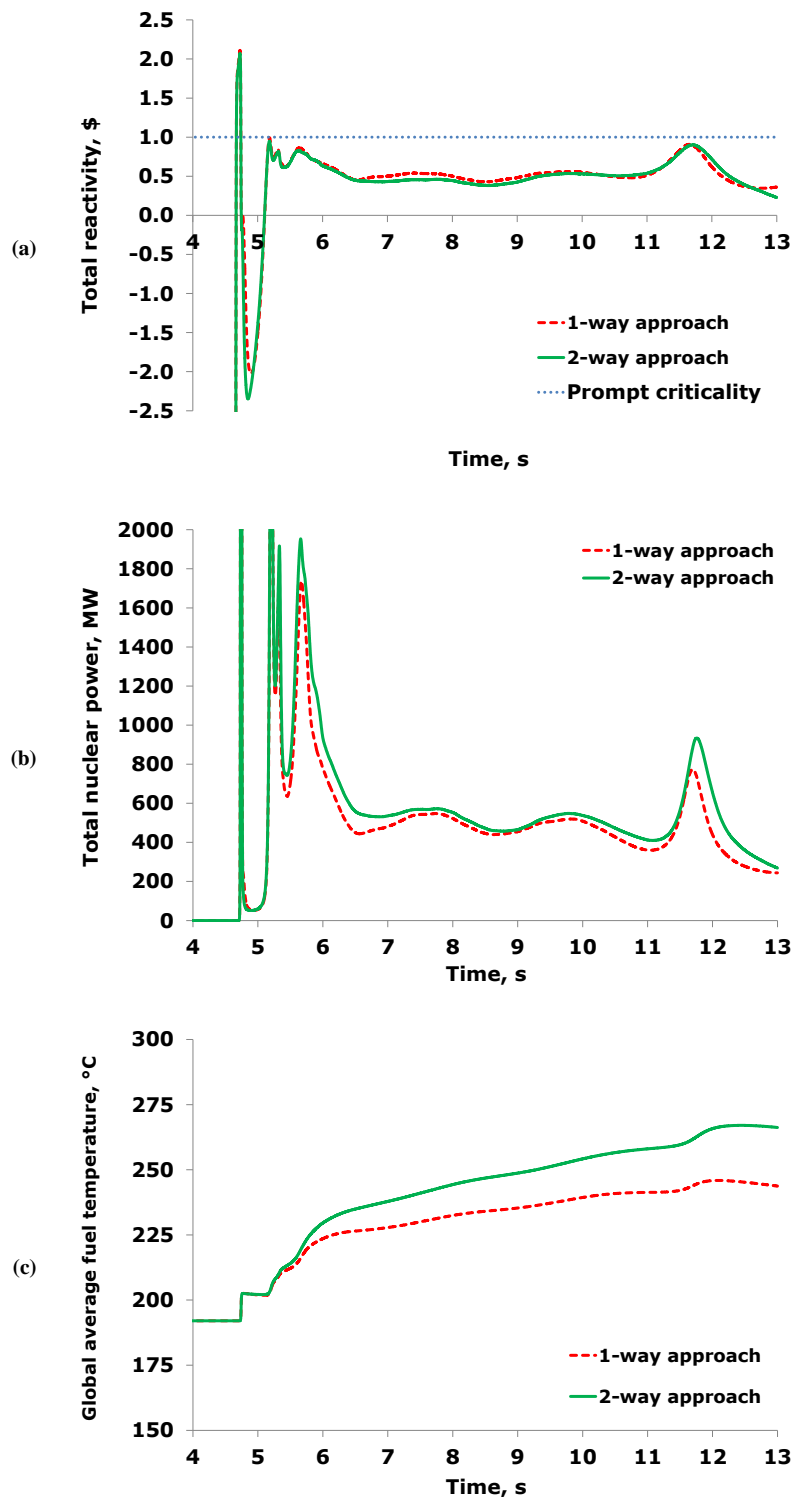


Figure 37: Total reactivity vs. time (a), total nuclear power zoomed in for showing differences vs. time (b) and global average fuel temperature vs. time (c) [values of the 1-way approach taken from the DYN3D part in the coupled code system]

Due to the upward movement of the boron dilution front in the core, secondary core power rises with smaller magnitudes occurred after the first peak (cf. Figure 37 (b)). For the first time, a difference in global average fuel temperature can be observed at 5.3 s. It increased over time between the one-way approach (values taken from the DYN3D part of the one-way coupling approach, hence identical to DYN3D standalone) and the two-way approach (cf. Figure 37 (c)). Despite the identical initial conditions, the fuel temperature increased slightly more for the two-way approach, reaching a maximum difference of 22 K (compared to maximum difference of 44 K during the CR ejection event in Ref. [10] (see subsection 6.4.2)). As mentioned above an increase in difference was expected, because recently DYN3D-TRANSURANUS showed a pronounced influence of detailed modelling on the heat transfer in the fuel rod for the CR ejection simulations [10].

Locally a large feedback on the thermal hydraulics could be observed in the boron dilution analysis, especially in those nodes where film boiling occurred (see subsection 6.4.3.2). The feedback on the thermal hydraulics affected slightly the global neutron kinetics, i.e. the peak in total reactivity around 11.7 s was slightly delayed in the two-way approach, mainly caused by the positive boron reactivity affected by the lower coolant density. However, the effect on the total reactivity and total nuclear power is limited, because film boiling was reached only in one node (best estimate ratio between CHF and actual heat flux) and in a few nodes (conservative ratio between CHF and actual heat flux).

Local feedback: injected energy and increase of assembly-wise fuel enthalpy

Nevertheless, the differences in global average fuel temperature can't explain completely the total reactivity evolution, shown in Figure 37 (a). For example, after the first power rise the total reactivity decreased to -2.02 \$ (one-way approach) and to -2.35 \$ (two-way approach) in spite of identical global average fuel temperatures at that time. Furthermore, the total nuclear power was higher in the two-way approach during the further course of the transient (cf. Figure 37 (b)), in spite of a higher global average fuel temperature. Both observations can be explained by the dependence of the total reactivity on the moderator density.

The moderator density was affected by local boundary conditions, which in turn led to local variations of the neutron kinetics. In the following, we will look at differences in local parameters like injected energy into the fuel in each node. Three main reasons can be identified for local dependencies: At first, the slug volume of unborated coolant is located in

one loop whose main coolant pump was started as first. Therefore, the distribution of the boron concentration over the core inlet plane is very heterogeneous and affected by complex turbulent mixing patterns. At second, the stuck CR conditions is responsible for the distortion of the regular power distribution in the core, and at third, the assembly-average burn-up is distributed heterogeneously over the core. They all contribute to an inhomogeneous injection of energy into the core (cf. Figure 38), hence the values of maximum enthalpy increase can strongly differ among fuel assemblies influencing locally the neutron kinetics (cf. Figure 39). For example, the maximum assembly-average fuel enthalpy rise occurred with 66.2 J/g in the fresh fuel assembly B6 (containing the stuck CR), followed by the neighboured fresh fuel assembly B7 with the second highest value in the calculated scenario. Furthermore, fuel enthalpy increases of up to more than 40 J/g could be seen for all average fuel assembly burn-up levels up to 50 MWd/kgHM. At the same time, fuel assemblies with larger burn-ups were located in the outermost row of the core (except for the central fuel assembly H8 with 53.2 MWd/kgHM).

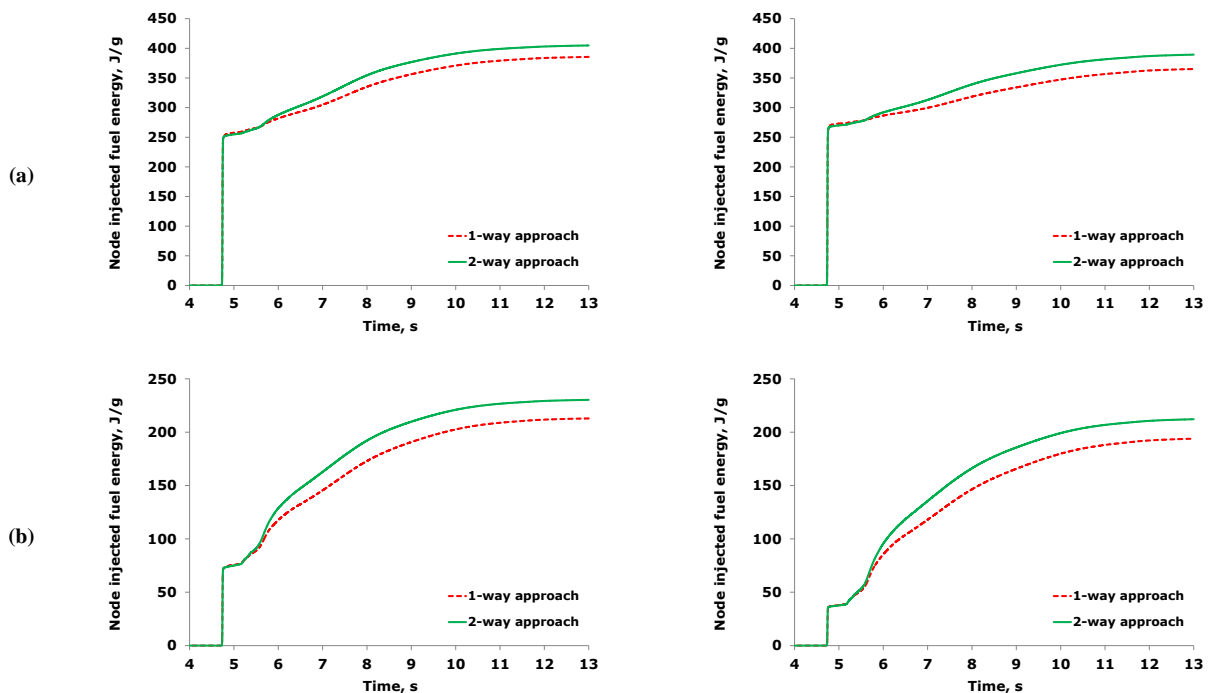


Figure 38: Node average injected energy vs. time. (a) For the node at the bottom of the fresh fuel assembly B6 (left) and for the 2nd lowest node of the same assembly (right). (b) For the node at the bottom of fuel assembly D5 with average assembly burn-up of 31.7 MWd/kgHM (left) and for the node at the bottom of fuel assembly E6 with average assembly burn-up of 50.0 MWd/kgHM (right).

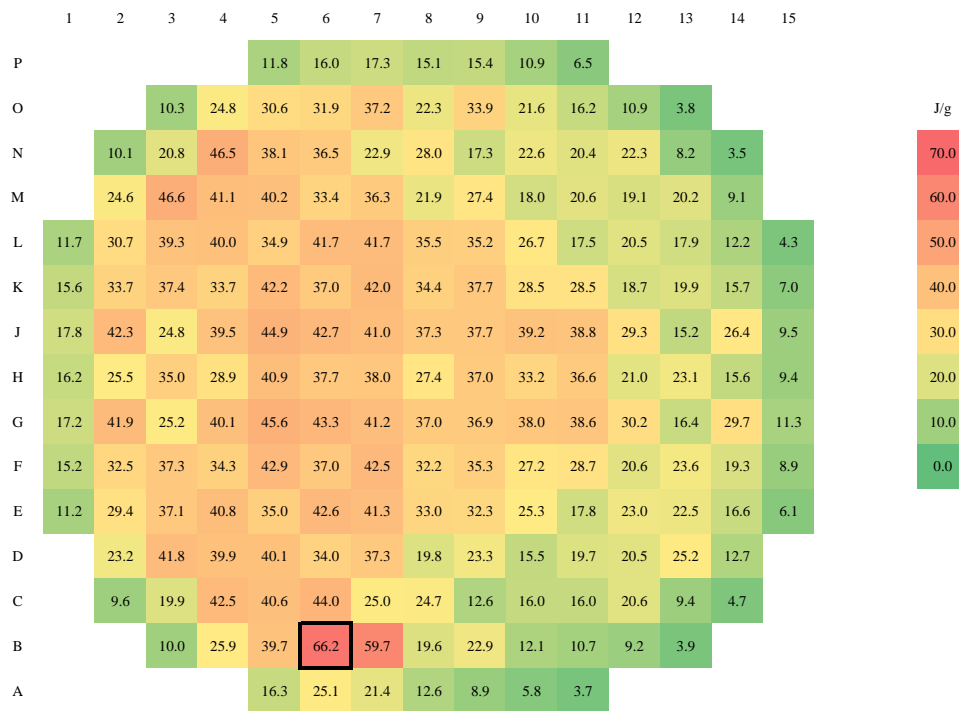


Figure 39: Maximum assembly-average fuel enthalpy increase Δh calculated by DYN3D-TRANSURANUS (two-way approach) [bordered fuel assembly contains the stuck CR]

As depicted in Figure 38, the injected energy was affected by the degree in detail in online fuel behaviour modelling. For all cases shown in Figure 38, the two-way approach calculated higher injected energies. A closer look at Figure 38 reveals that after the first power rise at 4.7 s the injected energy calculated in both approaches reached almost identical values in the 2nd lowest node of the fresh fuel assembly B6 (one-way approach: 268.2 J/g; two-way approach: 267.5 J/g). Afterwards the injected energy increased continuously slightly more in the two-way approach, following additional injected energy due to secondary power peaks of 96.9 J/g for the one-way approach and 121.8 J/g for the two-way approach. Thence, locally the neutron kinetics was influenced by the degree in detail in online fuel behaviour modelling. Due to its (strongly) coupling to the thermal hydraulics, this is discussed further in subsection 6.4.3.2.

6.4.3.2 Analysis of differences in feedback on thermal hydraulics

Local feedback: node average fuel enthalpy

Firstly, the differences in maximum node average fuel enthalpy were analysed, because a faster decrease can promote the onset of film boiling and a slower decrease PCMI and fuel melting. In case of the boron dilution transient, for all local burn-up levels, the two-way approach of DYN3D-TRANSURANUS calculated values between 0.5 J/g lower and 22.3 J/g higher, compared to the one-way approach (cf. Figure 40 (a) on the left). This is in line with (larger) differences observed already for low burn-up levels in case of the CR ejection event in a PWR (see subsection 6.4.2) [10]. At higher burn-ups the maximum differences decreased in both boron dilution transient and CR ejection event due to smaller transient power levels. When plotting the results from the two-way coupling against those of the one-way coupling in Figure 40 (b) on the left, the cloud of points was shifted in the direction of the two-way approach values. This shift is slightly larger with increase in maximum node average fuel enthalpies. The maximum shift included differences greater than 10 %. The envelope in the direction to the one-way approach values could be found around the 45° line at which the differences vanish. Nevertheless, there are four points for which both methods gave similar results even though the maximum node average fuel enthalpy exceeds 250 J/g. The two points with the highest values belong to the two lowest nodes of the fuel assembly B6. Due to the position of the stuck CR in this fuel assembly (cf. Figure 39) and the high amount of fissile material, the injection of the under-borated coolant from the bottom of the core induces a maximum increase in enthalpy. The other two values belong to the neighbouring fresh fuel assembly B7. Differences didn't occur for these nodes, because the maximum enthalpy value was reached during the first power rise with almost adiabatic fuel heat-up (see subsection 6.4.3.1).

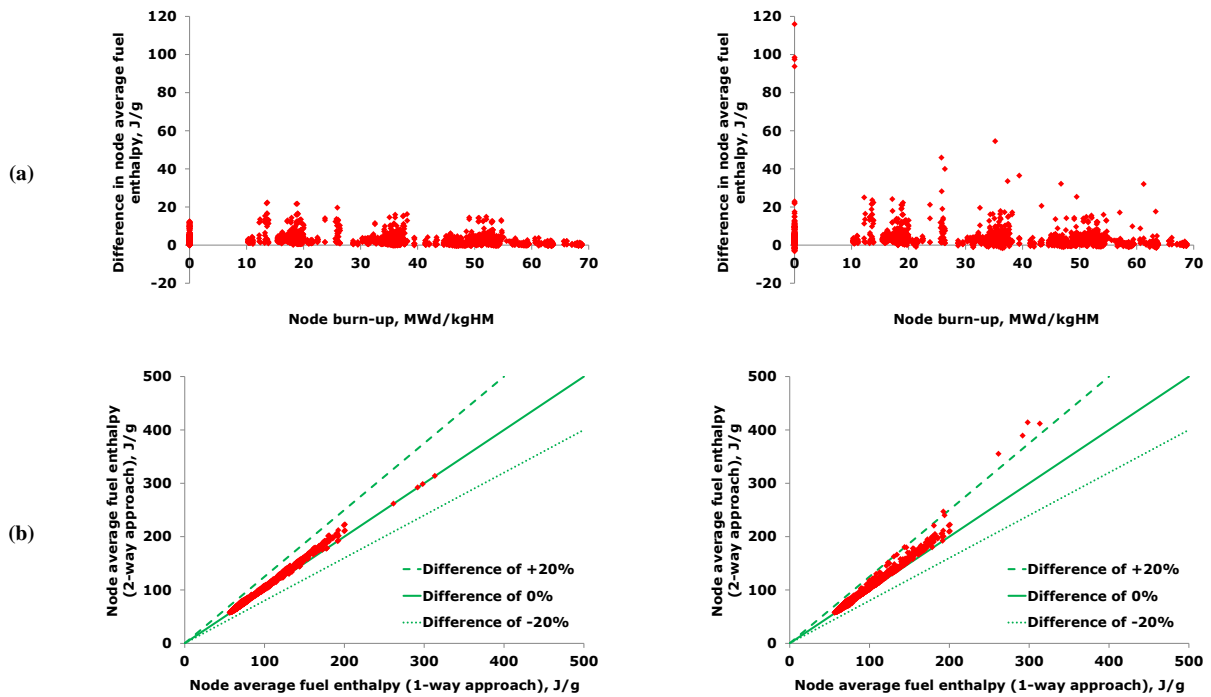


Figure 40: (a) Node-wise differences in maximum average fuel enthalpy as a function of the node burn-up. Differences are defined as the result of the two-way coupling approach minus the corresponding result of the one-way coupling approach of DYN3D-TRANSURANUS. (b) Maximum node average fuel enthalpy calculated by the two-way coupling approach versus the corresponding value of the one-way coupling approach. The ratio between the CHF and the actual heat flux, at which DNB is assumed, amounted to 1.0 (best estimate value) on the left and to 2.0 (conservative value) on the right.

The impact of more detailed fuel behaviour modelling on the evolution of node average fuel enthalpy was analysed to better understand the slightly higher increase in global average fuel temperature over time in Figure 37 (c) in the two-way approach. For the bottom node of fuel assembly B6 (core-wide with the second highest maximum node average fuel enthalpy), the evolution of the node average fuel enthalpy were very similar for both approaches (cf. Figure 41 (a) on the left). The peak values amounted 298.2 J/g for the one-way approach and 298.6 J/g for the two-way approach. However, beginning from 5.6 s the two-way approach of DYN3D-TRANSURANUS determined slightly higher values compared to the one-way approach. At the end of the calculation (13 s) the node average fuel enthalpies were almost identical. If the injected energy increases faster in the two-way approach (cf. Figure 38 (a) on the left), at the same time the node average fuel enthalpy will rise more compared to the one-way approach (cf. Figure 41). However, the node average fuel enthalpy will also decrease slightly faster in the two-way approach (higher temperature gradient) meaning both

evolutions come closer together. Altogether all difference lay in the uncertainty range of fuel performance codes (cf. results of the OECD RIA Fuel Codes Benchmark in Ref. [24, 25]).

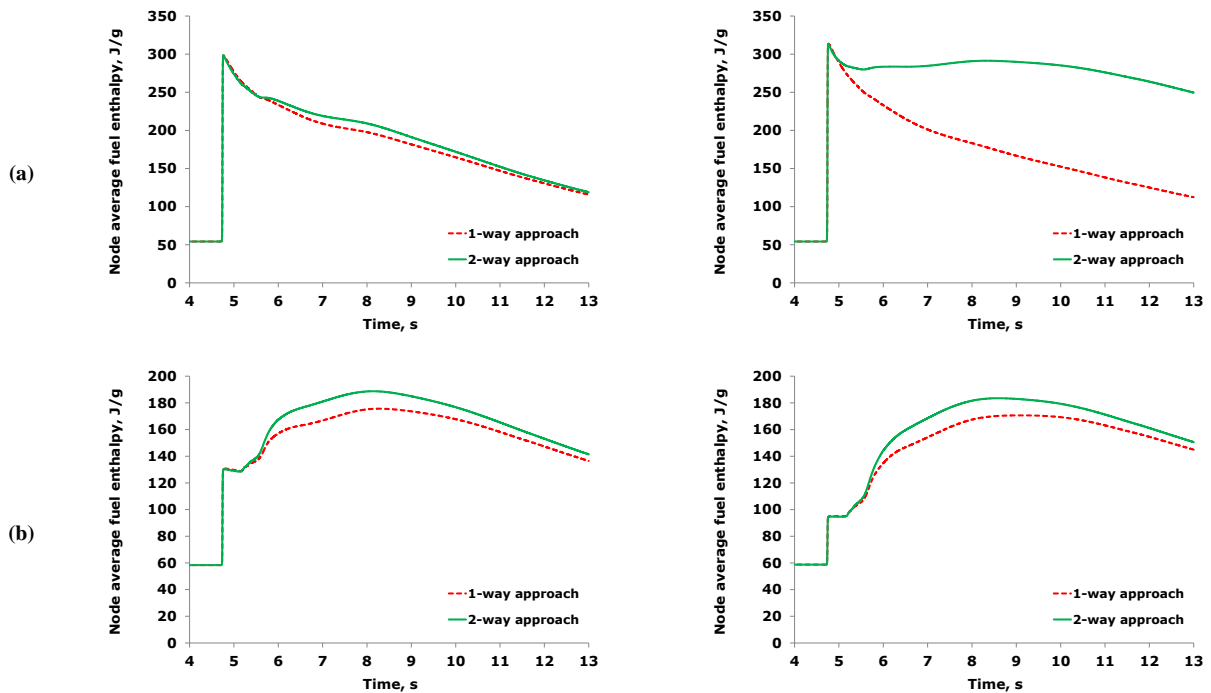


Figure 41: Node average fuel enthalpy vs. time. (a) For the node at the bottom of the fresh fuel assembly B6 (left) and for the 2nd lowest node of the same assembly (right). (b) For the node at the bottom of fuel assembly D5 with average assembly burn-up of 31.7 MWd/kgHM (left) and for the node at the bottom of fuel assembly E6 with average assembly burn-up of 50.0 MWd/kgHM (right).

Similar findings were expected for the fuel enthalpy of the 2nd lowest node of the same fuel assembly (core-wide with the highest maximum node average fuel enthalpy). The peak values are almost identical. Nevertheless, the average fuel enthalpy evolved completely different after 5 s (cf. Figure 41 (a) on the right). This couldn't be explained only by the injected energy (cf. Figure 38 (a) on the right). This seems to be mainly caused by the onset of film boiling in this node in the two-way approach. The improved fuel behaviour modelling interacting with a thermal hydraulic model, which is able to describe post-CHF heat transfer, resulted in different fuel thermal conductivity and heat transfer coefficient in the gap. This leads to a higher heat flux directly after the first power rise in the two-way approach. Since it occurred in fresh fuel, the detailed modelling in radial pellet power density profile couldn't be responsible. In the heat transfer regime of film boiling, the heat flux is significantly reduced, and the accumulated energy will be transferred to the coolant much slower. This effect explains the situation that the node average fuel enthalpy drops much slower than calculated

by the one-way approach (cf. Figure 41 (a) on the right). At the same time higher fuel enthalpies can promote PCMI and fuel melting. Thence altogether, the application of simplified fuel behaviour modelling and its associated influence should be analysed carefully, at least for conditions in the vicinity of film boiling.

As mentioned before the internal DYN3D fuel behaviour model is validated only for fresh and low burn-up fuel [94]. Potentially larger differences compared to TRANSURANUS were therefore expected for fuel rods with medium and high burn-up values. This was observable at the bottom node of fuel assemblies D5 with an assembly average burn-up around 32 MWd/kgHM and E6 with an assembly average burn-up around 50 MWd/kgHM. In these cases, maximum node average fuel enthalpies of 175.6 J/g (one-way approach) versus 188.7 J/g (two-way approach) for assembly D5 and of 170.6 J/g (one-way approach) versus 183.5 J/g (two-way approach) for assembly E6 were predicted. These peak values occurred at 8.1 s for assembly D5 and at 8.6 s for assembly E6, hence not during the first rise in total reactivity as for the two nodes of assembly B6. After this first rise the node average fuel enthalpy begun to increase for a second time, caused by the secondary rises in total reactivity (cf. Figure 41 (b)). Further analysis of the differences is provided in the following (see “Local feedback: node clad surface temperature”).

An additional set of calculations was accomplished performing a theoretical study in order to allow analysing nodes in which film boiling occurs in both approaches of the coupled system DYN3D-TRANSURANUS. For this purpose, the ratio between the CHF and the actual heat flux, at which DNB is assumed, was increased from 1.0 (best estimate value) to 2.0 (conservative value). This value is an optional input parameter in DYN3D. The node-wise differences in maximum average fuel enthalpy as a function of burn-up are shown in Figure 40 (a) on the right. In comparison to the best estimate results (cf. Figure 40 (a) on the left), larger changes in the differences between one-way and two-way approach could be seen. In particular, the two-way approach leads to film boiling in five nodes as summarised in Table 17. For these nodes, the effect of detailed online fuel behaviour modelling on the thermal hydraulics (coupled to the neutron kinetics) in the two-way approach was strong. In some cases, values higher than 30 % for the maximum node average fuel enthalpy compared to the one-way approach were calculated (cf. Figure 40 (b) on the right and Table 17). As main conclusion, the maximum node average fuel enthalpy will be affected strongly if film boiling is initiated leading to a maximum after the first peak of total reactivity.

Table 17 – Maximum node average fuel enthalpy for nodes with film boiling (simulation with increased ratio between CHF and actual heat flux)

Fuel assembly	C6	B6		B7	
Node	2 nd lowest	bottom	2 nd lowest	bottom	2 nd lowest
Fuel enthalpy [J/g] for one-way approach	192.4	298.2	313.3*	261.5	291.8*
Fuel enthalpy [J/g] for two-way approach	246.9*	414.1*	411.8*	355.3*	389.3*

*film boiling occurred

The differences shown in Figure 38, Figure 40 and Figure 41 were expected to be able to be minimized by adopting appropriate input values for the radial power density profile and for the gap heat transfer coefficient, and by replacing the model for fuel thermal conductivity (see subsection 6.4.2) [10]. This would require pre-calculations by a fuel performance code like TRANSURANUS. Nonetheless, an accurate provision of the heat transfer coefficient in the gap as a correlation is challenging, due to its sensitivity and complex modelling in the case of gap closure and film boiling.

Local feedback: node clad surface temperature

A conclusion about the conservatism of reactor safety analysis cannot be drawn from the fuel enthalpy alone: A higher fuel enthalpy can lead to more distinct PCMI with the increased potential for fuel rod failure, or to higher fuel temperatures inducing fuel melting. A lower fuel enthalpy caused by a higher heat transfer in the gap can lead to higher heat fluxes and might cause earlier onset of film boiling. In turn this can result in an increase of clad surface temperatures. Following the fuel enthalpy analysis, the nodes can be separated in two categories for the study of node-wise differences in clad surface temperature shown in Figure 42: those with only pre-CHF heat transfer and those with post-CHF heat transfer (e.g. film boiling) occurring in either only the two-way approach or in both approaches.

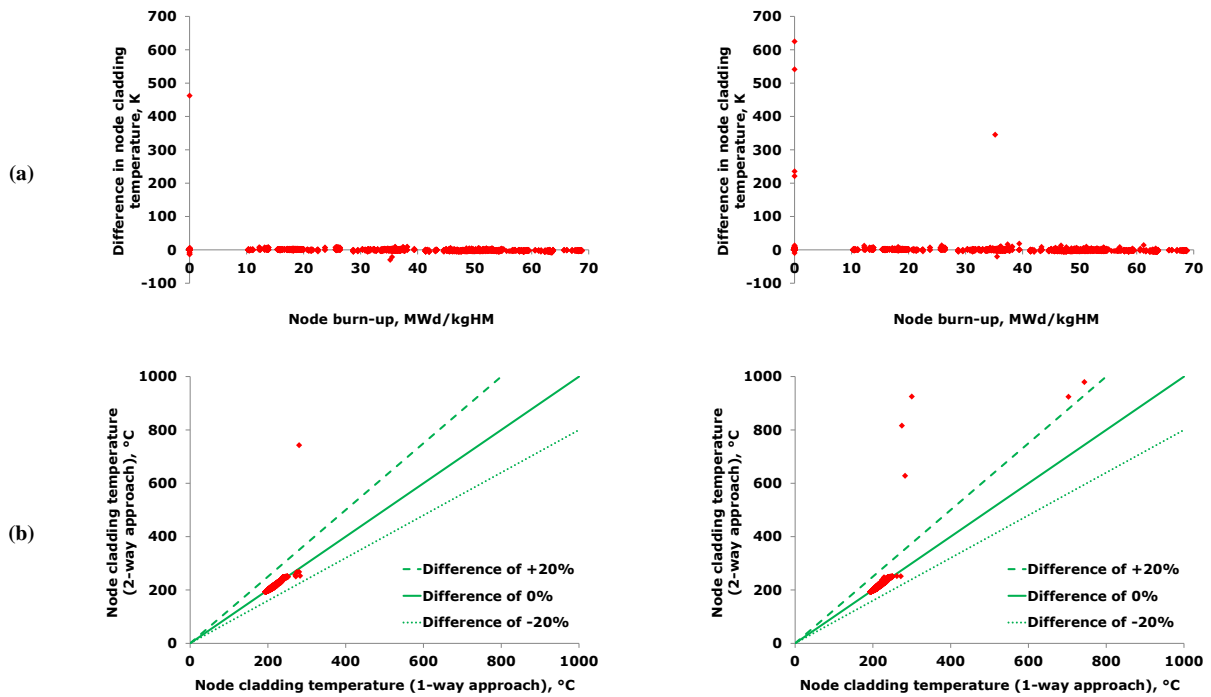


Figure 42: (a) Node-wise differences in maximum clad surface temperature as a function of the node burn-up. Differences are defined as the result of the two-way coupling approach minus the corresponding result of the one-way coupling approach of DYN3D-TRANSURANUS. (b) Maximum node clad surface temperature calculated by the two-way coupling approach versus the corresponding value of the one-way coupling approach. The ratio between the CHF and the actual heat flux, at which DNB is assumed, amounted to 1.0 (best estimate value) on the left and to 2.0 (conservative value) on the right.

For the first category of nodes, the differences in maximum clad surface temperature varied between -30.0 K and 9.3 K for the best estimate calculation (cf. Figure 42 (a) on the left) and between -20.4 K and 18.5 K for the calculation containing the increased ratio for DNB (cf. Figure 42 (a) on the right). All clad surface temperatures belonging to this first category remained below 300 °C (cf. Figure 42 (b)). Furthermore, only small differences appeared in the evolution of clad surface temperature over time (cf. Figure 43 (a) on the left as well as Figure 43 (b) on the left and right).

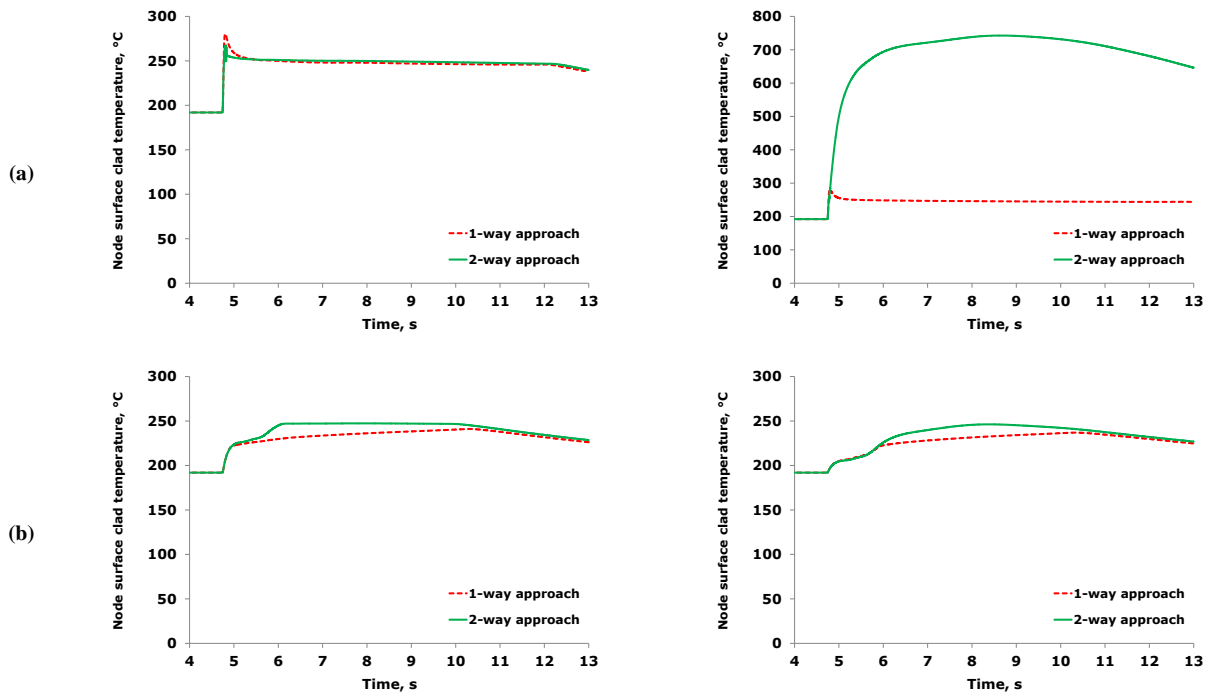


Figure 43: Node clad surface temperature vs. time. (a) For the node at the bottom of the fresh fuel assembly B6 (left) and for the 2nd lowest node of the same assembly (right). (b) For the node at the bottom of fuel assembly D5 with average assembly burn-up of 31.7 MWd/kgHM (left) and for the node at the bottom of fuel assembly E6 with average assembly burn-up of 50.0 MWd/kgHM (right).

There are only a limited number of nodes of the second category as can be seen in Figure 42. When applying the two-way approach, film boiling occurred in the 2nd lowest node in assembly B6 in the best estimate calculation (cf. Figure 42 (a) and (b) on the left) and in five nodes when applying a conservative CHF (cf. Figure 42 (a) and (b) on the right). For the best estimate calculation, the peak node clad surface temperature amounted to 280.4 °C (one-way approach) and to 742.6 °C (two-way approach), whereas post-CHF heat transfer didn't occur in the one-way approach. For the conservative CHF, the corresponding peak node clad surface temperatures are summarized in Table 18. These results confirm that the peak node clad surface temperature, hence the thermal hydraulics, depends strongly on the degree in detail in online fuel behaviour modelling if heat transfer crisis (e.g. film boiling) occurs.

Table 18 – Maximum node clad surface temperature for nodes with film boiling (simulation with increased ratio between CHF and actual heat flux)

Fuel assembly	C6	B6		B7	
Node	2 nd lowest	bottom	2 nd lowest	bottom	2 nd lowest
Clad surface temperature [°C] for one-way approach	282.9	300.1	743.9*	274.7	703.1*
Clad surface temperature [°C] for two-way approach	628.1*	925.0*	979.3*	815.8*	924.3*

*film boiling occurred

Besides the peak value, the corresponding evolution of the node clad surface temperature was strongly affected by film boiling. This is illustrated for the 2nd lowest node of assembly B6 in the best estimate calculation in Figure 43 (a) on the right. In this case, the peak was reached at the first power rise in the one-way approach and during the film boiling phase in the two-way approach. Thence, the modelling of the heat transfer in the fuel rod influenced also heavily the node average fuel enthalpy (cf. Figure 41 (a) on the right). More precisely, the heat transfer coefficient in the gap was almost identical until 5.2 s (cf. Figure 44 (a) on the right). Afterwards the value of the two-way approach stayed at greater values mainly due to the higher fuel thermal expansion associated with the fuel enthalpy (cf. Figure 41 (a) on the right). However, the heat flux between fuel and cladding depends on both the heat transfer coefficient in the gap and the temperature difference between the outer fuel temperature and the clad inner surface temperature. For example, this temperature difference was very high during the first power rise and decreased afterwards in 2nd lowest node of assembly B6, especially in case of post-CHF conditions due to higher clad surface temperatures. Furthermore, the outer fuel temperature is also influenced by the fuel thermal conductivity, which is almost always higher in the DYN3D internal fuel behaviour model (see subsection 6.4.2) [10]. This leads to a faster reduction in fuel enthalpy in the simplified fuel behaviour model.

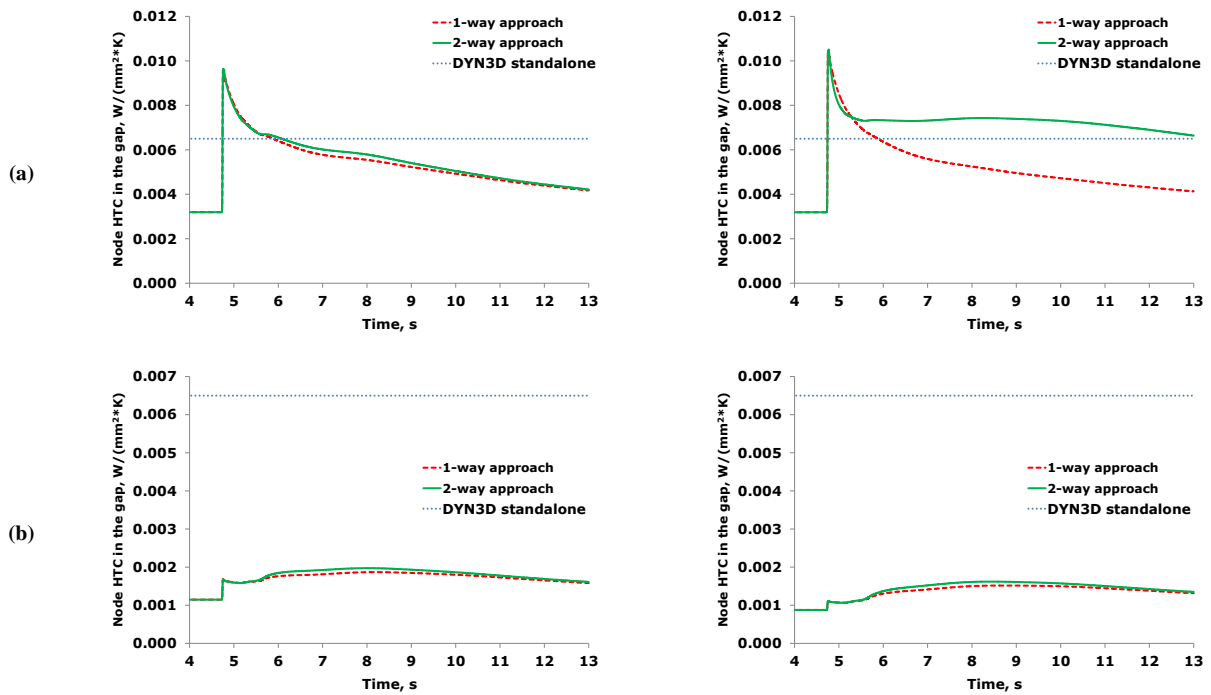


Figure 44: Node heat transfer coefficient (HTC) in the gap vs. time. (a) For the node at the bottom of the fresh fuel assembly B6 (left) and for the 2nd lowest node of the same assembly (right). (b) For the node at the bottom of fuel assembly D5 with average assembly burn-up of 31.7 MWd/kgHM (left) and for the node at the bottom of fuel assembly E6 with average assembly burn-up of 50.0 MWd/kgHM (right).

From the discussion above, it appears that for the second node category with occurrence of film boiling, the time at which the maximum clad surface temperature appeared and the time at which the maximum fuel enthalpy was predicted in that node did not match always. For the determined scenario and depending if post-CHF heat transfer occurs in the calculation, the peak node clad surface temperature will appear in the film boiling phase and not at the first power rise (cf. Figure 43). However, conclusion can't be drawn about the location of the maximum node average fuel enthalpy in case of film boiling. The fuel enthalpy was strongly affected by the local amplitude of the first power rise, by the amount of injected energy during the secondary power rises and the heat transfer in the fuel rod.

6.5 Computational costs

The calculations were executed with one core of an eight-core Intel Xeon processor (1.8 GHz). The different CPU times are summarized in Table 19. These include the time required to perform the transient calculation with inclusion of the time to search for starting conditions

defined by flux distribution and temperature distribution (values outside the parentheses), as well as the times for the transient calculation alone (values inside the parentheses). For the CR ejection transient initiated from 30 % of nominal reactor power (real time: 20 s), DYN3D-TRANSURANUS (two-way approach) needed computation costs acceptable for industry applications [10]. The simulation of the pure transient needed 28.9 min, compared to 372.9 min for searching the initial conditions for the transient. In contrast for the boron dilution transient initiated from sub-critical reactor conditions with zero power, the determination of the initial conditions took considerable more time in the two-way approach, compared to the simulation of the transient. This is caused by more iteration steps and/or more time for each iteration step, when we have a partial or full power state at the beginning of the transient. The boron dilution transient simulation (real time: 13 s) required longer CPU time in spite of both faster finding of the initial conditions and the shorter real time. This was triggered by the need of fixing small time step width of 0.001 s in the time interval between 4.65 s and 13 s process time in DYN3D, which was also applied in DYN3D-TRANSURANUS. This small DYN3D time step is requested to describe properly the neutron kinetics with an extreme power peak. Thence, TRANSURANUS was called by DYN3D more than 4.8 million times (i.e. more than 25,000 times for the representative rod of each assembly) in the two-way approach during this transient calculation.

Table 19 – Overview of computation times without parallelization [159]

Code (system)	CPU time [min]	
	CR ejection transient [10]	Boron dilution transient
DYN3D standalone	5.2 (4.9)	188.0 (187.9)
One-way coupling approach DYN3D-TRANSURANUS (best estimate)	26.8 (14.4)	752.8 (740.3)
Two-way coupling approach DYN3D-TRANSURANUS (best estimate)	401.8 (28.9)	1444.0 (1380.1)

It was also interesting that the computational time of the two-way approach was only a factor of 7.7 greater compared to DYN3D standalone and a factor of 1.9 greater compared to the one-way approach regarding to the boron dilution transient. This attested also the fast numerical performance of both components DYN3D and TRANSURANUS, and can be

further improved in the future thanks to a parallelization [10] (see subsection 5.1.6). Finally, it should be underlined that the convergence of DYN3D-TRANSURANUS was stable, even during the rapid increase in total nuclear power as well as during post-CHF conditions leading to a very rapid change of the boundary conditions at the clad surface.

6.6 Outlook on DYN3D-TRANSURANUS

The presented RIA simulations for Gen-II and -III can be completed in the future. On the one side, analyses of the CR ejection transient or/and the boron dilution transient implying TRANSURANUS correlations for MOX fuel can be carried out, on the other side the application of the coupled code system can be extended to VVER type reactors. DYN3D is comprehensively validated for VVER type reactors. Furthermore, the set of scenarios analysed by DYN3D-TRANSURANUS can be further enlarged. A further potential application of the two-way approach of the code system DYN3D-TRANSURANUS represents the application to fuel cycle calculations. For this purpose, the computational tools currently rely on simplified fuel behaviour models and/or a set-up of fuel rod parameters. More precisely, power density profiles and heat transfer coefficients in the gap are pre-calculated by e.g. a fuel rod performance code and provided as input tables. Nonetheless, an accurate provision of the heat transfer coefficient in the gap as a correlation is challenging due to its sensitivity and complex modelling in the case of gap closure. Therefore, a two-way coupling with a fuel performance code can improve the fuel cycle calculations and ultimately lead to a more efficient use of fuel. Another perspective can be the simulation of a whole nuclear power plant (i.e., including feedback from the secondary circuit of PWR), e.g., in case of ATWS or recriticality transients. For this, the next step would be the merging of the existing coupled code systems DYN3D-ATHLET and DYN3D-TRANSURANUS. Last one was designed from the beginning for this kind of extension.

Neutronics and thermal hydraulics codes [167, 168] are being extended and applied to safety analysis for Gen-IV reactors, enforced by the ASTRID [169] and the MYRRHA [170] projects for example. Such codes as well as the corresponding coupled code systems often either include a simplified Gen-IV fuel behaviour approach or still apply the LWR fuel behaviour models. On the contrary, TRANSURANUS provides correlations for Gen-IV fuel compositions and cladding materials, e.g., for FR [157]. A DYN3D version based on a multi-

group approach was developed, the thermal hydraulics model is going to be extended to other coolants than water (liquid metals, gases). Therefore, the coupling approach can be also adapted to the multi-group version of DYN3D for Gen-IV reactor designs with only small modifications.

A final perspective represents the application of DYN3D-TRANSURANUS to the analysis of RIA experiments, e.g., in the CABRI reactor in France and in the NSRR in Japan. The feedback on the neutronics and thermal hydraulics from detailed fuel behaviour modelling can be studied more precisely. At the end this can lead to improved models and to more accurate pre- as well as post-calculations.

6.7 Summary and recommendations for future work

Traditionally, licensing calculations rely either on simplified fuel behaviour models with appropriate sets of conservative model and material parameters, that are integrated in neutron kinetics and thermal hydraulics system codes, or on separated subsequent analyses of the neutron kinetics and thermal hydraulics of the transient and a follow-up fuel rod performance analysis based on the results of the first analysis used as boundary conditions. These calculations, however, neglect the dynamic interaction between neutron kinetics and thermal hydraulics on the one side, and greater degree in detail in online fuel behaviour modelling on the other side.

To investigate this potential feedback on neutron kinetics and thermal hydraulics in a RIA, a CR ejection initiated from 30 % of nominal reactor power in a PWR was first simulated with the code system DYN3D-TRANSURANUS [10, 120]. The feedback turned out to be almost negligible under transient conditions if the calculations begin from same initial conditions and film boiling doesn't occur during the transient.

As second scenario, a boron dilution transient in a PWR, initiated from sub-critical reactor conditions with zero power, was calculated with the one-way and two-way approaches of the code system DYN3D-TRANSURANUS in order to assess the impact of film boiling. A boron dilution transient represents a very challenging RIA scenario due to the initiation of a huge prompt power peak, on the one hand, and very quick changes in the thermal hydraulics

boundary conditions due to the possible heat transfer crisis occurrence at the fuel rod clad surface. According to our best estimate calculations, the feedback on the total nuclear power of the first power rise from detailed online fuel behaviour modelling is negligible because the heat transfers between cladding and coolant and inside the fuel rod aren't affected (delay caused by heat transfer time constant). In the further course of the transient, the total reactivity and total nuclear power were influenced by the detailed fuel behaviour modelling: it led to a steeper increase in global average fuel temperature in the two-way approach. The injected energies and clad-to-coolant heat transfer were also affected, hence there was feedback on thermal hydraulics beside the feedback on neutron kinetics. As a result, the one-way approach didn't predict film boiling at all, while the two-way approach determined film boiling in one node. To extend the analysis to the occurrence of film boiling in both coupling approaches, an additional set of calculations was performed. For this purpose, the ratio between CHF and actual heat flux, at which the switch to post-CHF heat transfer conditions is assumed, was conservatively increased by a factor of two. For the nodes with film boiling in both approaches, the two-way approach calculated still more than 30 % greater maximum node average fuel enthalpies and maximum node clad surface temperatures, compared to the one-way approach. This implies that the one-way approach potentially produces non-conservative results with respect to safety assessment, and an advanced coupling between neutron kinetics, thermal hydraulics and detailed fuel rod behaviour modelling is beneficial for reliable safety analysis.

Finally, typically for low leakage core loading pattern, the high burn-up fuel assemblies only underlay pre-CHF heat transfer in RIA scenarios. Thence, the impact from different degree in HBS modelling couldn't be analysed. For this purpose, the general TRANSURANUS coupling interface can be adopted to a thermal hydraulics system code. For LOCA simulations, especially with high burn-up rods studied in the Halden reactor in Norway, this would give the opportunity to consider the specific issues associated with the high burnup structure that are included in greater degree in detail in fuel performance codes.

7 Summary and conclusion

RIA belongs to the category of DBA; thence the reactor must be constructed to handle the consequences without environmental impact. Nuclear safety analysis has to demonstrate that the RIA safety criteria which limit the maximum increase in fuel enthalpy, the maximum fuel temperature, and the departure from nucleate boiling (DNB) / maximum clad surface temperature are ensured. Today's safety analysis is based on reactor dynamics codes containing simplified fuel behaviour models applying a set of conservative initial and boundary conditions. Calculations with (a sub-channel thermal hydraulics code and) a fuel performance code complete the safety analysis. This work contributes to the three areas of fuel performance analysis in advanced RIA simulation, which reflect general trends in this field.

Firstly, for advanced (RIA) safety analysis, fuel performance codes are still being extended to a wider range of application (e.g. capable for DBA like RIA). For example, the TRANSURANUS version for RIA is under development. Therefore, the performance of TRANSURANUS was evaluated by participation in the OECD RIA Fuel Codes Benchmark for highly irradiated rods, organized by the OECD/NEA Working Group on Fuel Safety (WGFS). In this regard the CABRI RIA test CIP0-1 with the coolant sodium was recalculated (benchmark case #1). In addition, the planned CABRI RIA test CIP3-1 with the coolant water was pre-calculated under the specific condition of both inhibition of boiling (benchmark case #2) and application of externally provided clad outer temperatures (benchmark case #3). The boundary condition of case #3 was determined by IRSN with its fuel performance code SCANAIR, containing well validated clad-to-coolant heat transfer correlations for RIA conditions. The TRANSURANUS results (HZDR) showed (very) good agreements in injected energy, variation of enthalpy, central fuel temperature, maximum fuel temperature and location of the maximum fuel temperature. Furthermore, TRANSURANUS shows a stable numerical behaviour which presents an important issue for (very) narrow and at the same time high power pulses occurring in RIA events. Nevertheless, TRANSURANUS underestimated the elongation of the fuel stack and the cladding. These might result from both a gaseous swelling model limited to normal and mild transients and the lack of clad properties for RIA conditions. According to more accurate simulations the development of a transient fission gas release model and the integration of a cladding failure model for RIA would be worthwhile for TRANSURANUS. Results of the other benchmark cases weren't provided in

the frame of this work. On the one side the TRANSURANUS thermal hydraulics model is based on a simplified approach covering the phases before DNB only. Thence the simulation of the benchmark cases #4, #6 and #8 with boiling (no provision of clad outer temperatures in the benchmark specification) couldn't be carried out with TRANSURANUS in standalone mode. On the other side numerical instabilities occurred under the specific condition inhibition of boiling for the NSRR capsuled RIA fuel tests performed in stagnant water (benchmark cases #5 and #7). They were caused by the thermal hydraulics modelling in TRANSURANUS.

Secondly for advanced (RIA) safety analysis, steady-state and transient fuel performance codes are still being improved for a more accurate simulation (e.g. of high burn-up phenomena). Today the HBS occurrence after a few cycles is one issue of major interest, especially due to its important influence on the fuel behaviour during DBA. Despite the many publications about the HBS made until now, there are still open questions. To take into account more properly the impact of the HBS in RIA analysis the modelling of the Xe depletion was improved in TRANSURANUS allowing a more accurate simulation of gaseous swelling and fission gas release in the future. For this purpose, the influence of the burn-up and irradiation temperature on the Xe concentration in the HBS was investigated using a multi-physics approach. The temperature influence was modelled by means of the temperature dependent effective burn-up. The fitting of the model on the basis of HBRP data showed that the HBS forms at a local burn-up level exceeding 49 ± 0.2 MWd/kgU and at temperatures below 1049 ± 17 °C. Thence good agreement was found between the modelled temperature threshold of the effective burn-up and the experimental temperature threshold between un- and restructured fuel in the HBRP. Furthermore, the fitted effective burn-up threshold lies in the experimentally observed range. However, a systematic difference is observed between the onset burn-up derived from the Xe measurements in highly enriched discs such as those of HBRP and the corresponding values derived from irradiated LWR fuel rods and reported in the open literature.

Thirdly for advanced (RIA) safety analysis in LWR, the benefit and potential were being analysed resulting from replacement of simplified fuel behaviour models in neutronics, thermal hydraulics and CFD codes by a full online two-way coupling approach to a fuel performance code. In today's licensing approaches these codes are still coupled offline to fuel performance codes. Furthermore, at the beginning of this work no full two-way coupling

approach has so far been reported in the open literature for calculating a whole LWR core online with detailed and well validated fuel behaviour correlations. A general interface was developed to couple the TRANSURANUS fuel performance code with reactor dynamics codes, thermal hydraulics codes or CFD codes. Beside its generality, other features of this interface are the application at either fuel assembly or fuel rod level, one-way or two-way coupling, automatic switching from steady-state to transient conditions in TRANSURANUS (including update of the material properties etc.), writing of all TRANSURANUS output files and the possibility of manual pre- and post-calculations with TRANSURANUS in standalone mode. The TRANSURANUS code can be used in combination with this coupling interface in various scenarios: different fuel compositions and cladding materials for the reactor types BWR, PWR, VVER, HWR, and FR with sodium as well as lead(-bismuth) coolant; normal operation, operational transients and DBA like LOCA; time scales from milliseconds/seconds (e.g. RIA) over seconds/minutes (e.g. LOCA) to years (e.g. normal operation or latterly also dry fuel storage) in the same simulation run.

As first application of the general TRANSURANUS coupling interface, the reactor dynamics code DYN3D was coupled at assembly level in order to describe the fuel behaviour in greater degree in detail. In the coupling, DYN3D provides process time, time-dependent rod power and thermal hydraulics conditions like heat transfer coefficient between clad to coolant, coolant temperature and coolant pressure to TRANSURANUS. For the two-way coupling, TRANSURANUS replaces the call of the simplified DYN3D fuel behaviour model, and is part of the iteration process in each time-step in DYN3D. Thence TRANSURANUS in turn transfers parameters like fuel temperature and clad temperature back to DYN3D. Results of the coupled code system were presented for two different RIA scenarios in a German PWR (Konvoi), initiated once by control rod ejection and secondly by boron dilution.

According to the RIA scenario control rod ejection starting from 30% of nominal reactor power, it appeared that for all burn-up levels the two-way coupling approach systematically calculated higher maximum values for the node fuel enthalpy (max. difference of 46 J/g) and node centreline fuel temperature (max. difference of 180.7 K), compared to DYN3D standalone in best estimate calculations. These differences could be completely explained by the more detailed TRANSURANUS modelling of fuel thermal conductivity, radial power density profile and heat transfer in the gap. The modelling of the heat transfer in the gap is sensitive. Only advanced fuel performance codes can consider the heat transfer in the gap in

an accurate manner. Since in this scenario no DNB occurred and the fuel enthalpy increases were relatively small, the feedback on the thermal hydraulics and neutron kinetics in the two-way approach calculations was very limited. Thence the difference in results between the one-way and two-way coupling approach were negligible. The results of the one-way coupling approach were generated applying the code system DYN3D-TRANSURANUS, but can be also obtained by standalone simulations of DYN3D and TRANSURANUS step-by-step. According to the RIA scenario boron dilution transient, the feedback from detailed fuel behaviour modelling was found negligible on the neutron kinetics and thermal hydraulics during the first power rise. In a later phase of the transient, the node injected energy can differ 25 J/g, even still around 20 J/g for nodes without film boiling. Furthermore, the thermal hydraulics can be affected strongly even in fresh fuel assemblies, where film boiling appeared in one node in the two-way approach in spite of no onset of film boiling in the one-way approach. For nodes with film boiling in both coupling approaches the two-way approach determined always higher maximum node average fuel enthalpies by about 100 J/g and higher maximum node clad surface temperatures by about 230 °C for the corresponding fresh fuel assemblies.

The numerical performance for DYN3D-TRANSURANUS was proved to be fast and stable. The coupled code system can therefore improve the assessment of safety criteria, at a reasonable computational cost. Both the numerical performance and the analysed differences between the coupled code system and DYN3D standalone substantiate the worldwide trend to integrate online detailed fuel behaviour approaches in safety analysis. However, this is realized sometimes as “half” / not full two-way coupling approach in other coupled code systems. Furthermore, the performance of DYN3D-TRANSURANUS demonstrated the potential to apply the general TRANSURANUS coupling interface to other codes. For example, the development of a coupling approach between the thermal hydraulics system code RELAP and TRANSURANUS was proposed in the frame of the international benchmark FUMAC, organized by IAEA. Such coupled code system will allow the performance of a large break LOCA analysis with great degree in detail in online fuel behaviour modelling.

8 Bibliography

- [1] F.-P. Weiss, F. Schäfer, S. Kliem, P. Tusheva, Analysis of design basis accidents, in: CEA-KIT (Ed.) Frédéric Joliot & Otto Hahn Summer School on Nuclear Reactors "Physics, Fuels and Systems", Aix-en-Provence, France, 2010.
- [2] IAEA, Assessment of Defence in Depth for Nuclear Power Plants, Safety Reports Series, No. 46, Vienna, Austria, 2005.
- [3] OECD/NEA, Nuclear fuel behaviour under Reactivity-Initiated Accident (RIA) Conditions. State-of-the-art report, NEA/CSNI/R(2010)1, Paris, France, 2010.
- [4] IAEA, Reactivity Accidents, Technical Reports Series No. 354, Vienna, Austria, 1993.
- [5] F. Lemoine, High burnup fuel behaviour related to fission gas effects under reactivity initiated accidents (RIA) conditions, *Journal of Nuclear Materials* 248 (1997) 238-248.
- [6] OECD/NEA, Proceedings of the workshop on Nuclear Fuel Behaviour during Reactivity Initiated Accidents (RIA), NEA/CSNI/R(2010)7, Paris, France, 2009.
- [7] A. Gensler, A. Schmidt, K. Kühnel, F. Wehle, LWR Core Safety Analysis with Areva's 3-dimensional Methods, *Atw/International Journal for Nuclear Power* 58(2) (2013) 82-88.
- [8] M. Seidl, Utility point of view: how to choose appropriate boundary conditions for PWR rod ejection accidents in safety analysis, *International DYN3D Users and Developers Meeting*, Rossendorf, Germany, 2013.
- [9] OECD/NEA, PWR Benchmark on Uncontrolled Rods Withdrawal at Zero Power, Final Report, NEA/NSC/DOC(96)20, Paris, France, 1997.
- [10] L. Holt, U. Rohde, M. Seidl, A. Schubert, P. Van Uffelen, R. Macián-Juan, Development of a General Coupling Interface for the Fuel Performance Code TRANSURANUS – Tested with the Reactor Dynamics Code DYN3D, *Annals of Nuclear Energy, Multi-Physics Modelling of LWR Static and Transient Behaviour* 84 (2015) 73-85.
- [11] T. Sugiyama, T. Nakamura, K. Kusagaya, H. Sasajima, F. Nagase, T. Fuketa, Behavior of irradiated BWR fuel under reactivity-initiated-accident conditions, Results of tests FK-1, -2 and -3, JAERI, 2003-033, 2004.
- [12] C. Vitanza, RIA failure threshold and LOCA limit at high burnup, *Journal of Nuclear Science and Technology* 43(9) (2006) 1074-1079.
- [13] J. Desquines, D.A. Koss, A.T. Motta, B. Cazalis, M. Petit, The issue of stress state during mechanical tests to assess cladding performance during a reactivity-initiated accident (RIA), *Journal of Nuclear Materials* 412 (2011) 250-267.
- [14] IAEA, Basis Safety Principles for Nuclear Power Plants, A report by the International Nuclear Safety Advisory Group, 75-INSAG-3 Rev. 1, INSAG-12, Vienna, Austria, 1999.

- [15] J. Papin, B. Cazalis, J.M. Frizonnet, J. Desquines, F. Lemoine, V. Georgenthum, F. Lamare, M. Petit, Summary and Interpretation of the CABRI REP-Na Program, *Nuclear Technology* 157 (2007) 230-250.
- [16] T. Fuketa, F. Nagase, K. Ishijima, T. Fujishiro, NSRR/RIA Experiments with High-Burnup PWR Fuels, *Nuclear Safety* 37 (1996) 328-342.
- [17] L. Yegorova, Data base on the behavior of high burnup fuel rods with Zr-1%Nb cladding and UO₂ fuel (VVER type) under reactivity accident conditions, NUREG/IA-0156, 1999.
- [18] L. Yegorova, e. al., Experimental study of narrow pulse effects on the behavior of high burnup fuel rods with Zr-1%Nb cladding and UO₂ fuel (VVER type) under reactivity-initiated accident conditions: Program approach and analysis results, NUREG/IA-0213, 2006.
- [19] R. Manzel, C.T. Walker, High burn-up fuel microstructure and its effect on fuel rod performance, Topical Meeting on LWR Fuel Performance (Oral Session), American Nuclear Society, Park City, Utah, USA, 2000, pp. 604-614.
- [20] L. Holt, A. Schubert, P. van Uffelen, C.T. Walker, E. Fridman, T. Sonoda, Sensitivity Study on Xe Depletion in the High Burn-up Structure of UO₂, *Journal of Nuclear Materials* 452 (2014) 166-172.
- [21] C. Sartoris, A. Taisne, M. Petit, F. Barré, O. Marchand, Example of Application of the IRSN Approach to Assess Safety Criteria for Reactivity Initiated Accidents, Workshop on Nuclear Fuel Behaviour during Reactivity Initiated Accidents, OECD-NEA, Paris, France, 2009.
- [22] NRC, Standard review plan, Chapter 4.2 fuel system design, Appendix B, NUREG-0800, Revision 3, March 2007.
- [23] OECD/NEA, Review of High Burn-up RIA and LOCA Database and Criteria, NEA/CSNI/R(2006)5, Paris, France, 2006.
- [24] OECD/NEA, RIA Fuel Codes Benchmark - Volume 1, NEA/CSNI/R(2013)7/VOL1, Paris, France, 2013.
- [25] OECD/NEA, RIA Fuel Codes Benchmark - Volume 2, NEA/CSNI/R(2013)7/VOL2, Paris, France, 2013.
- [26] P. Van Uffelen, C. Györi, A. Schubert, J. van de Laar, Z. Hozer, G. Spykman, Extending the application range of a fuel performance code from normal operating to design basis accident conditions, *Journal of Nuclear Materials* 383 (2008) 137-143.
- [27] K. Lassmann, C.T. Walker, J. van de Laar, F. Lindström, Modelling the High Burnup UO₂ Structure in LWR Fuel, *Journal of Nuclear Materials* 226 (1995) 1-8.
- [28] C.T. Walker, T. Kameyama, S. Kitajima, M. Kinoshita, Concerning the microstructure changes that occur at the surface of UO₂ pellets on irradiation to high burnup, *Journal of Nuclear Materials* 188 (1992) 73-79.

- [29] J. Spino, K. Vennix, M. Coquerelle, Detailed characterisation of the rim microstructure in PWR fuels in the burn-up range 40-67 GWd / tM, *Journal of Nuclear Materials* 231 (1996) 179-190.
- [30] J. Belle, Uranium Dioxide: Properties and Nuclear Applications, *Navel Reactors Handbooks*, United States Atomic Energy Commission, 1961.
- [31] J. Spino, J. Rest, W. Goll, C.T. Walker, Matrix swelling rate and cavity volume balance of UO₂ fuels at high burn-up, *Journal of Nuclear Materials* 346 (2005) 131-144.
- [32] K. Nogita, K. Une, Irradiation-induced recrystallization in high burnup UO₂ fuel, *Journal of Nuclear Materials* 226 (1995) 302-310.
- [33] I.L.F. Ray, H. Matzke, H.A. Thiele, M. Kinoshita, An electron microscopy study of the RIM structure of a UO₂ fuel with a high burnup of 7.9% FIMA, *Journal of Nuclear Materials* 245(2-3) (1997) 115-123.
- [34] J.O. Barner, M.E. Cunningham, M.D. Freshley, D.D. Lanning, Relationship between microstructure and fission gas release in high burn-up UO₂ fuel with emphasis on the rim region, *ENS International Topical Meeting on LWR Fuel Performance*, Avignon, France, 1991.
- [35] P. Blair, Modelling of Fission Gas Behaviour in High Burnup Nuclear Fuel, PhD thesis, École Polytechnique Fédérale de Lausanne, Switzerland, 2008.
- [36] J.A. Turnbull, The high burn-up restructuring of fuel, the so called rim effect: a consideration of its impact on steady-state and transient behaviour, HWR-709, *OECD Halden Reactor Project*, Halden, Norway, 2002.
- [37] J. Rest, G.L. Hofman, Dynamics of irradiation induced grain subdivision and swelling in U₃Si₂ and UO₂ fuels, *Journal of Nuclear Materials* 210 (1994) 187-202.
- [38] L.E. Thomas, C.E. Beyer, L.A. Charlot, Microstructural analysis of LWR spent fuels at high burnup, *Journal of Nuclear Materials* 188 (1992) 80-89.
- [39] D. Baron, M. Kinoshita, P. Thevenin, R. Largenton, Discussion about HBS transformation in high burn-up fuels, *Nuclear Engineering and Technology* 41(No. 2, Special issue on the water reactor fuel performance meeting 2008) (2009) 199-214.
- [40] E.K. M. Kinoshita, H. Matzke, V.V. Rondinella, High Burnup Rim Project (V) - Completed Scope and Needs for Further Study, EHPG, Lillehammer, Norway, 2001.
- [41] D. Baron, I. Arimescu, G. Shimanski, L. Hallstadius, S. Yagnik, The NFIR-V dimensional stability project: a method for transposing test reactor irradiation data for PWR and BWR applications, EPRI, Palo Alto, CA, U.S., 2009.
- [42] A. Bianco, M. Seidl, W. Faber, C. Vitanza, W. Wiesenack, R. Macián-Juan, Separate effects test to investigate fuel fragmentation during LOCA, KTG-Fachtag, Aktuelle Themen rund um das Brennelement, Karlsruhe, Germany, 2014.

- [43] W. Wiesenack, Overview of Halden LOCA tests: evaluation report, HPR-380, OECD Halden Reactor Project, Halden, Norway, 2013.
- [44] J.-P. Hiernaut, T. Wiss, J.-Y. Colle, H. Thiele, C.T. Walker, W. Goll, R.J.M. Konings, Fission product release and microstructure changes during laboratory annealing of a very high burn-up fuel specimen, *Journal of Nuclear Materials* 377 (2008) 313-324.
- [45] T. Fuketa, F. Nagase, T. Sugiyama, RIA- and LOCA-simulating experiments on high burnup LWR fuels, IAEA technical meeting on fuel behaviour modelling under normal, transient and accident conditions and high burnups, International Atomic Energy Agency, Kendal, United Kingdom, 2005.
- [46] D. Schrire, A. Kindlund, P. Ekberg, Solid swelling of LWR UO₂ fuel, EHPG Meeting, OECD Halden Reactor Project, Lillehammer, Norway, 1998.
- [47] T. Fuketa, T. Sugiyama, F. Nagase, Behaviour of 60 to 78 MWd/kgU PWR fuels under reactivity-initiated-accident conditions, *Journal of Nuclear Science and Technology* 43(9) (2006) 1080-1088.
- [48] F. Schmitz, J. Papin, High burnup effects on fuel behaviour under accident conditions: the tests CABRI REP-Na, *Journal of Nuclear Materials* 270 (1999) 55-64.
- [49] OECD/NEA, Nuclear Fuel Behaviour in Loss-of-coolant Accident (LOCA) Conditions. State-of-the-art report, NEA/CSNI/R(2009)15, Paris, France, 2009.
- [50] M. Ishikawa, S. Shiozawa, A study of fuel behavior under reactivity initiated accident conditions - review, *Journal of Nuclear Materials* 95 (1980) 1-30.
- [51] V. Bessiron, Modelling of Clad-to-Coolant Heat Transfer for RIA Applications, *Journal of Nuclear Science and Technology* 44(2) (2007) 211-221.
- [52] S. Saito, K. Sumita, Y. Emori, H. Kawamura, Development of inreactor fuel behavior observation system, *Journal of Nuclear Science and Technology* 18 (1981) 427-439.
- [53] T. Fujishiro, M. Hirose, S. Kobayashi, S. Tanzawa, Effects of coolant flow on light water reactor fuel behaviors during reactivity-initiated accident, *Journal of Nuclear Science and Technology* 18 (1981) 196-205.
- [54] V. Bessiron, T. Sugiyama, T. Fuketa, Clad-to-Coolant Heat Transfer in NSRR Experiments, *Journal of Nuclear Science and Technology* 44 (2007) 723-732.
- [55] V. Bessiron, Clad-to-coolant heat transfer during a RIA transient: Analysis of the PATRICIA experiments, modelling and applications, Fuel safety research meeting, Tokyo, Japan, 2004.
- [56] V. Georgenthum, J. Desquines, V. Bessiron, Influence of outer zirconia transient cracking and spalling on thermomechanical behaviour of high burnup fuel rod submitted to RIA, *Journal of Nuclear Science and Technology* 43 (2006) 1089-1096.
- [57] IAEA, Improvement of computer codes used for fuel behaviour modelling simulation (FUMEX-III). Final report of co-ordinated research project, Vienna, Austria, 2013.

- [58] M. Suzuki, H. Saitou, T. Fuketa, RANNS code analysis on the local mechanical conditions of cladding of high burnup fuel rods under PCMI in RIA-simulated experiments in NSRR, *Journal of Nuclear Science and Technology* 43 (2006) 1097-1104.
- [59] A. Zaruba, E.-M. Pauli, L.-P. Zeisler, Thermal-hydraulic study for the determination of fuel rod failure rate (FRFR) in case of 0.1A break LOCA, KTG-Fachtag, Aktuelle Themen rund um das Brennelement, Karlsruhe, Germany, 2014.
- [60] K. Lassmann, TRANSURANUS: a fuel rod analysis code ready for use, *Journal of Nuclear Materials* 188 (1992) 295-302.
- [61] K. Lassmann, URANUS - A Computer Programme for the Thermal and Mechanical Analysis of the Fuel Rods in a Nuclear Reactor, *Nuclear Engineering and Design* 45(No.2) (1978) 325-342.
- [62] Fuel Analysis and licensing Code: FALCON MOD01, Theoretical and Numerical Bases, EPRI, Palo Alto, CA, 2004.
- [63] R.L. Williamson, J.D. Hales, S.R. Novascone, M.R. Tonks, D.R. Gaston, C.J. Permann, D. Andrs, R.C. Martineau, Multidimensional multiphysics simulation of nuclear fuel behavior, *Journal of Nuclear Materials* 423 (2012) 149-163.
- [64] B. Michel, C. Nonon, J. Sercombe, F. Michel, V. Marelle, Simulation of Pellet-Cladding Interaction with the PLEIADES Fuel Performance Software Environment, *Nuclear Technology* 182 (2013) 124-137.
- [65] D. Gaston, C. Newman, G. Hansen, D. Lebrun-Grandié, MOOSE: A parallel computational framework for coupled systems of nonlinear equations, *Nuclear Engineering and Design* 239 (2009) 1768-1778.
- [66] R. Manzel, C.T. Walker, EPMA and SEM of fuel samples from PWR rods with an average burn-up of around 100 MWd/kgHM, *Journal of Nuclear Materials* 301 (2002) 170-182.
- [67] C.T. Walker, S. Bremier, S. Portier, R. Hasnaoui, W. Goll, SIMS analysis of an UO₂ fuel irradiated at low temperature to 65 MWd/kgHM, *Journal of Nuclear Materials* 393 (2009) 212-223.
- [68] T. Sonoda, M. Kinoshita, I.L.F. Ray, T. Wiss, H. Thiele, D. Pellottiero, V.V. Rondinella, H. Matzke, Transmission electron microscopy observation on irradiation-induced microstructural evolution in high burn-up UO₂ disk fuel, *Nuclear Instruments and Methods in Physics Research B* 191 (2002) 622-628.
- [69] G.A. Berna, H. Scott, FRAPTRAN: A computer code for the transient analysis of oxide fuel rods, U.S. Nuclear Regulatory Commission, 2001.
- [70] M. Suzuki, H. Saitou, T. Fuketa, Analysis on split failure of cladding of high burnup BWR rods in reactivity-initiated accident conditions by RANNS code, *Nuclear Engineering and Design* 236 (2006) 128-139.

- [71] K. Nogita, K. Une, Formation of pellet-cladding bonding layer in high burnup BWR fuels, *Journal of Nuclear Science and Technology* 34(7) (1997) 679-686.
- [72] G. Pastore, D. Pizzocri, J.D. Hales, S.R. Novascone, D.M. Perez, W. Spencer, R.L. Williamson, P. Van Uffelen, L. Luzzi, Modelling of transient fission gas behaviour in oxide fuel and application to the BISON code, EHPG Meeting, HRP, Røros, Norway, 2014.
- [73] L. Holt, A. Schubert, J. van de Laar, P. Van Uffelen, Stand-alone modelling of the high burnup structure formation and burst release during design basis accidents, EHPG Meeting, HRP, Røros, Norway, 2014.
- [74] A. Schubert, J. van de Laar, P. Van Uffelen, L. Holt, J. Klouzal, Simulation of LOCA tests carried out in Norway by means of the TRANSURANUS code, Presentation at 20th International QUENCH Workshop, collocated with the 1st IAEA Coordinated Research Project FUMAC Meeting, Karlsruhe, Germany, 2014.
- [75] C. Gyóri, Simulation of integral LOCA tests with high-burn-up fuel, in: INRNE (Ed.) 9th International Conference on WWR Fuel Performance, Modelling and Experimental Support, Burgas, Bulgaria, 2011.
- [76] C. Gyóri, P. Blair, An empirical model of fuel fragmentation and fission gas release under LOCA conditions, International TRANSURANUS Workshop "Towards Nuclear Fuel Modelling in the various Reactor Types across Europe", Hannover, Germany, 2011.
- [77] C. Gyóri, A 2D numerical method to simulate transient heat conduction in the plenum gas of LWR fuel rods, International TRANSURANUS Workshop "Towards Nuclear Fuel Modelling in the various Reactor Types across Europe", Karlsruhe, Germany, 2013.
- [78] K. Une, S. Kashibe, A. Takagi, Fission Gas Release Behavior from High Burnup UO₂ Fuels under Rapid Heating Conditions, *Journal of Nuclear Science and Technology* 43(9) (2006) 1161-1171.
- [79] M. Le Saux, J. Besson, S. Carassour, C. Poussard, X. Averty, A model to describe the anisotropic viscoplastic mechanical behaviour of fresh and irradiated Zircaloy-4 fuel claddings under RIA loading conditions, *Journal of Nuclear Materials* 378 (2008) 60-69.
- [80] OECD/NEA, Mechanical testing for RIA applications (under preparation).
- [81] V. Garat, D. Deuble, B. Dunn, J.P. Mardon, Quantification of the margins provided by M5 cladding in accidental conditions, LWR Fuel Performance Meeting (TopFuel), Manchester, United Kingdom, 2012.
- [82] V. Georgenthum, A. Moal, O. Marchand, SCANAIR a transient fuel performance code, Part two: Assessment of modelling capabilities, *Nuclear Engineering and Design* 280 (2014) 172-180.

- [83] J. Papin, M. Petit, C. Grandjean, V. Georgenthum, IRSN R&D studies on high burn-up fuel behaviour under RIA and LOCA conditions, Int. Meet. on LWR Fuel Performance, "Nuclear fuel: addressing the future", Topfuel, Salamanca, Spain, 2006, pp. 274-278.
- [84] R. Sanchez, A. Hebert, Z. Stankovski, M. Coste, S. Loubiere, C. Van der Gucht, I. Zmijarevic, APOLLO2: Twelve years later, Mathematics and computation, reactor physics and environmental analysis in nuclear applications (M&C99), American Nuclear Society, Madrid, Spain, 1999.
- [85] J. Rhodes, K. Smith, D. Lee, CASMO-5 Development and Applications, ANS Topical Meeting on Reactor Physics (PHYSOR-2006), Vancouver, Canada, 2006.
- [86] HELIOS Version 1.8, Generalized Geometry Lattice Analysis, Commercial computer code by Studsvik Scandpower Inc. and Studsvik AB, Nyköping, Sweden, 2003.
- [87] SIMULATE-3K, Commercial computer code by Studsvik Scandpower Inc. and Studsvik AB, Nyköping, Sweden, 2009.
- [88] U. Grundmann, U. Rohde, S. Mittag, DYN3D - Three-Dimensional Core Model for Steady-State and Transient Analysis of Thermal Reactors, Proc. of Int. Topl. Mtg. on Advances in Reactor Physics and Mathematics and Computation into the Next Millennium (PHYSOR-2000), Pittsburgh, USA, 2000.
- [89] U. Grundmann, U. Rohde, S. Mittag, S. Kliem, DYN3D Version 3.2 - Code for Calculation of Transients in Light Water Reactors (LWR) with Hexagonal or Quadratic Fuel Elements - Description of Models and Methods, Report FZR 434, Rossendorf, Germany, 2005.
- [90] C.L. Wheeler, C.W. Stewart, R.J. Cena, D.S. Rowe, A.M. Sutey, COBRA-IV-I: An interim version of COBRA for thermal-hydraulic analysis of rod bundle nuclear fuel elements and cores, BNWL-1962, 1976.
- [91] AREVA, COBRA-FLX: A Core Thermal-Hydraulic Analysis Code. Topical Report, ANP-10311NP, 2010.
- [92] U. Imke, V. Sanchez, R. Gomez, SUBCHANFLOW: a new empirical knowledge based sub channel code, Annual Meeting on Nuclear Technology, Berlin, Germany, 2010.
- [93] E. Federici, F. Lamare, V. Bessiron, J. Papin, The SCANAIR code version 3.2: main features and status of qualification, IAEA Technical Committee Meeting on Fuel Behaviour Under Transient and LOCA Conditions, IAEA, Halden, Norway, 2001, pp. 88-101.
- [94] U. Rohde, The modeling of fuel rod behaviour under RIA conditions in the code DYN3D, Annals of Nuclear Energy 28 (2001) 1343-1363.
- [95] H.-G. Sonnenburg, E. Hofer, A. Kloos, Development of methods for the analysis of the fuel rod behaviour in high burn-up regime, Final Report GRS-A-3079, Gesellschaft fuer Anlagen- und Reaktorsicherheit, Garching, Germany, 2002.

- [96] H.-G. Sonnenburg, M. Kloos, C. Müller, J.-D. Schubert, J. Herb, Development of methods for the analysis of the fuel rod behavior under both reactivity initiated accidents (RIA) and loss of coolant accidents (LOCA), Final Report GRS-A-3368, Gesellschaft fuer Anlagen- und Reaktorsicherheit, Garching, Germany, 2007.
- [97] H.-G. Sonnenburg, J. Herb, J. Sievers, H.-P. Bachmann, Development of methods for the analysis of the fuel rod behaviour under loss of coolant and reactivity initiated accidents, Final Report GRS-A-3519, Gesellschaft fuer Anlagen- und Reaktorsicherheit, Garching, Germany, 2010.
- [98] A. Schubert, P. Van Uffelen, J. van de Laar, C.T. Walker, W. Haeck, Extension of the TRANSURANUS burn-up model, *Journal of Nuclear Materials* 376 (2008) 1-10.
- [99] G.A. Berna, C.E. Beyer, K.L. Davis, D.D. Lanning, FRAPCON-3: A computer code for the Calculation of Steady-State, Thermal-Mechanical Behaviour of Oxide Fuel Rods for High Burnup, 1997.
- [100] K. Lassmann, J. van de Laar, Fission Gas Release Models of the TRANSURANUS version V1M2J98, IAEA RER/4/019, Licensing Fuel and Fuel Modelling Codes for WWER Reactors, Seminar "Implementation of the WWER version of the TRANSURANUS code and its application to safety criteria", Sofia, Bulgaria, 1998.
- [101] M. Ishikawa, T. Fujishiro, S. Kawasaki, LWR fuel safety research with particular emphasis on RIA/LOCA and other conditions, *Journal of Nuclear Science and Technology* 26 (1989) 118-125.
- [102] G.M. Grandi, D. Hagrman, Improvements to the INTERPIN code for high burnup and MOX fuel, International conference on making the renaissance real, Transactions of the American Nuclear Society and the European Nuclear Society, Washington, D.C., USA, 2007, pp. 614-615.
- [103] S. Kliem, A. Gommlich, A. Grahn, U. Rohde, J. Schütze, T. Frank, A. Gomez, V. Sanchez, Development of multi-physics code systems based on the reactor dynamics code DYN3D, *Kerntechnik* 76(3) (2011) 160-165.
- [104] C. Chauliac, J.-M. Aragonés, D. Bestion, D.G. Cacuci, N. Crouzet, F.-P. Weiss, M.A. Zimmermann, NURESIM - A European simulation platform for nuclear reactor safety: Multi-scale and multi-physics calculations, sensitivity and uncertainty analysis, *Nuclear Engineering and Design* 241(9) (2011) 3416-3426.
- [105] U. Grundmann, S. Kliem, U. Rohde, Analysis of the boiling water reactor turbine trip benchmark with the codes DYN3D and ATHLET/DYN3D, *Nuclear Science and Engineering* 148 (2004) 226-234.
- [106] S. Kliem, Y. Kozmenkov, T. Höhne, U. Rohde, Analyses of the V1000CT-1 benchmark with the DYN3D/ATHLET and DYN3D/RELAP coupled code systems including a coolant mixing model validated against CFD calculations, *Progress in Nucl. Energy* 48 (2006) 830-848.
- [107] J. Judd, G. Grandi, SIMULATE-3K/RELAP5-3D, A Coupled Code System, *Transactions of the American Nuclear Society* 97 (2007) 709-710.

- [108] The ARCADIA reactor analysis system for PWRs, Methodology description and benchmarking results, 2010.
- [109] P. Saha, N. Aksan, J. Andersen, J. Yan, J.P. Simoneau, L. Leung, F. Bertrand, K. Aoto, H. Kamide, Issues and future direction of thermal-hydraulics research and development in nuclear power reactors, Nuclear Engineering and Design 264(NURETH-14) (2013) 3-23.
- [110] G. Rossiter, Development of the ENIGMA Fuel Performance Code for Whole Core Analysis and Dry Storage Assessments, Nuclear Engineering and Technology 43(6) (2011) 489-498.
- [111] A. Worrall, A.S. DiGiovine, "ONUS": On-line fuel performance surveillance - Linking Studsvik's CMS with UK NNL's ENIGMA-B, Proceedings of Global 2009, Paper 9101, Paris, France, 2009.
- [112] K. Valtonen, A. Hamalainen, M.E. Cunningham, FRAPTRAN Fuel Rod Code and its Coupled Transient Analysis with the GENFLO Thermal-hydraulic Code, Twenty-Ninth Nuclear Safety Research Conference. NUREG/CP-0176, Washington, DC, 2002, pp. 381-396.
- [113] U.S. NRC, TRACE V5.0 assessment manual, Main report, Washington, DC, USA, 2005.
- [114] M. Suzuki, H. Saitou, Y. Udagawa, Light Water Reactor Fuel Analysis Code FEMAXI-7, model and structure, JAEA, 2010.
- [115] L. Holt, U. Rohde, M. Seidl, A. Schubert, P. Van Uffelen, Development of a General Coupling Interface for the Fuel Performance Code TRANSURANUS Tested with the Reactor Dynamic Code DYN3D, 10th International Conference on WWER Fuel Performance, Modelling and Experimental Support, Sandanski, Bulgaria, 2013.
- [116] G. Van Goethem, K. Lassmann, The coupling algorithm between fuel pin and coolant channel in the european accident code EAC-2, Nuclear Engineering and Design 113(3) (1989) 323-336.
- [117] J. Magedanz, M. Avramova, Y. Perin, A.K. Velkov, High-fidelity multi-physics system TORT-TD/CTF/FRAPTRAN for light water reactor analysis, Annals of Nuclear Energy, Multi-Physics Modelling of LWR Static and Transient Behaviour 84 (2015) 234-243.
- [118] A. Moal, V. Georgenthum, O. Marchand, SCANAIR: A transient fuel performance code, Part one: General modelling description, Nuclear Engineering and Design 280 (2014) 150-171.
- [119] S. Chemin, A. Moal, NURES SAFE, D11.11 - Specifications for SCANAIR Integration and D11.12 - Specifications CEA coupling in-core N/T-M/T-H, 2014.
- [120] L. Holt, U. Rohde, M. Seidl, A. Schubert, P. Van Uffelen, R. Macián-Juan, Two-way Coupling between the Reactor Dynamics Code DYN3D and the Fuel Performance Code TRANSURANUS at Assembly Level, 22nd International Conference on Nuclear Engineering (ICONE22), ASME, Prague, Czech Republic, 2014.

- [121] A. Schubert, V. Di Marcello, V.V. Rondinella, J. van de Laar, P. Van Uffelen, The data requirements for the verification and validation of a fuel performance code - The TRANSURANUS perspective, 10th International Conference on WWER Fuel Performance, Modelling and Experimental Support, Sandanski, Bulgaria, 2013.
- [122] E. Gailliez, Safety of nuclear fuels. New Cabri - water loop IPSN / OECD international research programme, INIS-FR--258, 2000.
- [123] IFPE, The Public Domain Database on Nuclear Fuel Performance Experiments for the Purpose of Code Development and Validation, International Fuel Performance Experiments (IFPE) Database. <<http://www.nea.fr/html/science/fuel/ifpelst.html>>, 2007).
- [124] RELAP5/MOD3.2 Code manual, Report NUREG/CR-5535, U.S. Nuclear Regulatory Commission, Washington, DC, USA, 1995.
- [125] R. Van Nieuwenhove, Instrumentation, measurement techniques and experimental systems, OECD - HRP Summer school on principles of fuel behaviour modelling and practical applications, Halden, Norway, 2013.
- [126] M. Suzuki, T. Fuketa, Analysis of Pellet-Clad Mechanical Interaction Process of High-burnup PWR Fuel Rods by RANNS Code in Reactivity-Initiated Accident Conditions, Nuclear Technology 155 (2006) 282-292.
- [127] A.M. Garde, W.H. Slagle, D. Mitchell, Hydrogen pick-up fraction for ZIRLO™ cladding corrosion and resulting impact on the cladding integrity, Water Reactor Fuel Performance Meeting (TopFuel), Paris, France, 2009, pp. 902-913.
- [128] L. Holt, Implementation of the 80% data set methodology into TRANSURANUS and validation, Diploma thesis, RWTH Aachen, Aachen, Germany, 2010.
- [129] J.B. Ainscough, B.W. Oldfield, J.O. Ware, Isothermal grain growth kinetics in sintered UO₂ pellets, Journal of Nuclear Materials. 49 (1973) 117-128.
- [130] C.S. Olsen, UO₂ pore migration and grain growth kinetics, Transactions on Structural Mechanics in Reactor Technology (SMiRT) C (1979) C1/9, 1-10.
- [131] P.T. Elton, K. Lassmann, Computational methods for diffusional gas release, Nuclear Engineering and Design 101(3) (1987) 259-265.
- [132] K. Lassmann, H. Benk, Numerical algorithms for intragranular fission gas release, Journal of Nuclear Materials 280(2) (2000) 127-135.
- [133] Y.K. Bibilashvili, RAPTA-5 code: modelling behaviour of VVER-type fuel rods in design basis accidents verification calculations, Proceedings of the IAEA Technical Committee on Behaviour of LWR Core Materials under Accident Conditions, Dimitrovgrad, Russia, 1996, pp. 139-152.
- [134] B. Cazalis, J. Desquines, S. Carassou, T.L. Jolu, C. Bernaudat, The plane strain tests in the PROMETRA program, Journal of Nuclear Materials 472 (2016) 127-142.

- [135] V.A. Adeev, V.V. Saprykin, A.A. Gagarinsky, Main operation results of the 3-rd generation nuclear fuel, 10th International Conference on WWER Fuel Performance, Modelling and Experimental Support, Sandanski, Bulgaria, 2013.
- [136] R. Hill, The mathematical theory of plasticity, Clarendon Press, Oxford, United Kingdom, 1950.
- [137] S. Yagnik, J. Turnbull, J. Noirot, C. Walker, L. Hallstadius, N. Waeckel, P. Blanpain, An Investigation into Fuel Pulverization with Specific Reference to High Burn-up LOCA (Paper 100145), WRFPM, Sendai, Japan, 2014.
- [138] J. Spino, D. Papaioannou, J.-P. Glatz, Comments on the Threshold Porosity for Fission Gas Release in High Burn-up Fuels, *Journal of Nuclear Materials* 328 (2004) 67-70.
- [139] J. Spino, A.D. Stalios, H. Santa Cruz, D. Baron, Stereological evolution of the rim structure in PWR-fuels at prolonged irradiation: Dependencies with burn-up and temperature, *Journal of Nuclear Materials* 354 (2006) 66-84.
- [140] G. Khvostov, V. Novikov, A. Medvedev, S. Bogatyr, High Burn-up Structure in LWR fuels: Experience of Modelling by the START-3 Code, International Workshop on the High Burn-up Structure in Nuclear Fuels, Karlsruhe, Germany, 2004.
- [141] G. Khvostov, K. Mikityuk, M.A. Zimmermann, A model for fission gas release and gaseous swelling of the uranium dioxide fuel coupled with the FALCON code, *Nuclear Engineering and Design* 241 (2011) 2983-3007.
- [142] M. Kinoshita, T. Sonoda, S. Kitajima, A. Sasahara, T. Kameyama, T. Matsumura, E. Kolstad, V.V. Rondinella, C. Ronchi, J.P. Hiernaut, T. Wiss, F. Kinnart, J. Ejton, D. Papaioannou, H. Matzke, High-Burnup Rim Project: (III) Properties of Rim-Structured Fuel (Paper 1102), International Meeting on LWR Fuel Performance, Orlando, Florida, 2004.
- [143] K. Une, K. Nogita, T. Shiratori, K. Hayashi, Rim structure formation of isothermally irradiated UO₂ fuel discs, *Journal of Nuclear Materials* 288 (2001) 20-28.
- [144] A.N. Kolmogorov, Statistical theory of crystallization of metals, *Izv. Akad. Nauk SSSR Ser. Math* 1 (1937) 355-360.
- [145] W.A. Johnson, R.F. Mehl, Reaction Kinetics in Processes of Nucleation and Growth, *Transactions AIME* 135, 1939, p. 416.
- [146] M. Avrami, Kinetics of Phase Change. I General Theory, *J. Chem. Phys.* 7 (1939).
- [147] M. Avrami, Kinetics of Phase Change. II Transformation-Time Relations for Random Distribution of Nuclei, *J. Chem. Phys.* 8 (1940).
- [148] M. Kinoshita, Mesoscopic Approach to Describe High Burn-up Fuel Behaviour (Paper F 1.2), EHPG, Leon, Norway, 1999.

- [149] J. Jonnet, P. Van Uffelen, D. Staicu, T. Wiss, C. Ronchi, Towards a Better Understanding of the Role of Stress in Restructuring of Radiation Damage, 18th International Conference Structural Mechanics in Reactor Technology, SMiRT18, Beijing, China, 2005.
- [150] K. Une, M. Hirai, K. Nogita, T. Hosokawa, Y. Suzawa, S. Shimizu, Y. Etoh, Rim structure formation and high burnup fuel behavior of large-grained UO₂ fuels, *Journal of Nuclear Materials* 278(1) (2000) 54-63.
- [151] G. Khvostov, V. Novikov, A. Medvedev, S. Bogatyr, Approaches to modeling of high burn-up structure and analysis of its effects on the behaviour of light water reactor fuels in the START-3 fuel performance code (Paper 1104), Water Reactor Fuel Performance Meeting, Kyoto, Japan, 2005.
- [152] D.W. Marquardt, An Algorithm for Least-Squares Estimation of Nonlinear Parameters, *Journal of the Society for Industrial and Applied Mathematics* 11(2) (1963) 431-441.
- [153] G. Lerchl, H. Austregesilo, P. Schöffel, D. von der Cron, F. Weyermann, ATHLET Mod 3.0 Cycle A. User's Manual, GRS-P-1 / Vol. 1 Rev. 6, Gesellschaft fuer Anlagen- und Reaktorsicherheit, Garching, Germany, 2012.
- [154] J. Jiménez, S. Alglave, M. Avramova, Coupling of TRANSURANUS with KTF for High Fidelity Fuel Rod Modeling, PHYSOR 2012, Knoxville, Tennessee, USA, 2012.
- [155] A. Schubert, C. Györi, P. Van Uffelen, J. van de Laar, L. Ott, Simulation of MOX and Gd containing fuel by means of TRANSURANUS, International Workshop: Towards nuclear fuel modelling in the various reactor types across Europe, Karlsruhe, Germany, 2007.
- [156] C. Györi, Z. Hózer, E. Perez-Feró, P. Van Uffelen, A. Schubert, J. van de Laar, Applying the TRANSURANUS Code to VVER Fuel under Accident Conditions, 18th International Conference on Structural Mechanics in Reactor Technology, SMiRT18, Beijing, China, 2005.
- [157] V. Di Marcello, A. Schubert, J. van de Laar, P. Van Uffelen, Extension of the TRANSURANUS plutonium redistribution model for fast reactor performance analysis, *Nuclear Engineering and Design* 248 (2012) 149-155.
- [158] P. Van Uffelen, J. van de Laar, A. Schubert, V. Di Marcello, L. Vlahovic, L. Holt, Modelling of Nuclear Fuel under Accident Conditions by means of TRANSURANUS, IAEA Technical meeting on modelling of water-cooled fuel including design basis accidents and severe accidents, Chengdu, China, 2013.
- [159] L. Holt, U. Rohde, S. Kliem, S. Baier, M. Seidl, P. Van Uffelen, R. Macián-Juan, Investigation of Feedback on Neutron Kinetics and Thermal Hydraulics from Detailed Online Fuel Behavior Modeling during a Boron Dilution Transient in a PWR with the Two-way Coupled Code System DYN3D-TRANSURANUS, *Nuclear Engineering and Design* 297 (2016) 32-43.

- [160] U. Grundmann, D. Lucas, U. Rohde, Coupling of the Thermohydraulic Code ATHLET with the Neutron Kinetic Core Model DYN3D, Int. Conf. on Mathematics and Computations, Reactor Physics and Environmental Analyses, Portland, Oregon, 1995, pp. 257-263.
- [161] J.F. Briesmeister, MCNP - A General Monte Carlo N-Particle Transport Code, Los Alamos National Laboratory, USA, 2000.
- [162] K. Lassmann, F. Hohlefeld, The Revised URGAP-Model to Describe the Gap Conductance Between Fuel and Cladding, Nuclear Engineering and Design 103 (1987) 215-221.
- [163] S. Kliem, S. Mittag, U. Rohde, F.-P. Weiss, Influence of System and Neutron-Kinetic Parameter Variations on an Anticipated Transient without Scram in a PWR, 17th International Conference on Nuclear Engineering (ICONE17), ASME, Brussels, Belgium, 2009.
- [164] S. Kliem, U. Rohde, F.-P. Weiß, Core response of a PWR to a slug of under-borated water, Nuclear Engineering and Design 230 (2004) 121-132.
- [165] S. Kliem, T. Sühnel, U. Rohde, T. Höhne, H.-M. Prasser, F.-P. Weiss, Experiments at the mixing test facility ROCOM for benchmarking of CFD codes, Nuclear Engineering and Design 238(3) (2008) 566-576.
- [166] A. Schubert, C. Györi, D. Elenkov, K. Lassmann, J. van de Laar, Analysis of Fuel Centre Temperatures with the TRANSURANUS Code, International Conference on Nuclear Fuel for Today and Tomorrow - Experiences and Outlook, ENS TopFuel 2003 / ANS LWR Fuel Performance Meeting, Würzburg, Germany, 2003.
- [167] B. Merk, V. Glivici-Cotruta, S. Duerigen, U. Rohde, S. Kliem, Overview of major HZDR developments for fast reactor analysis, Nuclear Engineering and Design 265 (2013) 1194-1204.
- [168] D. Tenchine, R. Baviere, P. Bazin, F. Ducros, G. Geffraye, D. Kadri, F. Perdu, D. Pialla, B. Rameau, N. Tauveron, Status of CATHARE code for sodium cooled fast reactors, Nuclear Engineering and Design 245 (2012) 140-152.
- [169] F. Gauche, J. Rouault, French SFR R&D Program and Design Activities for SFR Prototype ASTRID, Energy Procedia 7(Asian Nuclear Prospects 2010) (2011) 314-316.
- [170] L. Mansani, C. Artioli, M. Schikorr, G. Rimpault, C. Angulo, D.D. Bruyn, The European Lead-cooled EFIT Plant: an industrial-scale Accelerator-Driven System for Minor Actinide Transmutation, Nuclear Technology 180(2) (2012) 241-263.

Acknowledgements

Diese Doktorarbeit wurde im Rahmen einer einjährigen Tätigkeit als wissenschaftlicher Mitarbeiter und einer daran anschließenden Doktorandenzeit am Institut für Sicherheitsforschung (jetzt Institut für Ressourcenökologie) am Helmholtz-Zentrum Dresden-Rossendorf e. V. (HZDR) angefertigt. Finanziert und initiiert wurde dieses Vorhaben durch die E.ON Kernkraft GmbH im Rahmen der Sicherstellung des kerntechnischen Kompetenzerhalts in Deutschland. Hervorzuheben sind dabei die vom Auftraggeber gewährten großen Freiheiten in Hinblick auf die Ausgestaltung und Bearbeitung dieses Forschungsprojekts. Diese Industriemittel haben es dem HZDR ermöglicht, das Brennstabverhalten detailliert in seinen reaktorphysikalischen und thermohydraulischen Sicherheitsanalysen für Kernkraftwerke abzubilden. Die Wichtigkeit und Bedeutung dieses Doktorarbeitsthemas wurde anhand der gewonnenen Ergebnisse und Erkenntnisse nachgewiesen. Zudem wird diese durch einen gerade einsetzenden weltweiten Trend hin zu detaillierter Brennstabmodellierung in Reaktordynamik-, thermohydraulischen System- und thermohydraulischen Unterkanalprogrammen bestätigt.

Herrn Dr. Rohde danke ich für die Betreuung der Doktorarbeit am HZDR. Hervorzuheben sind u. a. die ausführliche Beantwortung vieler Fragen zum Reaktordynamikprogramm DYN3D (speziell zum von Herrn Dr. Rohde entwickelten Brennstabmodell in DYN3D), die gemeinsame Analyse der allerersten Ergebnisse des neuen Codesystems DYN3D-TRANSURANUS sowie die Durchsicht der Dissertation. Des Öfteren war es während der Doktorarbeit sehr hilfreich, die Hintergründe aus vergangenen Jahrzehnten zu erfahren. Diesbezüglich hatte Herr Dr. Rohde einen reichhaltigen Erfahrungsschatz. Weiterhin möchte ich dem Leiter der Abteilung Reaktorsicherheit Herrn Dr. Kliem für die wohlwollende Unterstützung dieser Doktorarbeit in seiner Abteilung sowie für die fachliche Begleitung der Simulation von Borverdünnungstransienten mit DYN3D-TRANSURANUS danken. Des Weiteren möchte ich mich beim gesamten DYN3D-Entwicklungsteam am HZDR für die fruchtbare Zusammenarbeit bedanken. Ein besonderer Dank gilt Herrn Dr. Baier für die Unterstützung bei der Umstrukturierung zweier komplexer DYN3D-Subroutinen zwecks Kopplung zum Brennstabcode TRANSURANUS. Außerdem möchte ich mich bei den Herren Berger und Gommlich für den exzellenten IT-Support am HZDR bedanken. Leider bot sich keine Möglichkeit mit Herrn Dr. Schäfer fachlich zusammenzuarbeiten, jedoch möchte ich mich für die sehr gute Zusammenarbeit bei der Öffentlichkeitsarbeit und für die

Unterstützung der kerntechnischen Exkursionen am HZDR bedanken. Herrn Kozmenkov danke ich für die sehr nette Atmosphäre im gemeinsamen Büro; die „Einführung in die russische Kerntechnik“ war hochinteressant. Vielen Dank auch an die Sekretärinnen / Assistentinnen Frau Gorzitze, Frau Kurde und Frau Losinski für die Organisation der vielen notwendigen Dienstreisen.

Ein ganz besonderer Dank gilt dem Unternehmen E.ON Kernkraft GmbH. Einerseits für die Initiierung des Projektes, Bereitstellung der Forschungsmittel und Projektbegleitung. Namentlich genannt seien diesbezüglich stellvertretend die Herren Dr. Faber, Dr. Sommer und Dr. Willschütz. Andererseits für die fachliche Betreuung dieser Doktorarbeit durch Herrn Dr. Seidl. Herr Dr. Seidl hat sich dabei immer – wie bereits bei meiner Diplomarbeit – sehr engagiert, z. B. bei der Durchsicht der Dissertation. Der fachliche Austausch mit Herrn Dr. Seidl in zahlreichen Telefongesprächen und E-Mails – gerade im ersten Jahr der Doktorarbeit – hat sehr zum Gelingen dieser Doktorarbeit beigetragen. Diesbezüglich kann auf zahlreiche fachliche Anmerkungen, Hinweise, Ideen und Vorschläge aus seiner jahrelangen Erfahrung in der Kernausslegung verwiesen werden. Diese gaben wichtige Impulse, Denkanstöße und zusätzlichen Optimismus für die Herausforderungen dieses Doktorarbeitsthemas. Weiterhin ermöglichte der fachliche Austausch mit der E.ON Kernkraft GmbH eine Vernetzung zwischen Wissenschaft und Praxis. Diese Vernetzung erachte ich persönlich als wichtige Voraussetzung für exzellente und zugleich relevante Ergebnisse in der anwendungsnahen Forschung. Zudem war es mir erst durch den fachlichen Austausch mit Herrn Dr. Seidl möglich, eine sowohl in der Forschung als auch in der Industrie anwendbare Innovation zu entwickeln.

Der Europäischen Kommission, Joint Research Centre, Institute for Transuranium Elements (JRC-ITU) in Karlsruhe gilt ebenso ein ganz besonderer Dank für die Ermöglichung der beiden Forschungsaufenthalte als Gastwissenschaftler (von 6 Monaten und 8 Monaten). Das letzte verbliebene Forschungsinstitut in Deutschland, das sich noch mit der nuklearen Sicherheitsforschung im Bereich Brennstoff beschäftigt und dadurch Einfluss auf die Sicherheit kerntechnischer Anlagen weltweit nimmt, bietet (fast) einmalige Chancen und Herausforderungen für junge, an der Kerntechnik interessierte Menschen. Meinen beiden dortigen Betreuern Herrn Dr. Schubert und Herrn Dr. Van Uffelen sowie Herrn van de Laar bin ich sehr dankbar für die nette und angenehme Atmosphäre, die exzellente Betreuung und die fachliche Integration meiner Person in das Entwicklungsteam des Brennstabprogrammes

TRANSURANUS. Den Experimentatoren am JRC-ITU danke ich für die Messung der Daten und für die Beantwortung meiner Fragen. Erwähnenswert ist zudem die sehr nette, multinational geprägte Atmosphäre unter den Trainees, Doktoranden und Postdocs am JRC-ITU. Die zahlreichen netten Gespräche und privaten Unternehmungen mit Menschen aus verschiedensten Staaten der Europäischen Union werden in sehr guter Erinnerung bleiben. Glücklicherweise macht es mich, dass meine Forschungsarbeiten am JRC-ITU weitergeführt werden und somit zukünftig allen TRANSURANUS-Nutzen zur Verfügung stehen.

Zudem gilt ein besonderer Dank Herrn Professor Dr. Macián-Juan, Inhaber des Lehrstuhls für Nukleartechnik an der Fakultät für Maschinenwesen an der Technischen Universität München; einerseits für die universitätsseitige Betreuung einschließlich der gründlichen Durchsicht dieser Dissertation, andererseits für seine damit verbundene Bereitschaft, als Prüfer in der Prüfungskommission an der Technischen Universität München zu fungieren. Weiterhin möchte ich mich bei Herrn Professor Dr. rer. nat. Allelein, Inhaber des Lehrstuhls für Reaktorsicherheit und -technik an der RWTH Aachen, für die Arbeit und Mühen, verbunden mit der Funktion als Prüfer in der Prüfungskommission, bedanken. Er hat schon meine externe Diplomarbeit über Modelle im Brennstabcode TRANSURANUS im Rahmen meines Maschinenbaustudiums betreut. Somit schließt sich der Kreis zu meiner ersten (kern)technischen Ausbildungsstätte der RWTH Aachen. Die damalige Betreuung meiner Diplomarbeit, die Vorlesungen und Übungen seines Vorgängers Herrn Prof. Dr.-Ing. Kugeler (Emeritus) und seiner Mitarbeiter im Hauptstudium sowie die zahlreichen (kerntechnischen) Exkursionen, organisiert durch Herrn Dr.-Ing. Jühe, an der RWTH Aachen werden auch weiterhin in sehr guter Erinnerung bleiben und haben mir zugleich das (kerntechnische und methodische) „Rüstzeug“ für die Erstellung dieser Dissertation gegeben.

Schließlich gilt noch ein besonderer und sehr großer Dank meiner Familie (insbesondere meinen Eltern und meinen beiden Brüdern), meinen Freundeskreisen und den Kommilitonen aus meiner Studentenzeit in Aachen. Durch alle wurde ich stark geprägt und ohne einen dieser drei würde ich mich nicht an dem Punkt befinden, an dem ich heute bin. Diese haben mir immer die Kraft gegeben, so manche fachliche und sonstige Herausforderung im Rahmen der Doktorarbeit zu meistern. Jedoch auch das gute Miteinander im Vorstand der Jungen Generation in der Kerntechnischen Gesellschaft e.V. (KTG) hat mir des Öfteren Kraft für die Anfertigung dieser Doktorarbeit gegeben. Dabei war mir das häufig nach Feierabend und am Wochenende geleistete Engagement für die Junge Generation in der KTG immer ein

Acknowledgements

Herzensanliegen. Der Austausch mit anderen jungen Kerntechnikern in Deutschland und Europa hat mir jederzeit Spaß und Freude bereitet.

Lingen (Ems), Mai 2016

Wass Hatt

Publications

Journal papers

L. Holt, A. Schubert, P. Van Uffelen, C.T. Walker, E. Fridman, T. Sonoda, Sensitivity Study on Xe Depletion in the High Burn-up Structure of UO₂, *Journal of Nuclear Materials*, 452 (2014) 166-172.

L. Holt, U. Rohde, M. Seidl, A. Schubert, P. Van Uffelen, R. Macián-Juan, Development of a General Coupling Interface for the Fuel Performance Code TRANSURANUS – Tested with the Reactor Dynamics Code DYN3D, *Annals of Nuclear Energy, Multi-Physics Modelling of LWR Static and Transient Behaviour*, 84 (2015) 73-85.

L. Holt, U. Rohde, S. Kliem, S. Baier, M. Seidl, P. Van Uffelen, R. Macián-Juan, Investigation of Feedback on Neutron Kinetics and Thermal Hydraulics from Detailed Online Fuel Behavior Modeling during a Boron Dilution Transient in a PWR with the Two-way Coupled Code System DYN3D-TRANSURANUS, *Nuclear Engineering and Design*, 297 (2016) 32-43.

U. Rohde, S. Kliem, U. Grundmann, S. Baier, Y. Bilodid, S. Duerigen, E. Fridman, A. Gommlich, A. Grahn, L. Holt, Y. Kozmenkov, S. Mittag, The Reactor Dynamics Code DYN3D – Models, Validation and Applications, *Progress in Nuclear Energy*, 89 (2016) 170-190.

Conference papers

L. Holt, U. Rohde, M. Seidl, A. Schubert, P. Van Uffelen, Development of a General Coupling Interface for the Fuel Performance Code TRANSURANUS Tested with the Reactor Dynamic Code DYN3D, 10th International Conference on WWER Fuel Performance, Modelling and Experimental Support, Sandanski, Bulgaria, 2013.

L. Holt, U. Rohde, M. Seidl, A. Schubert, P. Van Uffelen, R. Macián-Juan, Getting the details of fuel rod simulation in reactor safety analysis right: performance of the code coupling DYN3D-TRANSURANUS for RIA, 45th Annual Meeting on Nuclear Technology, INFORUM Verlags- und Verwaltungsgesellschaft mbH, Frankfurt, Germany, 2014.

L. Holt, U. Rohde, M. Seidl, A. Schubert, P. Van Uffelen, R. Macián-Juan, Two-way Coupling between the Reactor Dynamics Code DYN3D and the Fuel Performance Code TRANSURANUS at Assembly Level, 22nd International Conference on Nuclear Engineering (ICONE22), ASME, Prague, Czech Republic, 2014 (*Winner in the ICONE-22 Student Best Paper Competition - Europe*).

L. Holt, A. Schubert, J. van de Laar, P. Van Uffelen, Stand-alone modelling of the high burnup structure formation and burst release during design basis accidents, EHPG Meeting, HRP, Røros, Norway, 2014 (*presented by P. Van Uffelen from JRC-ITU*).

Technical reports

OECD/NEA, RIA Fuel Codes Benchmark - Volume 1, NEA/CSNI/R(2013)7/VOL1, Paris, France, 2013 (*containing simulation results of this work*).

OECD/NEA, RIA Fuel Codes Benchmark - Volume 2, NEA/CSNI/R(2013)7/VOL2, Paris, France, 2013 (*containing simulation results of this work*).

Technical meeting papers

P. Van Uffelen, J. van de Laar, A. Schubert, V. Di Marcello, L. Vlahovic, L. Holt, Modelling of Nuclear Fuel under Accident Conditions by means of TRANSURANUS, IAEA Technical meeting on modelling of water-cooled fuel including design basis accidents and severe accidents, Chengdu, China, 2013.

Presentations

L. Holt, U. Rohde, Validation of the TRANSURANUS code for RIA analysis and coupling with the reactor dynamics code DYN3D, International TRANSURANUS Workshop “Towards nuclear fuel modelling in the various reactor types across Europa”, Hannover, Germany, 2011.

L. Holt, RIA benchmark simulations with the fuel performance code TRANSURANUS, OECD/NEA, Second WGFS Seminar on RIA fuel code benchmark, Aix en Provence, France, 2012.

L. Holt, U. Rohde, M. Seidl, A. Schubert, P. Van Uffelen, R. Macián-Juan, Development of a general coupling interface for TRANSURANUS - Core Safety Analysis for high burn-up fuel during RIA, Kompetenzzentrum Ost fuer Kerntechnik, Rossendorf, Germany, 2012.

L. Holt, U. Rohde, M. Seidl, A. Schubert, P. Van Uffelen, R. Macián-Juan, PWR control rod ejection simulations including high burn-up phenomena - planned code coupling DYN3D-TRANSURANUS, International DYN3D Users and Developers Meeting, Rossendorf, Germany, 2013.

L. Holt, U. Rohde, M. Seidl, A. Schubert, P. Van Uffelen, R. Macián-Juan, Two-ways coupling of DYN3D and TRANSURANUS, Nuclear Reactor Safety Simulation Platform (NURESAFE) SP1 Meeting (FP7-EURATOM-Fission), Rossendorf, Germany, 2013.

L. Holt, A. Schubert, P. Van Uffelen, Modelling of the high burn-up structure and its processes in TRANSURANUS, International TRANSURANUS Workshop “Towards nuclear fuel modelling in the various reactor types across Europa”, Karlsruhe, Germany, 2013.

L. Holt, U. Rohde, M. Seidl, A. Schubert, P. Van Uffelen, R. Macián-Juan, A general coupling scheme for TRANSURANUS - development steps explained on the reactor dynamic code DYN3D, International TRANSURANUS Workshop “Towards nuclear fuel modelling in the various reactor types across Europa”, Karlsruhe, Germany, 2013.

L. Holt, U. Rohde, M. Seidl, A. Schubert, P. Van Uffelen, R. Macián-Juan, Getting the details of fuel rod simulation in reactor safety analysis right: performance of the code coupling DYN3D-TRANSURANUS for RIA, KTG-Fachtag, Aktuelle Themen rund um das Brennelement, Karlsruhe, Germany, 2014.

A. Schubert, J. van de Laar, P. Van Uffelen, L. Holt, J. Klouzal, Simulation of LOCA tests carried out in Norway by means of the TRANSURANUS code, 20th International QUENCH Workshop, Collocated with the 1st IAEA Coordinated Research Project FUMAC Meeting, Karlsruhe, Germany, 2014 (*presented by A. Schubert from JRC-ITU*).

L. Holt, Coupling of fuel performance codes – Replacement of simplified fuel behavior models through TRANSURANUS (part I), International TRANSURANUS Workshop “Towards nuclear fuel modelling in the various reactor types across Europa”, Karlsruhe, Germany, 2015.

L. Holt, Coupling of fuel performance codes – Replacement of simplified fuel behavior models through TRANSURANUS (part II), International TRANSURANUS Workshop “Towards nuclear fuel modelling in the various reactor types across Europa”, Karlsruhe, Germany, 2015.

Additional presentations at E.ON Kernkraft GmbH, Helmholtz-Zentrum Dresden-Rossendorf, European Commission (Joint Research Centre, Institute for Transuranium Elements) and Technische Universität München.